UDK 621.3:(53+54+621+66)(05)(497.1)=00 ISSN 0352-9045

INFORMACIJE MIDEM

Strokovno društvo za mikroelektroniko elektronske sestavne dele in materiale

4·2009

Strokovna revija za mikroelektroniko, elektronske sestavne dele in materiale
Journal of Microelectronics, Electronic Components and Materials

INFORMACIJE MIDEM, LETNIK 39, ŠT. 4(132), LJUBLJANA, december 2009

MIDEM 2009

45th INTERNATIONAL CONFERENCE
ON MICROELECTRONICS, DEVICES AND MATERIALS
and the WORKSHOP on
ADVANCED PHOTOVOLTAIC DEVICES

September 9.- September 11.2009
Jamski dvorec, Postojna, Slovenia

UDK 621.3:(53+54+621+66)(05)(497.1)=00 ISSN 0352-9045

INFORMACIJE MIDEM 4 ○ 2009

INFORMACIJE MIDEM LETNIK 39, ŠT. 4(132), LJUBLJANA, DECEMBER 2009
INFORMACIJE MIDEM VOLUME 39, NO. 4(132), LJUBLJANA, DECEMBER 2009

Revija izhaja trimesečno (marec, junij, september, december). Izdaja strokovno društvo za mikroelektroniko, elektronske sestavne dele in materiale - MIDEM.
Published quarterly (march, june, september, december) by Society for Microelectronics, Electronic Components and Materials - MIDEM.

Naslov uredništva
Headquarters
Uredništvo Informacije MIDEM
MIDEM pri MIKROIKS
Stegne 11, 1521 Ljubljana, Slovenija
tel.: + 386 (0)1 51 33 768
faks: + 386 (0)1 51 33 771
e-pošta: Iztok.Sorli@guest.arnes.si
http://www.midem-drustvo.si/

Letna naročnina je 100 EUR, cena posamezne številke pa 25 EUR. Člani in sponzorji MIDEM prejemajo Informacije MIDEM brezplačno.
Annual subscription rate is EUR 100, separate issue is EUR 25. MIDEM members and Society sponsors receive Informacije MIDEM for free.

Znanstveni svet za tehnične vede je podal pozitivno mnenje o reviji kot znanstveno-strokovni reviji za mikroelektroniko, elektronske sestavne dele in materiale. Izdajo revije sofinancirajo JAKRS in sponzorji društva.
Scientific Council for Technical Sciences of Slovene Research Agency has recognized Informacije MIDEM as scientific Journal for microelectronics, electronic components and materials.
Publishing of the Journal is financed by Slovenian Book Agency and by Society sponsors.

Znanstveno-strokovne prispevke objavljene v Informacijah MIDEM zajemamo v podatkovne baze COBISS in INSPEC.

Prispevke iz revije zajema ISI® v naslednje svoje produkte: Sci Search®, Research Alert® in Materials Science Citation Index™

Scientific and professional papers published in Informacije MIDEM are assessed into COBISS and INSPEC databases.

The Journal is indexed by ISI® for Sci Search®, Research Alert® and Material Science Citation Index™

Po mnenju Ministrstva za informiranje št.23/300-92 šteje glasilo Informacije MIDEM med proizvode informativnega značaja.

Grafična priprava in tisk
Printed by
BIRO M, Ljubljana

Naklada
Circulation
1000 izvodov
1000 issues

Poštnina plačana pri pošti 1102 Ljubljana
Slovenia Taxe Percue

UDK621.3:(53+54+621+66), ISSN0352-9045 Informacije MIDEM 39(2009)4, Ljubljana

Obnovitev članstva v strokovnem društvu MIDEM in iz tega izhajajoče ugodnosti in obveznosti

Spoštovani,

V svojem več desetletij dolgem obstoju in delovanju smo si prizadevali narediti društvo privlačno in koristno vsem članom.Z delovanjem društva ste se srečali tudi vi in se odločili, da se v društvo včlanite. Življenske poti, zaposlitev in strokovno zanimanje pa se z leti spreminjajo, najrazličnejši dogodki, izzivi in odločitve so vas morda usmerili v povsem druga področja in vaš interes za delovanje ali članstvo v društvu se je z leti močno spremenil, morda izginil. Morda pa vas aktivnosti društva kljub temu še vedno zanimajo, če ne drugače, kot spomin na prijetne čase, ki smo jih skupaj preživeli. Spremenili so se tudi naslovi in način komuniciranja.

Ker je seznam članstva postal dolg, očitno pa je, da mnogi nekdanji člani nimajo več interesa za sodelovanje v društvu, se je Izvršilni odbor društva odločil, da stanje članstva uredi in **vas zato prosi, da izpolnite in nam pošljete obrazec priložen na koncu revije.**

Naj vas ponovno spomnimo na ugodnosti, ki izhajajo iz vašega članstva. Kot član strokovnega društva prejemate revijo »Informacije MIDEM«, povabljeni ste na strokovne konference, kjer lahko predstavite svoje raziskovalne in razvojne dosežke ali srečate stare znance in nove, povabljene predavatelje s področja, ki vas zanima. O svojih dosežkih in problemih lahko poročate v strokovni reviji, ki ima ugleden IMPACT faktor.S svojimi predlogi lahko usmerjate delovanje društva.

Vaša obveza je plačilo članarine 25 EUR na leto. Članarino lahko plačate na transakcijski račun društva pri A-banki : 051008010631192. Pri nakazilu ne pozabite navesti svojega imena!

Upamo, da vas delovanje društva še vedno zanima in da boste članstvo obnovili. Žal pa bomo morali dosedanje člane, ki članstva ne boste obnovili do konca leta 2009, brisati iz seznama članstva.

Prijavnice pošljite na naslov:

MIDEM pri MIKROIKS

Stegne 11

1521 Ljubljana

Ljubljana, december 2009

Izvršilni odbor društva

MEASUREMENTS OF MATERIALS AT MICROWAVE FREQUENCIES

Jerzy Krupka

Institute of Microelectronics and Optoelectronics, Warsaw University of Technology, Warsaw, Poland

Key words: microwave frequency, electronic material, resonance measurement techniques

Abstract: Recent advances in measurements of various electronic materials at microwave frequencies are presented. Special attention is devoted to resonance techniques that are more sensitive and accurate than the transmission-reflection methods. Several specific measurement methods are described. Simultaneous use of whispering gallery and quasi TE modes allows for multi-frequency measurements of low loss materials. Modification of the split post dielectric resonator technique can be used for measurements of both permittivity and permeability of laminar low and medium loss metamaterial. Resistivity of conductive materials such as semiconductors metals and polymers can be measured in the range of several decades employing single post dielectric resonator technique.

Meritve materialov pri mikrovalovnih frekvencah

Kjučne besede: mikrovalovne frekvence, elektronski material, resonančne merilne tehnike

Izvleček: V članku predstavljamo napredne tehnike meritev karakteristik različnih elektronskih materialov pri mikrovalovnih frekvencah. Posebna pozornost je namenjena resonančnim tehnikam, ki so bolj občutljive in natančne kot oddajno-povratne metode. Opisanih je nekaj specifičnih metod merjenja, ki dovoljujejo meritve materialov z nizko izgubo pri različnih frekvencah. Spremenjena tehnika meritve z dielektričnim resonatorjem omogoča meritve dielektrične konstante in izgub v materialih s srednjimi in nizkimi izgubami. S to tehniko lahko merimo tudi upornost prevodnih materialov, kot so polprevodne kovine in polimeri v širokem območju.

1 Introduction

Measurement techniques of the complex permittivity and in some cases the complex permeability are described for the following four groups of materials:

a) Bulk low loss dielectric materials including ceramics and uniaxially anisotropic single-crystals;
b) Laminar type dielectric materials such as LTCC ceramics, PWB substrates and thin ferroelectric films;
c) Semiconductors and conductors;
d) Metamaterials

At frequency domain the complex permittivity of any linear material is generally defined as a tensor quantity describing relationship between the electric displacement ($\vec{D}$) and the electric field ($\vec{E}$) vectors (1) /1/.

$$\vec{D} = \bar{\varepsilon}\vec{E} \tag{1}$$

For passive reciprocal materials such as ionic dielectric single crystals permittivity tensor is symmetric and can be diagonalized which means that at certain specific coordinate system it takes the diagonal form (2)

$$\bar{\varepsilon} = \begin{bmatrix} \varepsilon_{11} & 0 & 0 \\ 0 & \varepsilon_{22} & 0 \\ 0 & 0 & \varepsilon_{33} \end{bmatrix} \tag{2}$$

For polycrystalline materials, glasses, plastics and some crystals (e.g. having cubic crystallographic structure) all diagonal elements become identical and the complex permittivity becomes scalar quantity. The complex permittivity of an isotropic material in general can be written as

$$\varepsilon = \varepsilon_0\varepsilon_r = \varepsilon_0(\varepsilon_r' - j\varepsilon_{rd}'' - j\frac{\sigma}{\omega\varepsilon_0}) = \\ = \varepsilon_0\varepsilon_r'(1 - j\tan\delta) \tag{3}$$

where - tan δ - total dielectric loss tangent

$$\tan\delta = \tan\delta_d + \frac{\sigma}{\omega\varepsilon_0\varepsilon_r'} \tag{4}$$

ε_r - relative complex permittivity
ω - angular frequency
σ - conductivity
$\varepsilon_0 = 1/(c^2\mu_0) \approx 8.8542x10^{-12}$ (F/m) - permittivity of vacuum
tan δ_d - dielectric loss tangent associated all other dielectric loss mechanisms except conductivity

When we measure the loss of a dielectric at a single frequency we cannot, in general, distinguish between them. Phenomenologically they all give rise to just one measurable quantity: namely the total measured loss tangent. Some materials commonly used at microwave frequencies such as ferrites, as well as metamaterials, exhibit magnetic properties that must be considered in measurements of their permittivity. Permeability tensor μ describes relationship between the magnetic induction $\vec{B}$ and magnetic field $\vec{H}$ vectors (5).

$$\vec{B} = \bar{\mu}\vec{H} \tag{5}$$

The most important microwave applications of ferrites are related to their non-reciprocal properties. In a presence of static magnetic field magnetizing ferrite material along z-axis of Cartesian or cylindrical coordinate system perme-

ability of ferrite material is represented by Polder's tensor (6) /6/. Off-diagonal components of Polder's tensor are purely imaginary but they don't describe any magnetic losses since they appear with opposite signs. If ferrite material is lossy than particular tensor components (μ,κ,μ_z) become complex.

$$\overleftrightarrow{\mu} = \mu_0 \begin{bmatrix} \mu & j\kappa & 0 \\ -j\kappa & \mu & 0 \\ 0 & 0 & \mu_z \end{bmatrix} \qquad (6)$$

This paper is principally devoted to the resonance techniques intended for the complex permittivity and the complex permeability measurements. These techniques are more sensitive and accurate than commonly used transmission-reflection methods.

Measured quantities in resonance techniques are the resonant frequency and the Q-factor of a specific mode excited in the resonant structure containing a sample under test. The complex permittivity of the sample can be evaluated from these two measured quantities providing that all other parameters of the structure are known. These parameters include dimension of the structure, surface resistance of metal parts, coupling coefficients, radiation losses, and the complex permittivities of dielectric supports. Usually advanced electromagnetic simulations are necessary to determine the complex permittivity even for relatively simple and regular shape of samples under test.

Resonant cavities having axial symmetry are the most often used in the dielectric metrology. Cavities of this kind can operate on different modes but in practice one of the few first modes of the frequency spectrum are used.

2 Measuremnts of bulk low loss dilectric materials

Bulk, low loss materials are usually measured employing dielectric resonator techniques when the sample under test concentrates most of the electromagnetic energy. These days the most frequently used method to measure bulk low loss dielectrics is the $TE_{01\sigma}$ mode dielectric resonator technique /2/ with geometry schematically shown in Fig.1a. The same structure can be used for multi-frequency measurements employing higher order TE /3/ and whispering gallery modes /4/, although Hakki-Coleman dielectric resonator technique /5/ is still frequently employed to measure the real part of the complex permittivity of low loss high permittivity ceramic materials. If the losses in samples under test increase then the Q-factor of the resonance structure becomes to small to be measured. In order to measure medium or even high loss bulk dielectric samples it is necessary to reduce the amount of the electromagnetic energy in the sample under test. This can be done for bulk samples in the way that is shown in Fig.1b /6/,/7/.

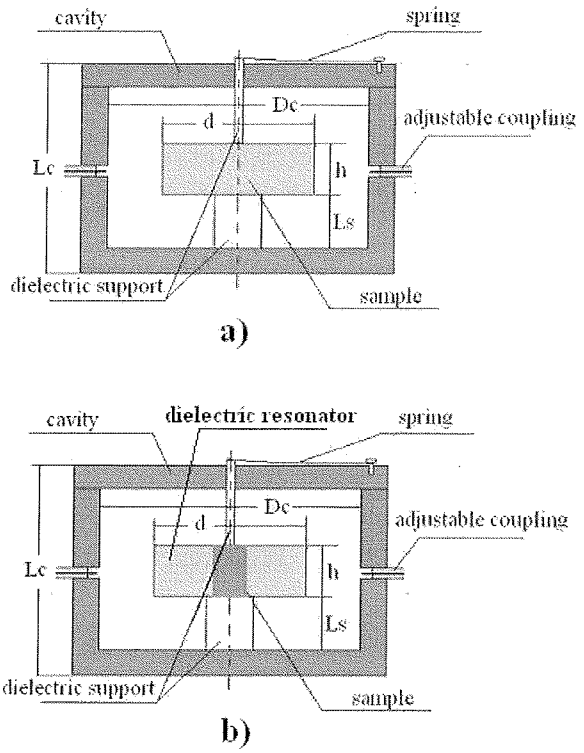

Fig. 1: Sketch of axially symmetric resonance structures used for measurements of bulk samples. a) TE or whispering gallery mode dielectric resonator intended for measurements of low loss samples, b) TE mode dielectric resonator intended for measurements of medium loss samples.

Measurement results of few bulk semi-insulating semiconductor and dielectric samples employing dielectric resonator techniques are shown in Figs.2-5.

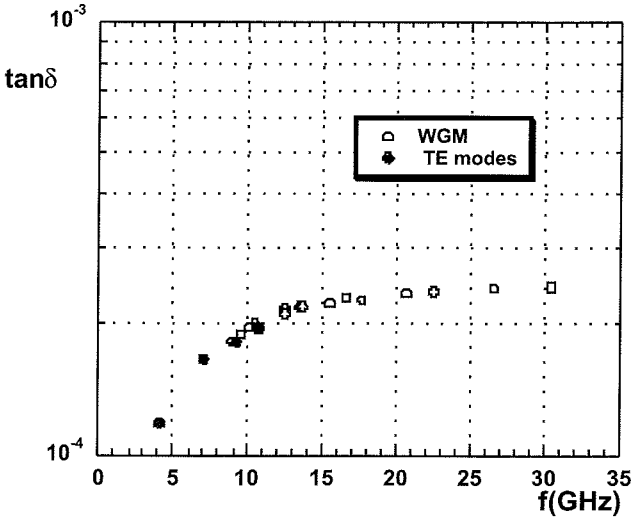

Fig. 2: Dielectric loss tangent for the GaAs sample versus frequency measured at room temperature employing several quasi TE and whispering gallery modes /8/.

Typical resolution of loss tangent resolution employing TE mode dielectric resonators technique with optimised enclosure is about 10^{-6} for high permittivity samples (ε_r>20) and uncertainty of the real part of permittivity measurements of the order of 0.3% (similar for low and high permittivities). For whispering gallery modes loss tangent resolution can be even better then 10^{-10} (dielectric loss tangent of high purity sapphire at 4 K) /4/.

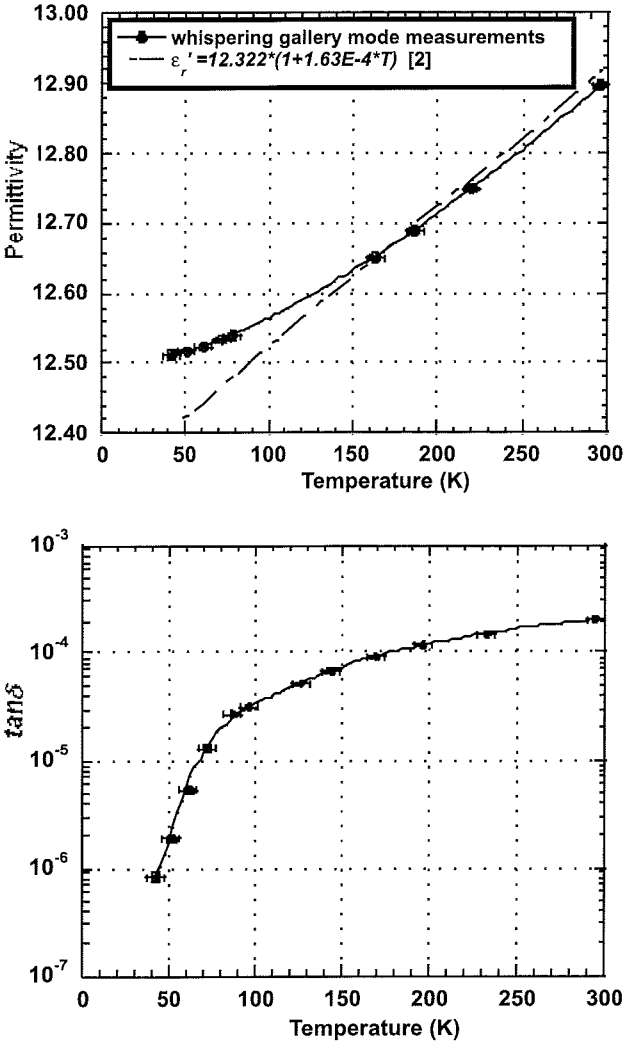

Fig. 3: Permittivity versus temperature for the GaAs sample. The experimental data points were extracted from measurements of the whispering gallery mode with frequencies near 18.9 GHz /8/.

Fig. 4: Measured and predicted theoretical loss at 3 GHz and zero bias for $KTaO_3$ /9/.

It should be pointed out that employing whispering gallery modes it is possible to measure two components of the complex permittivity tensor for oriented uniaxialy anisotropic crystals /10/.

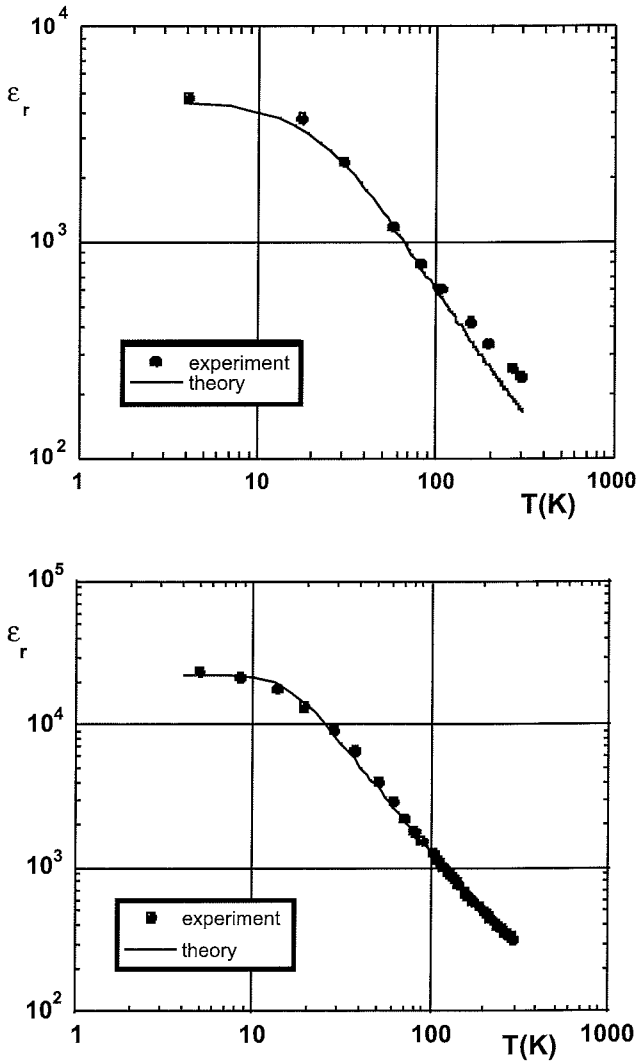

Fig. 5: Theoretical and measured real permittivities for high-purity single-crystals of $KTaO_3$ and $SrTiO_3$ /9/.

3 Measuremnts of laminar dielectric materials

The most convenient methods to measure the complex permittivity of isotropic laminar dielectric materials are the split cylindrical cavity method /11/ and the split post dielectric resonator method /12/. Schematic diagram of the split post dielectric resonator is shown in Fig. 6. In both methods the TE modes are employed that have only azimuthal component of the electric filed. This makes the methods no sensitive to the presence of air gaps between sample and the other parts of the resonance structures because due to their axial symmetry the electric field is tangential to the surface of test samples. Employing these methods one can measure permittivity to within 0.3%. The dielectric loss tangent resolution is typically better than 10^{-4}. Split post dielectric resonator can be also employed for the complex permittivity measurements of thin ferroelectric films /13/, as well as for the surface resistance meas-

urements of thin conducting films having surface resistance larger than 3 kΩ /14/.

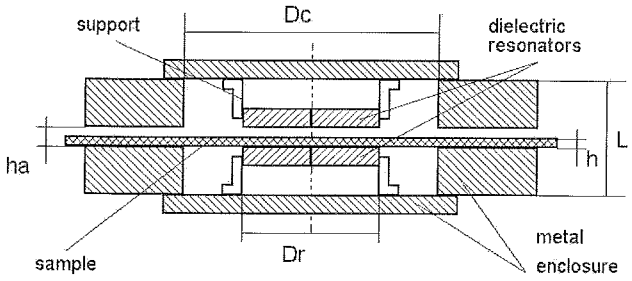

Fig. 6. Schematic diagram of split post dielectric resonator

4 Measurements of semiconductors and conductors

Contact-less conductivity measurements of semiconductors are very attractive especially for such materials for which it is difficult to create linear current contacts with four-point probe technique (e.g. SiC). This can be done with a single post dielectric resonator technique /15/. Schematic of the 10 GHz single post dielectric resonator intended for conductivity measurements of typical semiconductor wafers is shown in Fig.7.

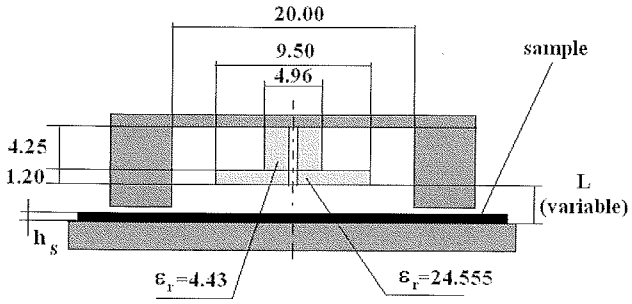

Fig. 7: Schematic of 10 GHz single post dielectric resonator intended for measurements of semiconductor wafers and thin conducting films deposited on dielectric substrates

Principles of conductivity measurements employing single-post dielectric resonators can be explained using graphs showing $TE_{01\sigma}$ mode resonant frequencies and Q-factors due to conductor losses (Q_S) in the sample versus conductivity for different thicknesses of samples. Such graphs are shown in Fig.8. One can observe that for σ<1 S/m Q_S-factors and resonant frequency shifts behave as for "proper dielectrics". In this conductivity range resonant frequency shifts depend on the real part of permittivity and thickness of samples, while Q_S-factors decrease with increase of conductivity. When σ>1000 S/m Q_S-factors and resonant frequency shifts behave as for metallic samples. In this case electromagnetic fields decay exponentially in the direction perpendicular to the surface of the sample (skin effect).

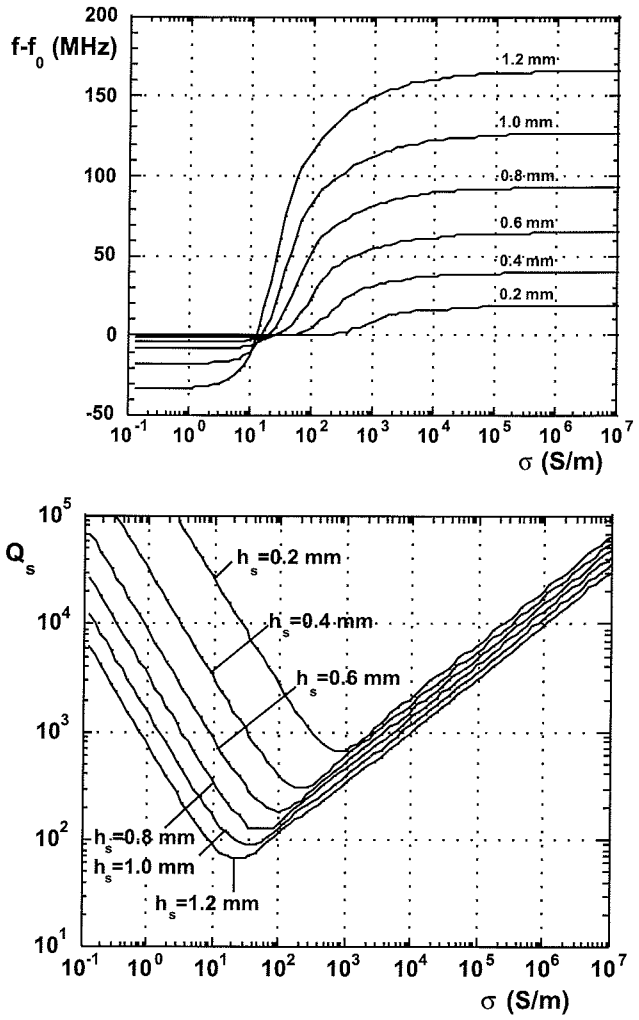

Fig. 8. Computed resonant frequency shifts and Q-factors due to conductor losses in the sample, (Q_S), for the single-post dielectric resonator shown in Fig. 7 with L=4.3 mm.

As one can notice unique determination of conductivity (resistivity) is possible if both the resonance frequency shift due to the presence of the sample and the Q-factor due to conductor losses in the sample are known.

The single post dielectric resonator technique can be also used for the measurements of the surface resistance of thin conducting films /14/.

5 Measurements of metamaterials

Metal films deposited on a dielectric substrate may exhibit dielectric properties that significantly deviate from those of the bulk metals /16/-/17/. Very rapid change of dielectric properties takes place near percolation threshold when films become very thin and have island structure. If one assumes that the island structure is periodic, such a patterned metal film can be considered as a 2D metamaterial /18/-/20/. Electromagnetic properties of periodic 2D heterogeneous structures consisting of unit cells of various shapes such as metal dots, rings, split rings, double split

rings and many other ones are of interest for many applications including manufacturing of a bulk artificial dielectric / 21/. If metal patterns posses high degree of symmetry than the in-plane electromagnetic properties of such created 2D metamaterial are expected to be isotropic. By stacking several layers of such 2D metamaterials one can obtain 3D metamaterials having uniaxialy anisotropy. It is known that the electromagnetic properties of such metamaterial can be characterized by the effective permittivity and the effective permeability. For more complicated structures that do not posses in plane symmetry it is necessary to introduce additional material parameters (material properties) that take into account the coupling between the electric displacement vector and the magnetic field as well as the coupling between magnetic induction and the electric field. Such metatamaterials are called bianisotropic. It is also possible to create isotropic 3D metamaterials by random mixing of dielectric and metal particles. Such isotropic metamaterials also exhibit both electric end magnetic properties but in this case permittivity and permeability are scalars. Measurements of both permittivity and permeability of metamaterials are difficult especially for relatively low loss materials.

I the recently published paper /23/ a method have been described that allows to measure the effective complex permittivity and the effective complex permeability of isotropic and uniaxialy anisotropic metamaterials. Separation of the complex permittivity from the complex permeability for a specific metamaterial was achieved performing measurements of the resonance frequencies and the Q-factors of a split post dielectric resonator with two samples having different diameters but identical film patterns as it is shown in Fig.9. Measurements of the resonance frequencies and Q-factors of empty substrates served as reference materials to determine the resonance frequency shifts and Q-factor changes due to the presence of the metamaterial only. electromagnetic Determinations of the effective complex permittivity and permeability were performed on the basis of rigorous modeling of the resonance structures containing the samples. To check the validity and accuracy of presented technique two reference "materials" were measured.

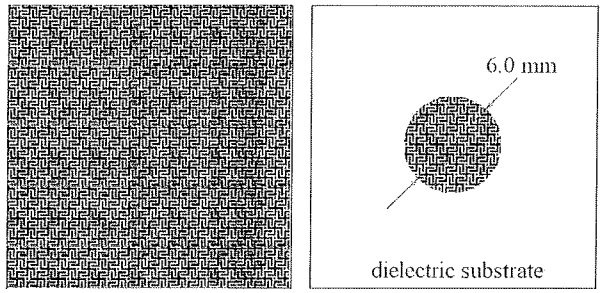

Fig. 9: Two samples of metamaterial having the same pattern that are used to determine both permittivity and permeability of this metamaterial.

The first reference material was made from a single piece of transparency foil, 122 mm thick placed on the substrate. A small sample of reference "material" was just cut from the transparency foil in a 6 mm diameter circle. Measurements of the dielectric reference "material" should yield known results (permittivity of 3.18 and unity permeability). Due to unavoidable measurement uncertainties real measurements would differ slightly. The second reference magneto-dielectric material was yttrium-iron garnet YIG. Again two samples of this material, 508 mm thick, have been used in our measurements, one was 30 mm x 30 mm sample and the other 6 mm diameter sample.

In the addition two metamaterial samples were measured. These samples were made as a random mixtures of very fine Aluminium powder (with a mean particle size of the order of 1 mm) and a polymer (PMMA) deposited by painting onto transparency polyester foils. The results of measurements on reference materials and on metamaterials at frequency 4.9 GHz are summarized in Table 1. Measurements on the reference materials (PET and YIG) are consistent with the literature values. It should be noted that permittivities of metamaterials are very large (comparable to the permittivity of ferroelectrics). The effective permeabilities of both metamaterials are smaller than unity which is related to the eddy currents induced in metal particles.

Table 1. Results of permittivity and permeability determination for "normal" reference materials and planar, isotropic 3D metamaterials

Material	$Re(\varepsilon_r)$	$Im(\varepsilon_r)$	$Re(\mu_{zy})$	$Im(\mu_{zy})$	$h_f(\mu_m)$
PET	3.145	-0.0154	1.00448	< 0.0001	122
YIG	15.45	-0.0011	0.64900	-0.00945	508
Metamaterial 1	341	-17.5	0.28900	-0.02870	7
Metamaterial 2	3146	-88	0.15100	-0.13400	4

6 Summary

This paper overviewed only small fraction of available techniques for measurement of material properties at microwave frequencies. A lot of techniques exist that were not mentioned in this paper that utilize microstrip, stripline and coplanar waveguide cells (both transmission line and resonant ones). Typically transmission/reflection technique are useful for characterization of high and medium loss materials and resonant techniques can be in principle used for measurements of materials having arbitrary losses. On the other hand resonant techniques are in most cases limited to one fixed frequency (although as it has been shown multi-frequency measurements in one measurements cell are possible) while transmission/reflection techniques can typically operate at broad frequency bands. One of the most important issues for all techniques is their sensitivity to the presence of air gaps between the sample and other parts of the measurement cell. Resolution of loss tangent measurements for arbitrary technique is associated with the presence of parasitic losses in measuring cells. They must be calculable and relatively small with respect to the

losses in the sample to in order to measure precisely losses in the material under test.

Acknowledgments

This work was partly supported by the Polish Government Research Grant No 0592/T02/2007/32

References

/1/ J. Krupka, "Frequency Domain Complex Permittivity Measurements at Microwave Frequencies", *Measurement Science and Technology*, vol.17, R55-R77, 2006 .

/2/ J.Krupka, K. Derzakowski, B. Riddle and J. Baker-Jarvis, "A dielectric resonator for measurements of complex permittivity of low loss dielectric materials as a function of temperature", Measurements Science and Technology, vol.9, pp.1751-1756, Oct.1998

/3/ J. Krupka, Wei-Te Huang and Mean-Jue Tung "Complex Permittivity Measurements of Low Loss Microwave Ceramics Employing Higher Order Quasi TE0np Modes Excited in a Cylindrical Dielectric Sample", Measurements Science and Technology, vol 16, pp.1014-1020, 2005

/4/ J. Krupka, K. Derzakowski, A. Abramowicz, M. E. Tobar and R. G. Geyer "Whispering Gallery Modes for Complex Permittivity Measurements of Ultra-Low Loss Dielectric Materials", *IEEE Trans. Microwave Theory Tech.*, vol. MTT-47, pp.752-759, June 1999

/5/ B. W. Hakki and P. D. Coleman "A dielectric resonator method of measuring inductive capacities in the millimeter range", IEEE Trans. Microwave Theory Tech. Vol. 8, pp. 402-410, 1960

/6/ J. Krupka, J. Breeze, A. Centeno, N. Mc N. Alford, T. Claussen, and L. Jensen, "Measurements of permittivity, dielectric loss tangent, and resistivity of float zone Silicon at microwave frequencies," IEEE Trans. on Microwave Theory Tech, vol.54, pp.3995-4001, November 2006

/7/ J. Krupka, T. Zychowicz, V.Bovtun, and S. Veljko, "Complex Permittivity Measurements of Ferroelectrics Employing Composite Dielectric Resonator Technique", IEEE Transactions on Ultrasonics, Ferroelectrics and Frequency Control, pp.1883-1888, vol.53, No 10, October 2006

/8/ J. Krupka, D. Mouneyrac, J.G. Hartnett, and M.E. Tobar, "Use of whispering-gallery modes and quasi-TE0np modes for broadband characterization of bulk gallium arsenide and gallium phosphide samples", IEEE Trans. on Microwave Theory Tech, vol.56, pp.1201-1206, May 2008

/9/ R. G. Geyer, J. Krupka, B. Riddle, and L. A. Boatner "Microwave dielectric properties of single crystal quantum paraelectrics KTaO3 and SrTiO3 at cryogenic temperatures", Journal of Applied Physics, vol.97, No10, p.104111 (6pages), Part 1, May 15, 2005

/10/ J. Krupka, K. Derzakowski, M.E. Tobar, J. Hartnett, and R.G. Geyer, "Complex permittivity of some ultralow loss dielectric crystals at cryogenic temperatures", Measurement Science and Technology, vol.10, pp.387-392, Oct.1999

/11/ G. Kent, "An evanescent-mode tester for ceramic dielectric substrates", IEEE Trans. on Microwave Theory Tech, vol.36, pp.1451-1454, 1988.

/12/ J. Krupka, A P Gregory, O. C. Rochard, R N Clarke, B Riddle and J Baker-Jarvis, "Uncertainty of Complex Permittivity Measurements by Split-Post Dielectric Resonator Technique", *Journal of the European Ceramic Society*, vol.21, pp.2673-2676, 2001

/13/ J. Krupka, Wei-Te Huang and Mean-Jue Tung, „Complex Permittivity Measurements of Thin Ferroelectric Films Employing Split Post Dielectric Resonator", Ferroelectrics, vol.335, issue 1, pp.89-94, 2006

/14/ J. Krupka, "Measurement of the complex permittivity of metal nanoislands and the surface resistance of thin conducting films at microwave frequencies", Measurements Science and Technology, Vol. 19, Iss. 6 Article Number: 065701. June, 2008

/15/ J. Krupka and J. Mazierska, „Contact-less measurements of resistivity of semiconductor wafers employing single-post and split-post dielectric resonator techniques", *IEEE Trans. IM*, pp.1839-1844, October 2007.

/16/ J. J. Tu, C. C. Homes and M. Strongin, "Optical Properties of Ultrathin Films: Evidence for a Dielectric Anomaly at the Insulator-to-Metal Transition", *Phys. Rev. Lett.* vol.90, 017402, 2003

/17/ A.P. Boltaev, L.S. Podlesnykh, F.A. Pudonin, "Anomalously high effective permittivity of a system of FeNi metal nanoislands", *Kratkie Soobshcheniya po Fizike*, vol. 34, No. 8, pp. 3-9. 2007

/18/ N. Engheta and R.W. Ziolkowski, Metamaterials - Physics and Engineering Explorations, Chapter 3, IEEE Press, Wiley Interscience, 2006.

/19/ O. F. Siddiqui and G.V. Eleftheriades, "Resonant modes in continuous metallic grids over ground and related spatial-filtering applications", *J. Appl. Phys.*, vol. 99 , Issue 8, 083102, 2006

/20/ J. B. Pendry, J.A. Holden, J.D. Robbins, and J.W. Steward, "Magnetism from conductors and enhanced nonlinear phenomena", *IEEE Trans. Micro. Theory and Tech.*, vol. 47, pp.2075-2084, November 1999.

/21/ H. Kubo, T. Mukai, and A. Sanada; "High Q or high effective permittivity artificial dielectric resonator in a waveguide", *IEICE Trans. on Electronics*, vol.E88C, Iss.7, pp.1412-1419, July 2005

/22/ J. Krupka, K. Derzakowski and J.G. Hartnett, " Measurements of the Effective Permittivity and the Effective Permeability of Low and Medium Loss Planar Metamaterials at Microwave Frequencies", To be published in Measurements Science and Technology

Jerzy Krupka
Institute of Microelectronics and Optoelectronics, Warsaw University of Technology, Koszykowa 75, 00-662 Warsaw, Poland, krupka@imio.pw.edu.pl

Prispelo (Arrived): 15.08.2009 *Sprejeto (Accepted): 09.10.2009*

MODERN THICK-FILM AND LTCC PASSIVES AND PASSIVE INTEGRATED COMPONENTS

Andrzej Dziedzic

Faculty of Microsystem Electronics and Photonics, Wroclaw University of Technology, Wroclaw, Poland

Key words: LTCC technologies, modern passives, thick-film, passive integrated components, modern electronic circuits

Abstract: The dimensions of modern passives and passive integrated components should be reduced significantly in the nearest future. The aim of this paper is to present current situation in the area of discrete, integrated and integral passives made using thick-film or Low Temperature Co-Fired Ceramic (LTCC) technologies. The role of these components in modern electronic circuits is discussed too. The concept of such passives is very simple and they are very cheap in mass production. But from materials science point of view they are complicated, non-equilibrium systems with physical and electrical properties dependent on microstructure, which is determined in turn by proper arrangement of raw materials properties and conditions of fabrication process.

The material, technological and constructional solutions and their relation with electrical and stability properties are analyzed in details for thick-film and LTCC micropassives - microresistors, microcapacitors, microinductors and microvaristors - both described in the literature as well as fabricated and characterized at the Faculty of Microsystem Electronics and Photonics, Wroclaw University of Technology. Moreover the relations between minimal geometrical dimensions, technological accuracy and limitations on the one hand and electrical properties and stability behavior on the second hand are presented and discussed.

Moderne pasivne in integrirane pasivne komponente izdelane z debeloplastno in LTCC tehnologijo

Kjučne besede: LTCC tehnologije, moderne pasivne komponente, debeloplastne pasivne integrirane komponente, moderna elektronska vezja

Izvleček: Velikosti modernih pasivnih in integriranih pasivnih komponent moramo v bližnji prihodnosti še dodatno zmanjšati. Namen tega članka je predstaviti trenutno situacijo na področju diskretnih, integriranih in integralnih pasivnih komponent, narejenih s pomočjo debeloplastnih filmov ali LTCC tehnologij. Omenjamo tudi vlogo the komponent v modernih elektronskih vezjih. Koncept teh pasivnih komponent je zelo enostaven, v široki potrošnji pa so zelo poceni. Toda s stališča materialoznanstva pa gre za zapletene, neravnovesne sisteme, katerih fizikalne in električne lastnosti so odvisne od mikrostrukture, ki je na drugi strani določena z lastnostmi osnovnega materiala in pogojev proizvodnega procesa.

V prispevku analiziramo material, tehnološke in konstrukcijske rešitve ter njihov vpliv na stabilnost in električne lastnosti debeloplastnih in LTCC pasivnih komponent. - mikroupori, mikrokondenzatorji, mikroinduktivnosti in mikrovaristorji - oboje opisano v literaturi, kakor tudi proizvedeno in okarakterizirano na Fakulteti za Mikrosisteme, elektroniko in fotoniko na Univerzi Wroclaw. Obravnavamo tudi povezavo med minimalnimi dimenzijami, tehnološko točnostjo in omejitvami na eni strani in električnimi lastnostmi in zanesljivostjo na drugi strani.

1. Introduction - characterization of modern passives

Electronic devices, components, circuits and systems should be faster, smaller, lighter and cheaper. Proper functionality of modern electronic circuits demands both active devices and passives (primarily resistors, capacitors and inductors, but also nonlinear resistors - thermistors and varistors, potentiometers, transformers, filters, fuses, mechanical switches and electromechanical relays).

About 10^{12} of passives, which undergo deep technological and constructional transformation, are used by electronic industry every year and the world wide market in this segment is equal to about 35 billions of US dollars. Around 1980's the through-hole packaging moved towards surface mount technology (SMT). Wirewound components were replaced gradually but rapidly by surface mount ones and about 90% passives is SMT adapted at present.

According to the classification of National Electronics Manufacturing Initiative (NEMI, USA) the following generation of passives can be distinguished /1-4/:

- Discretes - traditional single purpose surface mount or through-hole passives,
- Arrays - multiple passive components with identical function in a single SMT case,
- Networks - multiple passive components of more than one function in a single SMT case, usually 4 to 12 elements,
- Integrated - a package containing multiple passive elements of more than one function and possibly a few active elements in a single SMT or Chip Scale Package (CSP),
- Integral - passives embedded in or incorporated on the surface of an interconnecting substrate,
- On-chip passives - passive components that are fabricated along with the active ICs as a part of semiconductor wafer.

The requirements for passives are dependent on type of circuits (Table 1).

Table 1. Typical passive components requirements for various electronic circuits (based on /5/)

Analog and mixed-signal circuits		
Application	Value range	Tolerance [%]
Resistors	10 Ω– 100 MΩ	1 – 10
Signal capacitors	10 pF– 10 nF	5 – 10
Decoupling capacitors	0.01 – 0.1 μF	10 – 20
EMI filter capacitors	1 – 10 nF	10 – 20
Choke inductors	1 – 10 μH	10 – 20
RF and microwave circuits		
Application	Value range	Tolerance [%]
Terminating resistors	20 – 100 Ω	1 – 10
Signal resistors	10 – 100 Ω	1 – 10
Signal capacitors	1 – 20 pF	5 – 10
Decoupling capacitors	0.01 – 0.1 μF	10 – 20
Choke inductors	1 – 10 μH	10 – 20
Signal inductors	1 – 20 nH	1 – 10

The average linear dimension (Table 2) and complexity of passives was decreased during recent years much less than characteristic dimension and complexity of integrated circuits. This is the reason why the ratio between passives and active devices is increased almost all the time.

Table 2. Percentage contribution of package sizes of passive components (based on /6/)

Year / Pack. size	1980	1990	2000	2010
1206	89.5	13.0	5.0	1.0
0805	10.5	78.0	22.0	2.5
0603		9.0	60.0	20.0
0402			13.0	60.0
0201				15.0
01005				1.5

Further miniaturization of passives reaches the equipment barrier – for example modern pick-and-place machines are not adjusted for accurate placement of 01005 components. Therefore an old idea of planar arrays and networks was reanimated.

Four 0603 capacitors, together with solder pads and technological margins, need 17.5 mm^2 area. But array of 4 identical capacitors placed in one 1206 structure needs only 7.75 mm^2 of printed circuit board area. Moreover, considering the necessary technological margins, the contribution of area (volume) of active layer in relation to nominal device dimensions is decreased for smaller packages. For example, this is 43% in 1206 multilayer ceramic capacitors and only 19% in 0402 ones. Moreover passive arrays and networks are characterized by smaller serial inductance and better frequency behavior as well as lower assembly cost and higher circuit reliability.

The integration of passives is the best solution for very high component density with increased electrical performance, improved reliability, reduced size and weight as well as lower cost. This process causes reduction or elimination of discrete SMT components and the same reduction of overall part count, elimination of solder joints, improvement of wireability and frequency behavior due to elimination of parasitic inductance. The above advantages are possible thanks to multichip module (MCM) technologies /7,8/ - an extension of hybrid technologies permitting a higher packaging density than can be assures by other approaches.

The signal transmission lines in MCM are placed at many levels and the ratio of bare VLSI circuits' area (mounted on MCM surface) to MCM area is greater than 20%. Therefore MCM can transmit signals with frequency higher than 100 MHz. There are three kinds of MCM technology:

- MCM-D, where interconnections are formed in a similar manner as in thin-film circuits, i.e. by depositing alternate layers of conductors and dielectrics onto an underlying substrate,
- MCM-L, where multilayer structures are formed by lamination of printed circuit board materials with etched patterns in copper foils and metalized vias,
- MCM-C, where multilayer structures are made by co-firing of ceramic or glass/ceramic tapes, similar to thick-film process. This means that vias are punched in green tapes and then filled with conductive electronic paste. The individual layers are screen-printed to create desired metallization patterns. Several such prepared tapes are laminated at elevated temperature and then co-fired at proper temperature to form a monolithic structure.

Modern MCM substrates consist not only interconnections but also many integral (embedded) passives. In this manner they fulfill the demands for the next generation of packaging needs. For example, integral passives significantly reduce inherent parasitics connected with the current discrete passive packages.

This paper concentrates on author and his co-workers activity in the area of thick-film and LTCC passives.

2. Fabrication of thick-film and LTCC fine lines

In thick-film and LTCC technologies screen-printing is the most reliable and cost-effective process for film deposition on tape or ceramic substrates. The standard screen-printing resolution (line width and line-to-line space) is equal to 100-125 μm /9/. The fine line print resolution is limited both by ink rheology as well as by screen properties (mesh size, wire thickness, calendaring and angle of the screen fabric in the frame) and the current achievable print resolution is about 50 μm for curved structures and 30-40 μm for straight lines /10,11/.

There are also other techniques developed for deposition of fine lines - in general they are based on printing processes, like printing through etched solid metal masks, offset printing (eg. gravure-offset printing /12/, where as narrow as 25 μm wide conductors have been printed), stamping or pad printing.

Next techniques are based on combination of standard screen-printing with photolithography. This attempt is present in photosensitive inks, where pattern is defined after film drying /13,14/ – this method enables to produce fine lines narrower than 20 μm in the case of Hibridas-like materials. Also standard screen-printing can be connected with photoetching, where patterns are defined after firing of the layer. There are also tests with diffusion patterning /15/ or nanoinprint technologies /16/.

There are also a group of methods involves the deposition of thick-films by capillary action from a precious stylus (nozzle) that also serves as the ink reservoir. Three methods are used to deposit inks through the writing orifice:

- Hydraulic positive displacement pumping synchronized with substrate stage motion (direct write printing) where standard inks can be applied,
- Non-contact electrostatic thick-film printing where ink is ejected by a high electrostatic field applied between the nozzle and the substrate,
- Drop-on-demand ink-jet printing, in which drop-lets of ink are jetted from small aperture directly to a specified position by application of a voltage pulse to a piezoelectric material that is coupled directly or indirectly to the printed fluid; typically drop-on-demand systems are able to produce droplets of diameter between 25 and 100 μm /17/; the ink-jet process made it possible to metalize fine lines with line/space = 30/30 μm /10/.

Investigation of author and his PhD and MSc students in this area /18,19/ was devoted to preparation of set-ups for exposure and development of miniature photoimageable thick films, self-building of apparatus for deposition of thick-film with the usage of ink-jet technique, elaboration of technology of stamping and geometrical characterization of lines obtained in these techniques and set-ups. Our Fodel made lines had minimal width of about 50 μm, ink-jet printed lines – 90 μm and stamped lines – 80 μm. Examples of stamped 80 μm lines are shown in Fig. 1.

4. Laser-shaped micropassives

Many laser applications, especially related to complete microcircuit size reduction and packaging density increase are reported in the literature (please see eg. /20-24/). This chapter presents the systematic studies of fabrication as well as geometrical, electrical and stability properties of thick-film or LTCC micro-resistors, microcapacitors and microinductors made with the aid of laser-shaping.

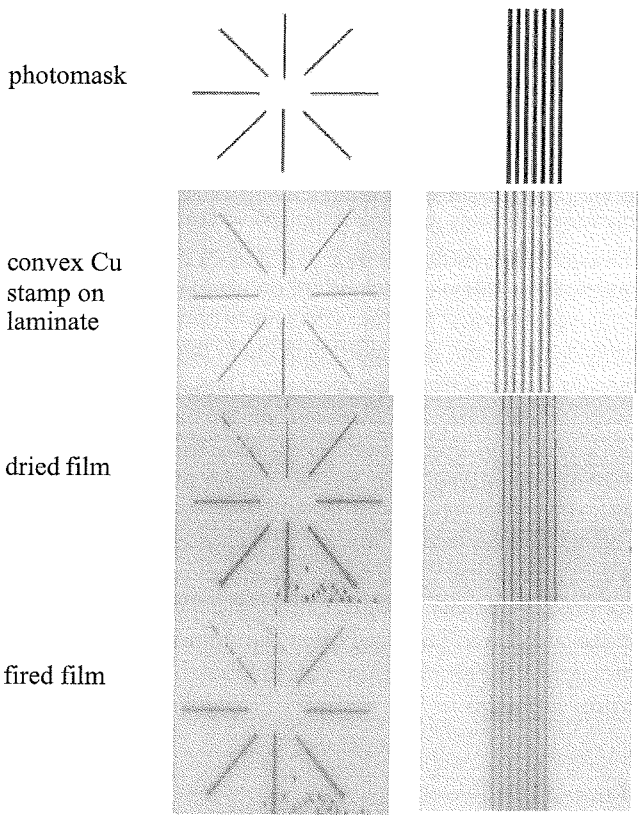

Fig. 1. Quality of 80 μm PdAg lines made by stamping method with the aid of convex Cu stamp

Micropassives were patterned by means of three lasers:

- Nd:YAG laser - arc lamp pumped Nd:YAG (cur-rent industrial standard in LTCC and thick-film technology); the Aurel NAVS-30 Laser Trimming and Cutting System (Aurel, Italy) with pulse Nd:YAG laser (1064 nm wavelength) and special software was used,
- frequency-tripled Nd:YAG laser (third harmonic generated with two extra-cavity LBO-crystals, beam length of 355 nm) - Microline 350L laser system (LPKF, Germany) equipped with an arc lamp pumped Nd:YAG-laser with Q-switching; the resulting beam is guided by two galvanoscan-ners on a *f*-Θ lens; the typical repeating precision of the *x-y*-stage was 1 μm and typical laser spot velocity on the surface between 1 and 400 mm/s,
- KrF excimer laser - LPX 210 Lambda Physik model, wavelength λ = 248 nm, 30 μm laserspot diameter on the surface, repetition rate - 200 Hz, energy density on the surface - 40 J/cm^2, shaping by scanning with 1 pulse per μm.

The laser parameters in every case depend on patterned material. In case of fired thick-film conductive layers relatively low energy laser beam is needed to avoid injury of the substrate.

4.1. Thick-film and LTCC microresistors /21, 25-27/

Laser-shaped microresistors were made on alumina (96% Al_2O_3) or LTCC (DP 951 tape from DuPont) substrates. The distance between electrodes, i.e. proper resistor length, was created by laser cutting of conductive films. Nd:YAG laser was used for cutting of dried conductors and because of various behavior of cut films during firing, the real notch width was dependent on conductor metallurgy. The spaces equal to 109, 120 and 96 μm have been received for 80 mm designed distance in the case of PdAg-, Au- or Ag-based films, respectively. These differences between particular conductors are larger than for laser cut performed on fired ones. Therefore frequency-tripled Nd:YAG laser was used for fabrication of microresistors with regulated length (30 to 300 μm), created by laser cutting of fired PdAg-, Au- or Ag-based conductive films (Fig. 2). Next DP 2021 (100 ohm/sq.) or DP 2041 (10 kohm/sq.) ink was screen-printed and fired. To compare these structures standard ones the screen-printed resistors with 300 to 1800 μm length were prepared on the same substrate.

Microresistors with constant length and regulated width down to 30 μm were made by proper cutting of 1×1 mm^2 fired resistors (Fig. 2) - this shaping method permits to eliminate conductor distance beyond resistor width.

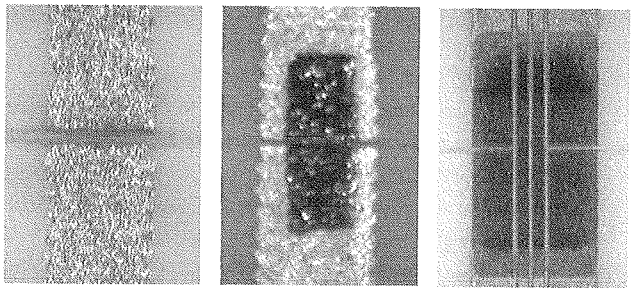

Fig. 2. Conductive path with laser made gap, gap filled with screen-printed resistive ink and top view of resistors with regulated width

Laser profilometer was used for three-dimensional characterization of investigated structures. A typical cross-section profile is shown in Fig. 3. The thickness of resistive film is not identical at every point. The mean thickness of these films is about 10 μm, both on alumina and LTCC substrates. The depth of laser kerf is dependent on scribed material and kind of substrate - the same pulse energy of laser gives much deeper notches in LTCC substrates in comparison with alumina ones. Moreover it is much more difficult to cut fired conductive films than resistive ones.

Example of sheet resistance (R_{sq}) versus resistor length dependences is shown in Fig. 4. The sheet resistance is increased with resistor length. The increase level is dependent on kind of resistive film. Resistors with regulated width exhibit hot temperature coefficient of resistance (HTCR) practically independent of their width (Fig. 5).

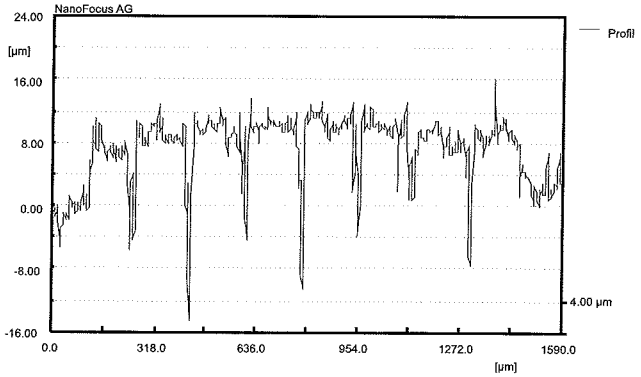

Fig. 3. Profile through six 800x170 μm^2 laser-shaped resistors (DP2031/LTCC substrate)

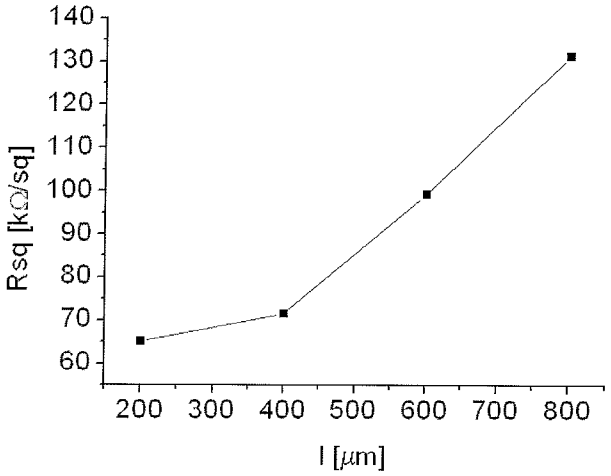

Fig. 4. Sheet resistance of R8951/Al_2O_3 resistors vs. resistor length

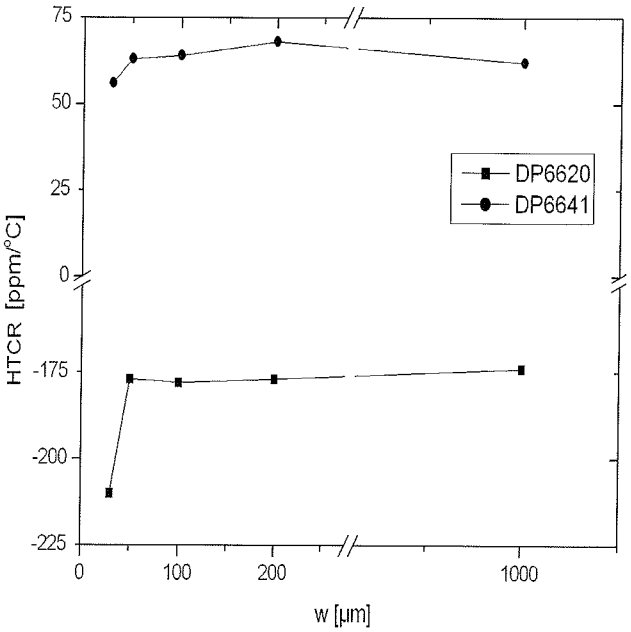

Fig. 5. HTCR as a function of resistor width

Long-term stability was characterized based on resistance drift induced by long-term thermal ageing at three different temperatures- 150°C, 200°C and 250°C. The samples

were kept at every temperature for about 300 hours. Some examples of fractional resistance changes are shown in Fig. 6. Insignificant resistance changes are observed in general. Resistors with Au-based terminations have better stability as those with Ag- or PdAg-based contact layers. Longer and wider resistors exhibit smaller resistance drift. This means that ageing processes within resistor volume give smaller fractional resistance changes than those appearing at the resistor/conductor interface. Screen-printed resistors exhibit similar stability level under the same ageing conditions /28,29/. This suggests that laser affected zone, appearing during shaping, is very small and can be neglected during analysis of electrical and stability properties for structures with resistor width larger than 150 µm.

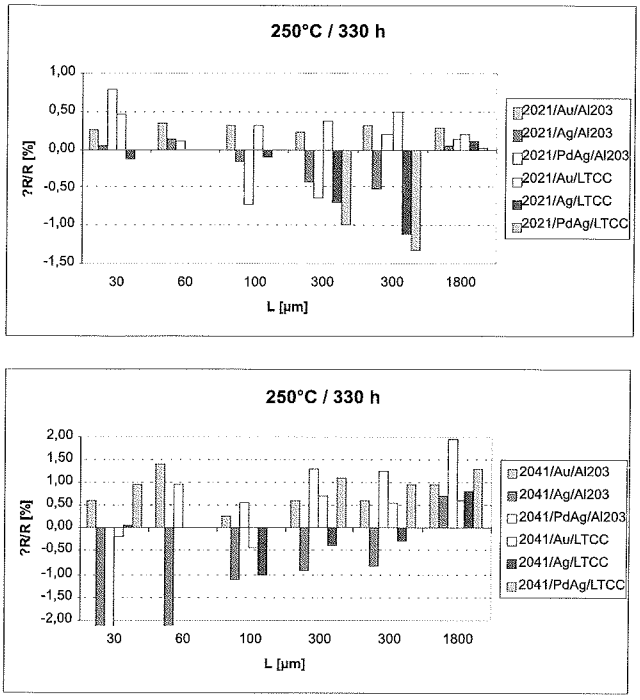

Fig. 6. Long-term stability of laser-shaped microresistors - resistive ink DP 2021 (top) and DP 2041 (bottom)

4.2. Thick-film and LTCC microcapacitors /30,31/

Capacitance density of thick-film components ranges from few pF/mm^2 up to few nF/mm^2. This is a result of relatively large thickness of dielectric layer - it must be printed at least twice for prevention from shorts. Thus, considering area occupied, only small and medium capacitances are achievable in thick-film technology. Multilayer LTCC structures allow circuit integration and miniaturization. But LTCC process differs from typical thick-film one, what results in significant difference of component properties.

Below fabrication and electrical as well as stability characterization of 2.5×2.5 mm^2 comb laser-shaped planar capacitors (Fig. 7) is presented. Basic electrical properties of components were measured as a function of frequency and temperature. Two dielectric inks - ESL4164 (K = 250) and DP5674 (K = 50÷80) were used. PdAg-based ESL963 and DP6146 conductive inks served for electrodes. Moreover Ag-based ESL9912-A conductive ink was applied in combination with both dielectrics for surface capacitors. Each capacitor layer on alumina and post-fired LTCC substrate was fired at standard 850°C/60 min. profile after printing. Two prints were used for all capacitors except buried planar ones.

Finger electrodes (50/50 and 75/75 µm line/space) were formed by Nd:YAG frequency-tripled laser. In addition standard Nd:YAG laser was used to cut 120/80 µm electrodes in dried conductive inks both for surface and buried capacitors.

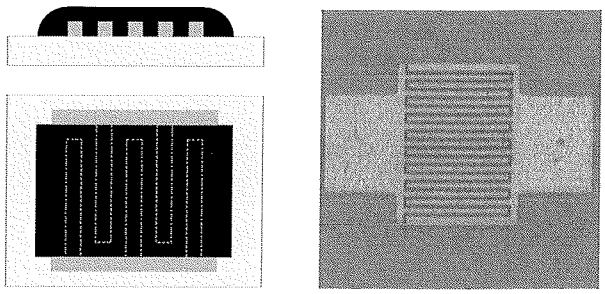

Fig. 7. Planar comb capacitor configuration

The frequency (1 kHz÷30 MHz i.e. from acoustic to UHF frequency range) and temperature (25°C÷145°C) characteristics of comb capacitors were measured and analyzed. Some examples of capacitance versus frequency characteristics (compared with fitting results) are shown in Fig. 8.

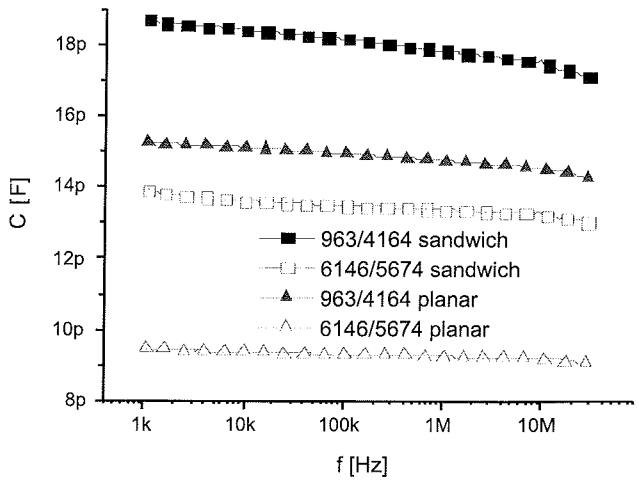

Fig. 8. Capacitance vs. frequency (sandwich buried 0.5×0.5 mm^2 capacitors and comb planar ones, LTCC substrate)

4.3. Thick-film and LTCC microinductors /32,33/

Modern circuits operate at higher and higher frequencies. Therefore inductors are used more frequently. Such thick-film passives also can be laser-shaped. Air-cored, one-side

ferrite covered and planar inductors with conductive tracks (silver ink ESL 9912-A with 14-16 μm thickness) embedded in ferrite material (Fig. 9) in three different shapes (meander inductors with 100 μm conductor width/50 μm conductor spacing, and square spiral ones with 100 μm conductor width/50 μm conductor spacing or 50 μm width/50 μm spacing) were designed and laser-shaped (by frequency-tripled Nd:YAG laser). Next their elect-rical and stability properties were investigated. The inductors of meander form consist of 17 sections whereas those of rectangular form of 5 (for 100 μm track width/50 μm spacing) or 8 turns (for 50 μm track width/50 μm spacing). The size of the fabricated inductors was about 2.5x2.5 mm^2.

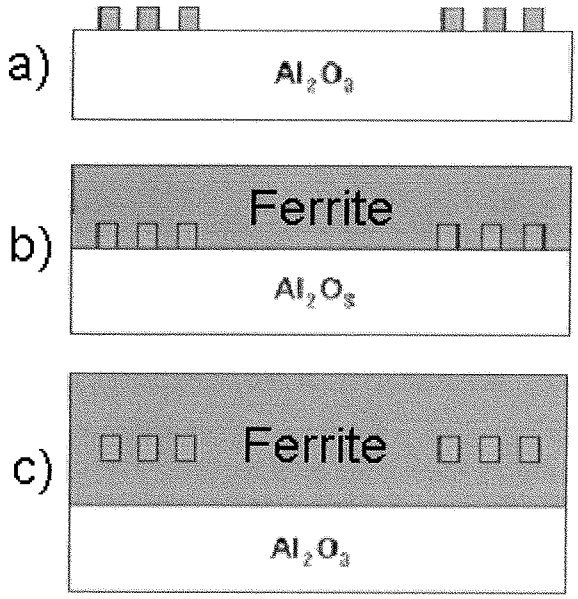

Fig. 9. Schematic cross-sections of realized inductors

Next ferrite layer, based on ESL 40011 magnetic tape /34/, was prepared in the following way - the organic medium was removed from the magnetic tape by firing at 550°C, the remaining part was thoroughly powdered and mixed with typical ethylcellulose-terpineol binder to obtain an appropriate thick-film ink. This ink was screen-printed below or onto planar inductors through proper screen and fired in 850°C/60 min cycle.

Inductance, resistance and quality factor, Q_L were determined in a wide frequency (10 kHz - 110 MHz) and temperature (20°C - 250°C) range and analyzed as a function of inductor geometry (shape and width of conductive tracks) and presence/absence of magnetic core. The stability properties, i.e. fractional inductance and resistance changes after long-term thermal ageing at elevated temperature (150°C and/or 250°C, 250 hours each) were also investigated and analyzed.

The inductances of structures with ferrite layer were from the range 29-31 nH for 100/50 μm meander inductors, 91-102 nH for 100/50 μm and 179-232 nH for 50/50 μm spiral square inductors. The inductances of air-cored inductors were from the range 10-13 nH for 100/50 μm meander inductors, 55-60 nH for 100/50 μm and 137-143 nH for 50/50 μm spiral square inductors This means that the inductance is increased for 1.6-2.9 times for one-side ferrite covered inductors (Fig. 10).

Ag-based spiral square inductors have the quality factor $Q_L = \omega L/R$ from the range 15 to 18 at 90 MHz frequency, independently on kind of substrate. However *Q*-factor of inductors with ferrite layer becomes lower in higher frequencies (about 1.5 - 5.3 for 90 MHz) than for air-cored coils. It might be caused by loses of magnetic field energy for induction of eddy currents in ferrite.

The stability properties, which are not analyzed too often for such components, i.e. fractional inductance and resistance changes after long-term thermal ageing at elevated temperature (150°C and/or 250°C, 250 hours each) were also investigated. The inductors are very stable - long-term thermal ageing did not change inductance level and caused only small resistance increase in the whole frequency range - this is con-nected with good temperature stability of applied thick-film conductors (Fig. 11). Therefore ageing pro-cess practically do not affect $Q_L = f(\omega)$ dependence.

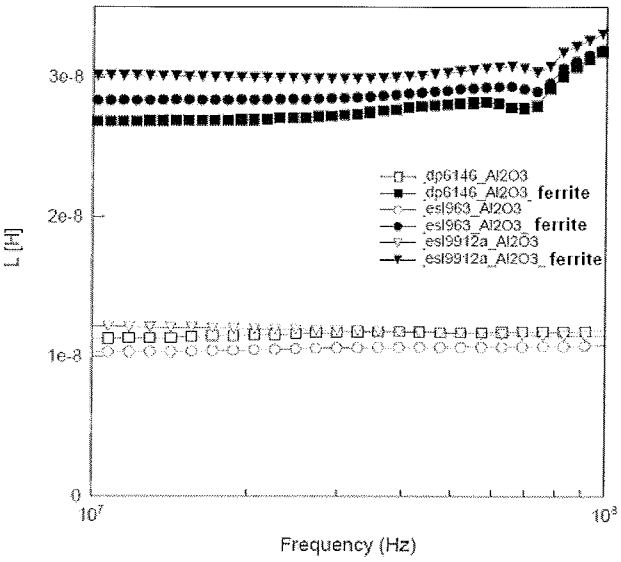

Fig. 10. Inductance vs. *frequency for meander air-cored and with ferrite layer inductors on alumina substrates*

The impedance spectra of inductors with ferrite core were also measured in temperature range from 30 to 210°C. As is shown in Fig. 12 decrease of inductance in higher temperature was observed. At temperature above 180°C the value of inductance is almost the same as for air-cored structures. This indicates that the Curie point (temperature above which core loses its characteristic ferromagnetic ability) was crossed. Parasitic resistance proves typical for metals linear increase with temperature - is a strong function of temperature and is slightly affected by thermal ageing.

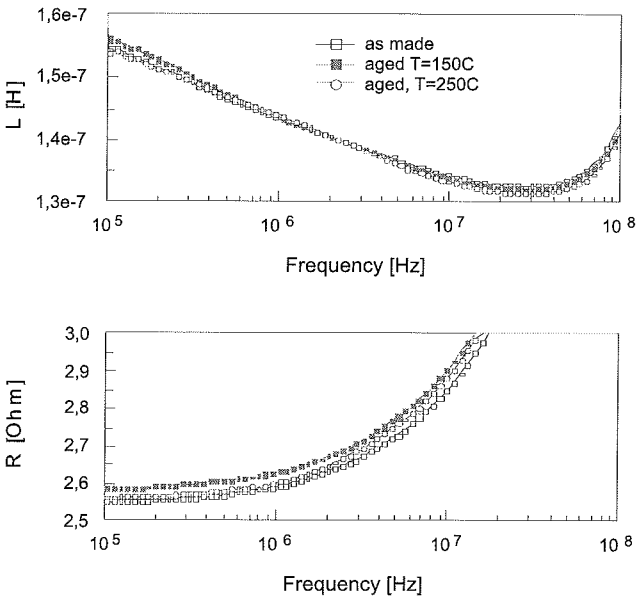

Fig. 11. Behavior of inductance and parasitic series resistance of Ag-based thick-film inductors after long-term thermal ageing

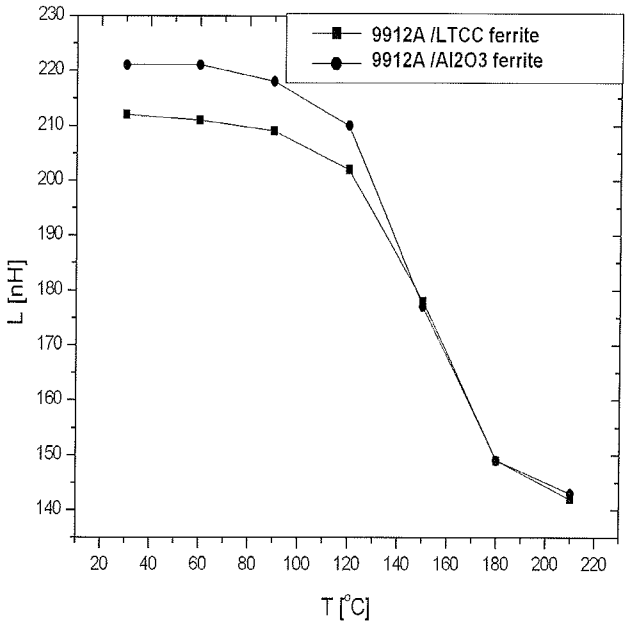

Fig. 12. Inductance vs. temperature for Ag-based square inductors with ferrite layer on different substrates

5 Fodel microresistors

So far various photosensitive conductor and dielectric inks are commercially available. But such resistive compositions are still only at the research and development stage. For example Du Pont mentioned about Fodel photopatternable resistive inks /35/. We investigated the fabrication and preliminary electrical characterization of microresistors made of experimental DP E-93350-153 (1 kohm/sq.) Fodel resistive ink (based on RuO_2) and Ag-based DP6453 Fodel conductor, both from Du Pont. Screen-printed or fully photopatternable test resistors with designed dimensions from 50x50 to 800x200 μm^2 were made and tested. Results related with geometrical, electrical and stability properties of microresistors were described in /28,36,37/. During examinations the following were found:

- The 3D geometry of microcomponents is strongly affected by applied fabrication method. The screen-printed resistors are wider whereas the Fodel one - narrower than designed. To obtain assumed planar dimensions the technological offset should be included into the design procedure. Moreover microresistors made in Fodel process have much smoother surface.
- Microresistors made in full Fodel process exhibit weaker dependence of sheet resistance on resistor length and better long-term stability.
- In spite of significantly reduced dimensions (even down to 50x50 μm^2) the R(T) characteristics of microresistors are typical for thick-film resistors with resistance minimum at certain temperature. The minimum shifts towards lower temperatures when the resistor aspect ratio is decreased.
- Much better reproducibility of this technology leads also to much better pulse behavior of Fodel microresistors (increase of critical electrical field and surface power density approximately by 20-30% in comparison with standard ones).
- The long-term stability of 200x200 μm^2 Fodel microresistors was similar to typical thick-film resistors. The 100x100 and 50x50 μm^2 microresistors exhibited somewhat worse long-term stability (after 500 h ageing at 150°C the resistance increased by about 1.0 - 1.5%).

Probably the problems with long-term stability were the reason that Fodel resistive system was not commercialized and photosensitive resistive inks are still at the research and development stage in laboratories of ink manufacturers.

6 Microvaristors

ZnO-based varistors are widely used for overvoltage protection of electronic circuits. High firing tempe-rature (1150°C÷1300°C) has to be applied in order to obtain satisfactory nonlinearity properties of such devices. However recently various thick-film varistor ceramics and structures possessing nonlinearity coefficient from the range 20-35, but fabricated in the temperature range between 850°C and 1000°C, were presented /38-45/.

Our varistor ink was prepared from ZnO-based powder consisting of ZnO (97.54 mol.%) and such additives as $BaBiO_3$ (0.7 mol.%), $Bi_4Ti_3O_{12}$ (0.16 mol.%), Sb_2O_3 (0.125 mol.%), MnO_2 (0.125 mol.%), NiO (0.5 mol.%), Cr_2O_3 (0.5 mol.%), and Co_3O_4 (0.35 mol.%). Next 1 wt% of Bi_2O_3

was added to improve sintering process of such ink /12/. Three conductive inks - DP6146 (PdAg), DP9894 (Pt) and ESL8880-H (Au) - were used for electrodes. Alumina and fired LTCC tape (DP951) served as substrates. Two varistor configurations were designed - planar with finger-like electrodes with 0.25 mm spacing and 2 mm wide varistor layer and sandwich one (with dimensions of 0.5×0.5 or 2×2 mm^2 - Fig. 13).

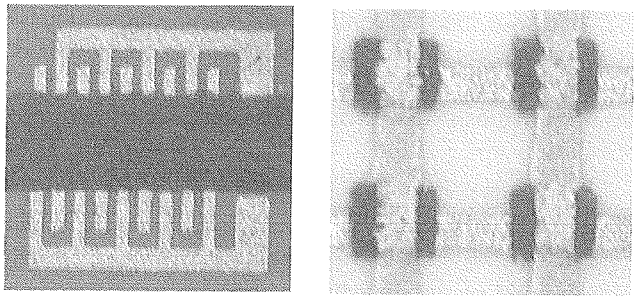

Fig. 13. Planar and sandwich varistor configuration

I-V characteristics of varistors were measured with pulse generator (0.1 ms pulses duration, 1 s interval). Obtained curves were fitted using $I = kV^{\alpha}$ formula and the nonlinearity coefficient α and characteristic voltage V_{1mA} were calculated (Fig. 14).

Electrical properties of varistors were significantly dependent on technology. The strongest factor was electrode material. Nonlinearity coefficient α in the range of 9÷23 was obtained for Pt terminations, 3÷8 for PdAg and 3÷11 for Au ones. Structures on LTCC substrate exhibited higher nonlinearity in comparison with those on alumina, especially in the case of Pt metallurgy. Moreover platinum terminations made *a* dependent on firing profile; in the case of Au and PdAg electrodes nonlinearity changed weakly. In general sandwich varistors showed higher α. The distribution of *a* values was about 25% for sandwich varistors and 10% for planar ones.

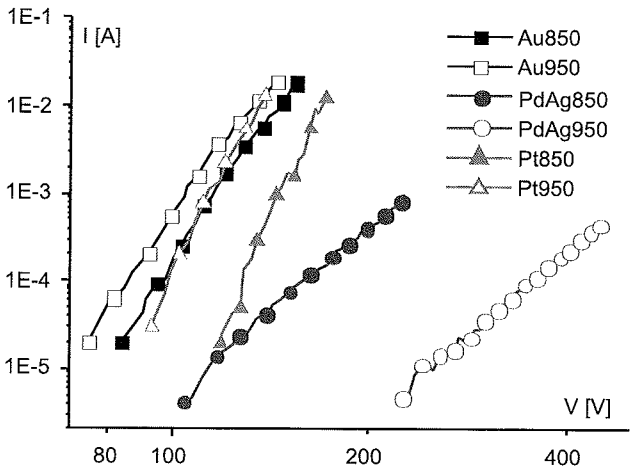

Fig. 14. I-V characteristics of planar varistors on LTCC substrate

Wide range of characteristic voltage, V_{1mA} (10÷200 V for sandwich varistors and 100÷460 V for planar ones), strongly affected by electrode metallurgy, was obtained. Its value was weakly correlated with *a*.

The stability of thick-film and LTCC varistors is not described yet. This is why we decided to characterize long-term thermal and electrical ageing and pulse durability of such devices.

Varistors were thermally aged at 150°C for 250 h. Examples of their *I-V* characteristics, measured before and after ageing, are shown in Fig. 15.

Generally thermal ageing slightly deteriorated varistors properties - small decrease in *a* and 10÷15% decrease in V_{1mA} was observed in most cases.

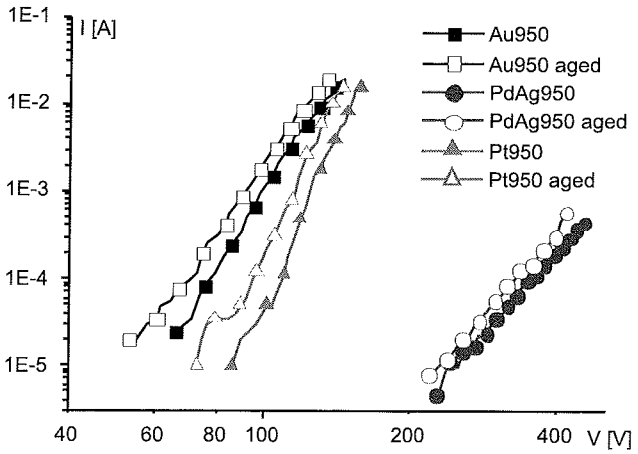

Fig. 15. I-V characteristics of planar varistors on LTCC substrate fired at 950°C before and after ageing

Sandwich varistors with easy solderable PdAg electrodes were chosen for long-term electrical ageing. They were loaded with 100 µA current for 250 h at room temperature. Varistors made on alumina practically were not affected by electrical load. Also α value for LTCC components remained unchanged. Only their *I-V* characteristics shifted toward lower voltages. Changes were in the range from a few to about 40 V.

Durability of varistors to high voltage pulses was also investigated. Components were subjected to series of 1000 pulses with 10 mA amplitude and 5 ms duration each. Test was done at room temperature. Examples of changes in I-V characteristics for as-fired and pulse exposed varistors are shown in Fig. 16. Varistors showed good durability. Generally small drop in α were found, although in some cases its value remained the same or even increased. V_{1mA} changes were very small, either positive or negative. Structures with Au electrodes were the most reliable, no breaks during test occurred.

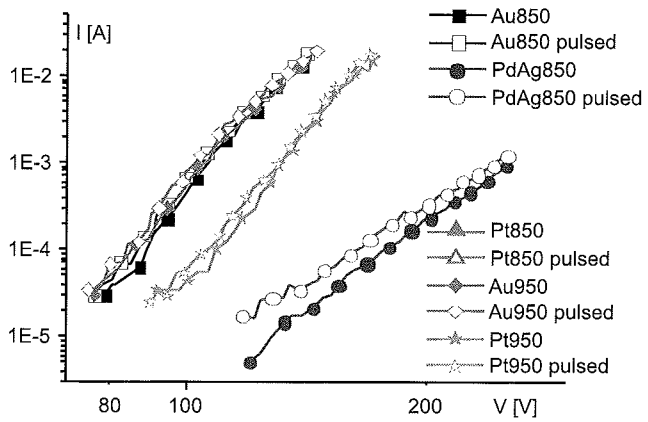

Fig. 16. I-V characteristics of planar varistors on LTCC substrate before and after exposure

Acknowledgments

This work was supported by Wroclaw University of Technology, Grant 343 578 W-12 - statutory research activity

References

/1/ Fundamentals of Microsystems Packaging, Edited by R.R. Tummala, McGraw-Hill, 2001

/2/ L.J. Golonka, K.-J. Wolter, A. Dziedzic, J. Kita, L. Rebenklau; Embedded passive components for MCM, Proc. 24th Int. Spring Seminar on Electronics Technology, Calimanesti-Caciulata (Romania), 2001, p.73-77

/3/ A. Dziedzic, Electrical and structural invest-tigations in reliability characterisation of modern passives and passive integrated components, Microelectron. Reliab., vol.42 (2002), p.709-719

/4/ Integrated Passive Component Technology, Edited by R.K. Ulrich and L.W. Schaper, Wiley Inter-science, 2003

/5/ R.C. Frye, Passive components in electronic applications; requirements and prospects for integration, Int. J. Microelectronics and Electronics Packaging, vol.19 (1996), p.483-489

/6/ R. Lasky, Growth continues for passive components, Electronic Packaging and Production, March 1998, p.77-78

/7/ Electronic Packaging and Interconnection Handbook, Edited by C.A. Harper, McGraw-Hill, 2000

/8/ T.P. Gupta, Handbook of Thick- and Thin-Film Hybrid Microelectronics, Wiley Interscience, 2003

/9/ A. Dziedzic, J. Nijs, J. Szlufcik, Thick-film fine-line fabrication techniques - application to front metallization of solar cells, Hybrid Circuits, No. 30 (Jan. 1993), p. 18-22, 26

/10/ A. Albertsen, K. Koiwai, K. Kobayashi, T. Oguchi, K. Aruga, Combined manufacture met-hods for high density LTCC substrates: thick film screen printing, ink jet, postfiring thin film pro-cesses, and laser-drilled fine vias, J. Microelectro-nics and Electronic Packaging, vol.6 (2009), p.6-12

/11/ D. Schwanke, J. Pohlner, A. Wonisch, T. Kraft, J. Geng, Enhancement of fine line print resolution due to coating of screen fabrics, J. Microelectro-nics and Electronic Packaging, vol.6 (2009), p.13-19

/12/ M. Lahti, S. Leppavuori, V. Lantto, Gravure-offset-printing technique for the fabrication of solid films, Applied Surface Science, vol.142 (1999), p.367-370

/13/ B. Dziurdzia, S. Nowak, M. Ciez, W. Gregorczyk, H. Thust, E. Polzer, Low cost high performance microwave structures fabricated by advanced thick film technologies, Microelectronics Int., vol.16 no.3 (Sept. 1999), p.46-53

/14/ J. Minalgiene, V. Baltrusaitis, Photoimageable thick film implementation of very high density ceramics technology products, Proc. 39th IMAPS Nordic Conf., Stockholm, 2002, p. 233-242

/15/ D. Belavic, M. Hrovat, M. Pavlin, J. Holc, Some results obtained with diffusion patterning techno-logy, Microelectronics Int., vol.18 no.1 (Jan. 2001), p.7-18

/16/ P. Carlberg, Development of nanoimprint litho-graphy for applications in electronics, photonics and life science, PhD thesis, Lund University (Sweden), 2006

/17/ J.B. Szczech, C.M. Megaridis, D.R. Gamota, J. Zhang, Fine-line conductor manufacturing using drop-on-demand PZT painting technology, IEEE Trans. on. Electronic Packaging Manufacturing, vol.25 (2002), p.26-33

/18/ P. Markowski, Thermoelectric properties of thick-film composites, PhD Thesis, Wroclaw University of Technology, 2009

/19/ MSc theses of W. Bobrowski (2007), M. Wojtaszczyk (2007), M. Bugajny (2008), P. Kacperczyk (2008), T. Józenków (2009), Ł. Kaźmierczak and G. Zięba (2009) - supervisor A. Dziedzic

/20/ J.H. Lau, C. Chang, An overview of microvia technology, Circuit World, vol.26 no.1 (2000), p.22-32

/21/ J. Kita, A. Dziedzic, L. Golonka, Nonconven-tional application of laser in LTCC and thick-film technology - preliminary results, Proc. 23rd Int. Spring Seminar on Electronics Technology, Balatonfured (Hungary), 2000, p.219-224

/22/ Z. Illyefalvi-Viteez, Laser processing for micro-electronics packaging applications, Microelectron. Reliab., vol.41 (2002), p.563-570

/23/ K.-H. Drue, Precise drilling and structuring of LTCC materials using a 355 nm YAG-laser, Proc. Eur. Microelectronics and Packaging Conf., Brugge (Belgium), 2005, p.410-415

/24/ J. Borecki, H. Hackiewicz, G. Kozioł, W. Falin-ski, UV laser microvias formation in build-up glass fiber prepeg, Proc. 3rd Eur. Microelectronics and Packaging Symp., Prague, 2004, p.571-576

/25/ E. Miś, M. Borucki, A. Dziedzic, S. Kaminski, L. Rebenklau, K.-J. Wolter, F. Sonntag, Laser-shaped thick-film and LTCC microresistors, Proc. 1st Eur. Systemintegration Technology Conf., Dresden, 2006, p.954-96

/26/ D. Nowak, T. Jozenków, A. Dziedzic, J. Kita, Miniaturization of thick-film and LTCC resistors by laser-shaping, Proc. 32nd Int. Conf. IMAPS-CPMT Poland 2008, Pułtusk (Poland), 2008, 5 p.

/27/ D. Nowak, E. Miś, A. Dziedzic, J. Kita, Fabrication and electrical properties of laser-shaped thick-film and LTCC microresistors, Microelectron. Reliab., vol.49 (2009), p.600-606

/28/ A. Dziedzic, L. Rebenklau, L. Golonka, K.-J. Wolter, Fodel microresistors - processing and basic electrical properties, Microelectron. Reliab., vol.43 (2003), p.377-383

/29/ A. Dziedzic, A. Kolek, A. Ehrhardt, H. Thust, Advanced electrical and stability characterization of untrimmed and variously trimmed thick-film and LTCC resistors, Microelectron. Reliab., vol.46 (2006), p.352-359

/30/ E. Miś, A. Dziedzic, T. Piasecki, J. Kita, R. Moos, Geometrical, electrical and stability proper-ties of thick-film and LTCC microcapacitors, Microelectronics Int., vol.25 no.2 (2008), p.37-41

/31/ E. Miś, A. Dziedzic, K. Nitsch, Electrical proper-ties and electrical equivalent models of thick-film and LTCC microcapacitors, Microelectronics Int., vol.26 no.2 (May 2009), p.45-50

/32/ M. Bąk, M. Dudek, A. Dziedzic, J. Kita, Chosen electrical and stability properties of laser-shaped thick-film and LTCC inductors, Proc. 2nd Eur. Systemintegration Technology Conf., London-Greenwich, 2008, vol. 1, p.101-103

/33/ D. Nowak, T. Piasecki, A. Dziedzic, Influence of ferrite layer on electrical and stability properties of laser-shaped thick-film and LTCC inductors, Proc. 32nd Int. Conference of IMAPS-CPMT Poland 2008, Pułtusk (Poland) 2008, 5 p.

/34/ ESL 40011 Magnetic Tape - *www.electroscience.com*

/35/ Y.L. Weng, P.J. Ollivier, M.A. Skurski, Photoformed thick film materials and their application to fine feature circuitry, Proc. 2000 Int. Conf. on High-Density Interconnect and System Packaging, Denver 2000, p.579-584

/36/ A. Dziedzic, E. Miś, L. Rebenklau, K.-J. Wolter, LTCC and Thick-Film Microresistors, Proc. 54th Electronic Components and Technology Conf., Las Vegas (USA), 2004, p.1885-1890

/37/ A. Dziedzic, E. Miś, L. Rebenklau, K.-J. Wolter, Geometrical and electrical properties of LTCC and thick-film microresistors, Microelectronics Int., vol.22, no.1 (Jan. 2005), p.26-33

/38/ H. Debeda-Hickel, C. Lucat, F. Menil, Influences of the densification parameters on screen-printed component properties, J. Eur. Ceram. Soc., vol.25 (2005), p.2115-19

/39/ M.A. de la Rubia Lopez, M. Peiteado, J.F. Fernandes, A.C. Caballero, J. Holc, S. Drnovsek, D. Kucser, S. Macek, M. Kosec, Thick film ZnO based varistors prepared by screen printing, J. Eur. Ceram. Soc., vol.26 (2006), p.2985-2989

/40/ A. Dziedzic, E. Miś, W. Mielcarek Micro-varistors for thick-film and LTCC microcircuits, Proc. 1st Electronics Systemintegration Techno-logy Conf., Dresden (Germany), 2006, p.961-965

/41/ E. Miś, A. Dziedzic, W. Mielcarek Thick-film and LTCC microvaristors, Proc. 30th Int. Spring Seminar on Electronics Technology, Cluj-Napoca (Romania), 2006, p.53-58

/42/ C. Lucat, M.-P. Martin, H. Debeda-Hickel, A. Largeteau, F. Menil, Screen-printed varistors: New strategy for high non-linear coefficient, J. Eur. Ceramic Soc., vol.27 (2007), p.3883-3886

/43/ M.A. de la Rubia Lopez, M. Peiteado, J. de Frutos, F. Rubio-Marcos, J.F. Fernandes, A.C. Caballero, Improved non-linear behaviour of ZnO-based varistor thick films prepared by tape casting and screen printing, J. Eur. Ceram. Soc., vol.27 (2007), p.3887-3891

/44/ J. Honkamo, J. Hannu, H. Jantunen, M. Moilanen, W. Mielcarek, Microstructural and electrical properties of multicomponent varistor ceramics with PbO-ZnO-B_2O_3 glass addition, J. Electroceram., vol.18 (2007), p.175-181

/45/ E. Miś, A. Dziedzic, W. Mielcarek, Micro-varistors in thick-film and LTCC circuits, Microelectron. Reliab., vol.49 (2009), p.607-613

/46/ E. Olsson, G.L. Dunlop, The effect of Bi_2O_3 content on the microstructure and electrical properties of ZnO varistor materials, J. Applied Physics, vol.66 (1998), p.4317-4325

Andrzej Dziedzic
Faculty of Microsystem Electronics and Photonics,
Wroclaw University of Technology, Wybrzeze
Wyspianskiego 27, 50-370 Wroclaw, Poland,
andrzej.dziedzic@pwr.wroc.pl

Prispelo (Arrived): 15.08.2009 *Sprejeto (Accepted): 09.10.2009*

III-V MULTI-JUNCTION SOLAR CELLS - SIMULATION AND EXPERIMENTAL REALIZATION

S. P. Philipps, W. Guter, M. Steiner, E. Oliva, G. Siefer, E. Welser, B. M. George, M. Hermle, F. Dimroth, A. W. Bett

Fraunhofer Institute for Solar Energy Systems ISE, Freiburg, Germany

Key words: Multi-junction solar cells, numerical modelling, record solar cell

Abstract: III-V multi-junction solar cells are the state-of-the-art approach for high-efficiency photovoltaic energy conversion. Due to the structural complexity of these devices numerical modelling and simulation for analysis and optimization has found increasing attention in recent years. This work presents an overview of the modelling techniques for III-V multi-junction solar cells applied at the Fraunhofer Institute for Solar Energy Systems (ISE). These are in particular the detailed balance model used in the program "etaOpt", the numerical semiconductor simulation using Sentaurus TCAD from Synopsys as well as classical network simulations. Our latest modelling results, the capabilities of the different approaches as well as their limitations are discussed. In addition, a focus is set on a recent record triple-junction solar cell with an efficiency of 41.1 % at a concentration ratio of 454 suns. Its key design factors are indicated and it is shown in which aspects numerical modelling supported this development and what extensions will be needed in the future.

III-V večspojne sončne celice – simulacije in praktične izvedbe

Kjučne besede: večspojne sončne celice, rekordna sončna celica, numerično modeliranje

Izvleček: III-V večspojnespoje sončne celice so trenutno najboljši pristop za doseganje visoke učinkovitosti pretvorbe. Zaradi strukturne kompleksnosti teh celic se je v zadnjih letih izredno povečalo zanimanje za njihovo numerično modeliranje, simulacijske analize in optimizacijo.V članku je predstavljen pregled tehnik modeliranja II-V sončnih celic, ki jih uporabljajo na Fraunhofer Institute for Solar Energy Systems (ISE).Te tehnike so: ravnovesni model, ki ga uporablja program "etaOpt", numerične polprevodniške simulacije z uporabo programa Sentaurus TCAD od Synopsysa, kakor tudi klasične mrežne simulacije. Predstavljeni so naši zadnji rezultati, kakor sposobnosti in omejitve posameznih pristopov. Dodatno je v članku povdarek na trenutni rekordni trispojni sončni celici z izkoristkom 41.1 % pri koncentraciji 454 sonc. Predstavljeni so ključni dejavniki pri razvoju strukture, podpora numeričnega modeliranja in kakšne nadgradnje bodo potrebne v prihodnosti.

1 Introduction

Monolithically stacked multi-junction solar cells based on III-V semiconductor materials, such as the GaInP/GaInAs/Ge triple-junction solar cell, are the state-of-the-art approach for high-efficiency photovoltaic energy conversion. Consisting of stacked p-n junctions with different band gap energies, these devices can exploit the solar spectrum very profitably. Just recently an efficiency of 41.1% was achieved for a metamorphic $Ga_{0.35}In_{0.65}P$/ $Ga_{0.83}In_{0.17}As$/Ge triple-junction solar cell under the standard AM1.5d ASTM G173-03 spectrum and a concentration of 454 suns /1,2/.

A multi-junction solar cell structure consists of a high number of layers of different III-V compound semiconductor materials. Due to the complex electrical and optical interactions between the different layers, a pure experimental optimization of these sophisticated structures would be very expensive and protracted. An accurate and reliable modelling is desirable in order to accelerate the optimization procedure considerably.

In recent years the use of numerical modelling and simulation of III-V multi junction solar cells has found increasing attention. Different approaches and tools are in use. The following seem to be most common: Very prevalent is the evaluation of theoretical efficiencies for specific structures. A good overview of the different approaches is presented in Ref. /3/. Several groups use semiconductor simulation environments for the analysis and optimization of the semiconductor layer structure, e.g. /4-8/. For the optimization of the front contact grid, network simulations were repeatedly used, e.g. /9,10/. In addition, some specialized programs for solar cell modelling have been developed of which the most common ones - such as PC1D and AMPS - are reviewed in Ref. /11/. These programs have also been used for III-V solar cells, e.g. /12-14/. Thus, numerical modelling and simulation have become common methods in the development of III-V multi-junction solar cells.

At Fraunhofer ISE different simulation techniques are used for the analysis and optimization of III-V multi-junction solar cells. The aim of this paper is to present an overview of the three modelling approaches applied and to present our recent findings. The capabilities and limitations of the models are also discussed. Concerning the current status of the experimental realization the focus is set on a recent highlight, which is the development of a metamorphic triple-junction solar cell with an efficiency of 41.1% /1/ under the AM1.5d ASTM G173-03 spectrum and 454 kW/m^2. It is shown in which aspects numerical modelling supported this development and what extensions will be needed in the future.

2 Numerical modelling

The parameter space for the structure optimization of III-V multi-junction solar cells is very large. In principle, the number of subcells, the layer structure and the materials in each subcell as well as the thickness and doping level of each semiconductor layer need to be determined. In addition, the front contact grid layout needs to be optimized in respect to the designated concentration and concentrating system. Obviously an experimental procedure would be very time-consuming and expensive. However, a numerical modelling tool that is able to search the whole parameter space does not yet exist. Therefore, different modelling tools are used for the analysis of the parameter space. In the III-V group at Fraunhofer ISE three different approaches are used. The optimal number of band gaps and the ideal band gap combination is evaluated with a modelling tool described in Section 2.1, which is based on the Shockley-Queisser limit. We analyze the semiconductor layer structure with the commercially available semiconductor simulation environment Sentaurus TCAD from Synopsys (see Section 2.2). Finally, the grid design is optimized with the circuit simulator LTSpice from Linear Technology Corporation /15/ described in Section 2.3.

2.1 Ideal efficiency calculation

One of the central benefits of using III-V semiconductors as material for solar cells is the wide choice of band gaps that can be experimentally realized and stacked. A valuable guidance for finding the most efficient set is the evaluation of ideal efficiencies, which could be realized without any, but the physically inevitable losses. At Fraunhofer ISE the program "etaOpt" was developed to calculate these ideal efficiencies /16/.

2.1.1 Modelling approach

The model used in "etaOpt" is based on the detailed balance method first introduced by Shockley and Queisser /17/, i.e. only radiative recombination is considered. All subcells have an external quantum efficiency (EQE) equal to one and it is assumed that photocurrent from upper subcells can be transferred to lower ones to improve current-matching. In reality this is achieved by thinning the absorbing layers.

2.1.2 Results for triple-junction solar cells

This section focuses on triple-junction solar cells as they currently have the highest efficiencies realized for terrestrial as well as for space applications. Figure 1 shows the optimal band gap combinations for triple-junction solar cells under the extraterrestrial AM0 spectrum (1367 W/m^2, 298 K) as well as under the terrestrial AM1.5d ASTM G173-03 spectrum with a concentration ratio of 500 suns (500 kW/m^2, 298 K). Optimal band gap combinations with efficiencies above 48% (AM0) or 60.5% (AM1.5d) are marked with black dots, while the grey dots represent structures with efficiencies of 48 to 49% and 59.0 to 60.5% respectively. Due to the homogeneous extraterrestrial AM0 spectrum, a large compound field of optimal band gap combinations is formed, whereas the absorption band of atmospheric water and carbon dioxide lead to the formation of two local maxima under AM1.5d.

The band gap combinations of five specific triple-junction solar cell structures, for which efficiencies of over 40% under the concentrated AM1.5d spectrum have already been experimentally realized, are indicated: lattice-matched $Ga_{0.5}In_{0.5}P$/ $Ga_{0.99}In_{0.01}As$/Ge (LM) /18-20/; metamorphic $Ga_{0.44}In_{0.56}P$/$Ga_{0.92}In_{0.08}As$/Ge (MM1) /18/; metamorphic $Ga_{0.35}In_{0.65}P$/$Ga_{0.83}In_{0.17}As$/Ge (MM2) /1/; inverted metamorphic $Ga_{0.5}In_{0.5}P$/GaAs/ $Ga_{0.73}In_{0.27}As$ (Inv1), inverted (double) metamorphic device $Ga_{0.63}In_{0.37}As$/$Ga_{0.96}In_{0.04}As$/GaAs (Inv2) /21/. A more detailed discussion of the particularities of these designs can be found in Ref. /1/.

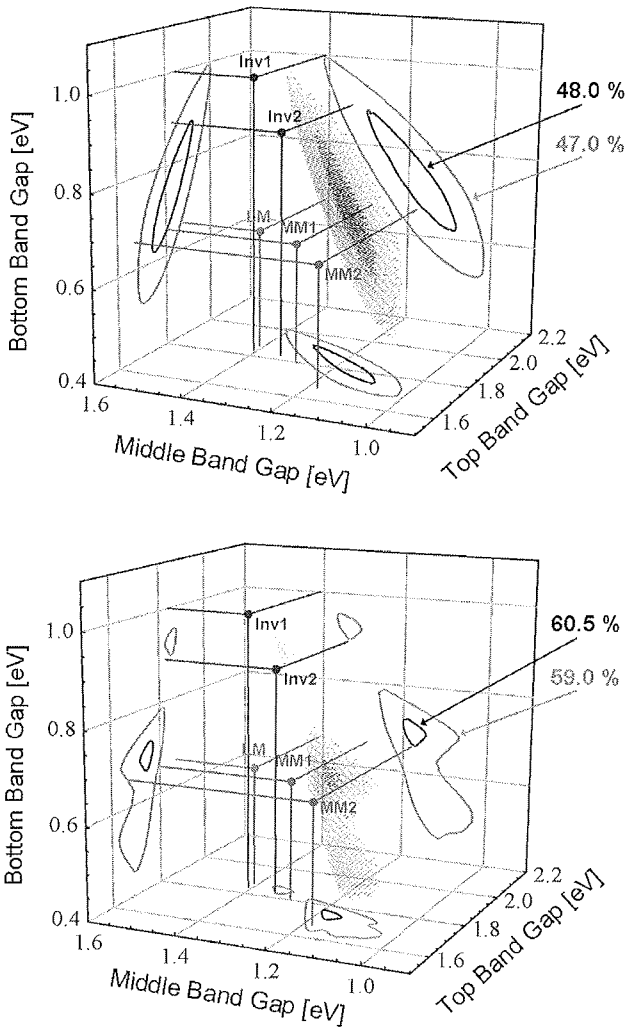

Fig. 1: Ideal efficiencies of triple-junction solar cell structures calculated with etaOpt under the AM0 (top) and the AM1.5d ASTM G173-03 spectrum with a concentration ratio of 500 suns (bottom, after Ref. /1/).

2.2 Numerical modelling of the cell structure

After the identification of the optimal band gap combinations using "etaOpt", the realistic cell structure with real material properties has to be designed. The optimization of the semiconductor layer structure is highly complex due to the high number of layers and the strong optical as well as electrical interactions between the layers. At Fraunhofer ISE the commercially available semiconductor simulation environment Sentaurus TCAD from Synopsys is used to analyze and optimize the layer structure.

2.2.1 Modelling approach

For the simulations presented here, different tools of the simulation environment Sentaurus TCAD are used. After defining the solar cell structure and meshing it with the tools Sentaurus Structure Editor and Mesh, the calculation of the optics and the electrical features are performed with the device simulator Sentaurus Device /22/.

We model the smallest two-dimensional symmetry element of the solar cell, which is constructed by a cut through the layers from cap to substrate perpendicular to the grid fingers. The element covers a width corresponding to half of the finger spacing. This ensures that series resistance effects caused by lateral current flow in the device are taken into account.

Realistic simulations with Sentaurus TCAD have two prerequisites: Firstly, the necessary models describing the occurring physical phenomena need to be implemented and validated. Of particular importance for solar cell modelling are optical interference effects, optical generation and recombination of minority carriers, carrier transport at hetero-interfaces and tunnelling effects. Secondly, material parameters such as optical constants, carrier mobilites, band gap energies, electron affinity and parameters for radiative, Auger, Shockley-Read-Hall as well as interface recombination are required for each semiconductor layer in the structure. In the following it will be shown that both prerequisites are satisfactory fulfilled for the materials used in our GaAs single-junction solar cells as well as in our lattice-matched GaInP-GaAs dual-junction solar cells. However, for other materials especially those in metamorphic III-V multi-junction solar cells the lack of material data limits the modelling capabilities.

2.2.2 Results for single-junction solar cells

In the past excellent results have been obtained for the modelling of III-V single-junction solar cells using numerical semiconductor simulation tools, e.g. /4,12,23/. Thereby, it was shown that the particular physical phenomena in III-V solar cells, such as carrier transport at hetero-interfaces as well as optical interference effects, are well described. However, the application of these relatively new models for design optimization has rarely been reported. In the following we present first optimization results for single-junction GaAs solar cells. Details about the underlying model and the material parameters can be found in Ref. /4/. Figure 2 shows a comparison between measured and simulated EQE and reflection of two GaAs solar cells with different material for the window (FSF) layer. All parameters of the solar cell except for the window layer have been identical.

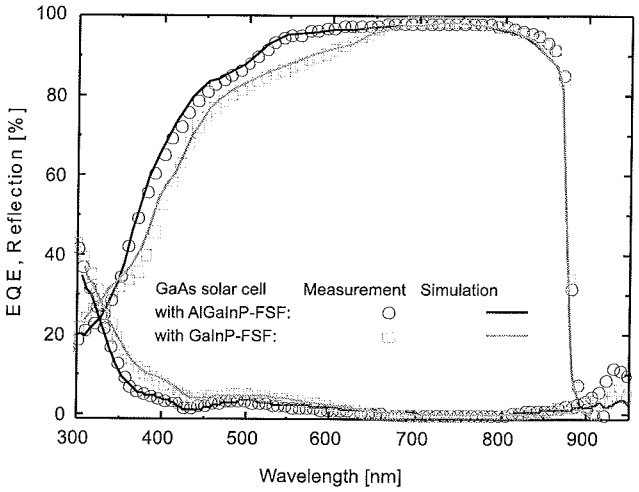

Fig. 2: Comparison between measured and simulated EQE and reflection for two GaAs solar cells with different window (FSF) layer material.

The good agreement between measurement and simulation proves the validity of the numerical model. The GaInP window layer leads to significant absorption in the short wavelength range between 300 - 650 nm and therefore reduces the EQE. This underlines the importance of a high band gap material for the window layer. After setting the material to high band gap $Al_{0.35}Ga_{0.16}In_{0.49}P$, the next task is to find the optimal window thickness and doping. Figure 3 shows based on the results of the high band gap $Al_{0.35}Ga_{0.16}In_{0.49}P$ window layer, how the efficiency of the investigated GaAs solar cell varies for different thicknesses and doping levels of the window layer. Two trends influence the optimum configuration: The window should lead to low absorption, but should also serve as a good passivation layer. The first demand favours thin window layers, whereas the second demand sets a lower boundary to the minimum thickness which is necessary for a sufficient passivation. Additionally the passivation properties are favouring high doping levels in the window material. Thus, the optimum configuration lies at high doping levels > $2x10^{18}$ cm^{-3} and a thin window layer around 20 nm.

Following a one-layer-at-a-time optimization approach, the next layer to be analyzed is the emitter. The efficiency contour plot (Figure 4) shows a plateau with quite stable efficiency values ranging from very thin but highly doped configurations to rather thick, but low doped values. The strong drop in efficiency for configurations in the upper right corner is caused by the decrease of the short-circuit current due to low diffusion lengths of the minority carriers. In contrast the drop in the lower left corner is caused by the increasing lateral sheet resistance of the emitter.

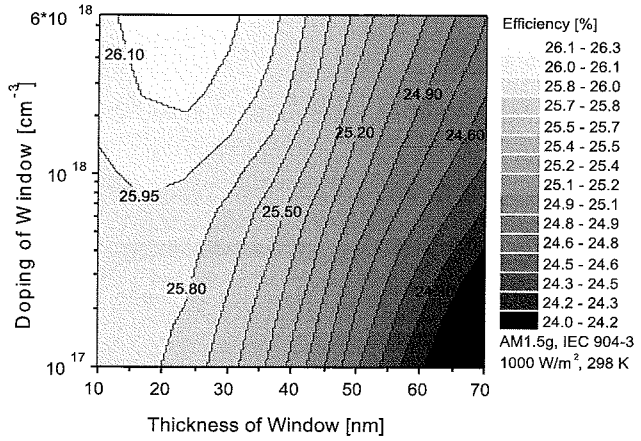

Fig. 3: Efficiency contour of a GaAs solar cell as a function of the thickness and doping level of the $Al_{0.35}Ga_{0.16}In_{0.49}P$ window layer.

These two trends are commonly observed for emitter variations. Yet, their individual strength strongly depends on the particular material parameters. The shape of the plateau is also influenced by the voltage, which shows a strong dependence on material parameters, especially on the carrier lifetime. Usually, the voltage increases with higher doping levels and lower thicknesses. However, for solar cells with very high SRH lifetime in the emitter the influence of the doping level on the open-circuit voltage can be inverted due to the increase of radiative and Auger recombination with higher doping.

It is important to note that the results of the optimization strongly depend on the material parameters of the individual cell. Of particular importance are the Shockley-Read-Hall lifetimes and the interface recombination velocities, which can vary significantly with the doping level and the growth conditions. Therefore, the results of this study are only valid for the material parameters obtained for our grown layers. It should also be mentioned that the analysis presented here uses the approach of optimizing one-layer-at-a-time, which will not necessarily lead to the global optimum for the device structure.

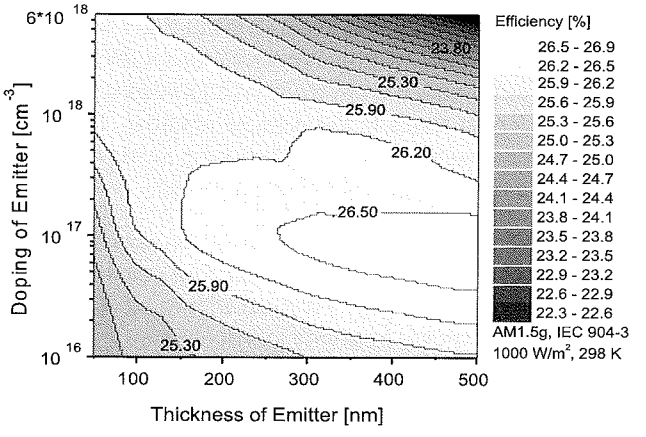

Fig. 4: Efficiency contour of a GaAs single-junction solar cell as a function of the thickness and doping level of the emitter layer.

2.2.3 Results for dual-junction solar cells

The modelling of multi-junction solar cells poses additional challenges. First, a proper and numerically stable model for the tunnel diode, which connects the subcells in series, is required. Second, the numerical complexity is highly increased due to the simultaneous computation of two or more subcells. Only few research groups have presented results on the modelling of III-V multi-junction solar cells within semiconductor simulation environments /5-8,24,25/. Recently, we presented a numerical model of a $Ga_{0.51}In_{0.49}P$-GaAs dual-junction solar cell taking into account the necessary material parameters and physical processes /8/. The theoretical modelling results were shown to be in good agreement with measurements. Figure 5 shows a comparison of the measured and simulated EQE and reflection for the investigated dual-junction solar cell.

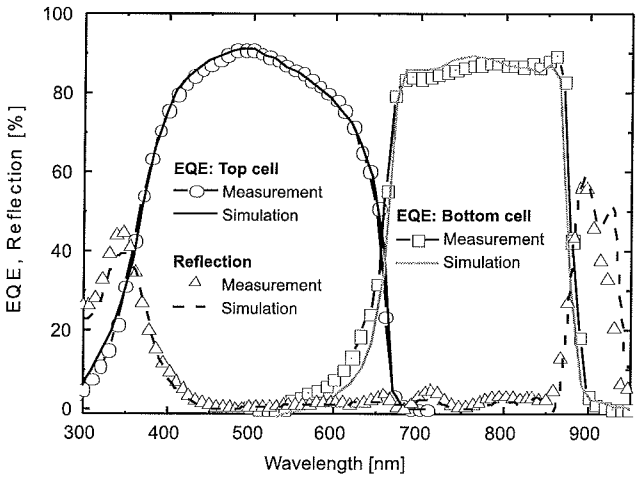

Fig. 5: Simulated and measured EQE and reflection of the investigated $Ga_{0.51}In_{0.49}P$-GaAs dual-junction solar cell agree well (after Ref. /8/).

Based on the effect of current-limitation in a series interconnected multi-junction solar cell, a special calculation method was developed to compute the quantum efficiencies of the subcells. This method follows the measurement procedure for the EQE in which appropriate bias light conditions are chosen to determine the EQE of the current limiting subcell. With the developed simulation tools specific aspects of the device behaviour can now be theoretically predicted and understood. An example is the optimization of the top and bottom cell thickness as shown in Ref. /8,25/.

2.3 Optimization of the front contact grid

As shown above, the semiconductor layer structure can be very well modelled with a two-dimensional symmetry element. Yet, for the optimization of the front contact grid such a model is not sufficient. In principle it would be possible to model and simulate a complete solar cell in all three dimensions within the Sentaurus TCAD simulation environment. However, due to the high number of mesh points necessary for a realistic model, the computational effort

would be enormous, leading to intolerable computing time of weeks or even months. Therefore, we optimize the front contact separately with an electrical network model, which will be discussed in this section.

2.3.1 Modelling approach

The IV-characteristic of a solar cell is often described with the two diode model. The lack of this model is the missing spatial distribution, thus neglecting the influence of the distributed series resistance and the perimeter effects at the solar cell surrounding. The two diode model can be enhanced by dividing the solar cell in elementary cells consisting of diodes, resistances and current sources to model the saturation currents and the photo generated current. The elementary cells are connected in parallel through ohmic resistances representing e.g. the lateral conducting emitter layer or the metal fingers. Thereby a network of electrical components is created, which describes the whole solar cell. The IV-characteristic is calculated with the circuit simulator LTSpice, which uses a SPICE (Simulation Program with Integrated Circuit Engineering) approach. More details about our network model can be found in Ref. /26/.

Compared to the modelling approach described in Section 2.2 a network model requires more integral parameters such as the short-circuit current density, the resistances of emitter and base layers, the dark current density as well as the parallel resistance. This has the advantage that most of these values can be measured or fitted directly from existing solar cell samples. Of course the obtained results are strongly connected to the particular epitaxial structure as well as to the technological processing and may differ significantly for other solar cell structures.

2.3.2 Exemplary results

The network model was validated through a comparison of measured and simulated data. The measured data was gained by a flash-lamp based system described in /27/. For the validation GaAs single-junction solar cells with the same epitaxial structure as in Section 2.2.2 were used. Figure 6 shows a good match between simulation and measurement for a concentration ratio of up to 1000 suns. The increase of efficiency caused by the increase in open-circuit voltage and fill factor is well reproduced by the simulation as well as the drop caused by the losses through series resistances. The optimum efficiency for this specific GaAs solar cell is reached at about 100 suns.

The network simulation now enables the prediction of device parameters for variations in the front contact metallization. This makes it a suitable tool for the grid optimization. Figure 7 shows the calculated dependency between efficiency and grid finger distance for the same GaAs solar cell under a concentration ratio of 100 suns. The best finger spacing turns out to be about 260 µm. For this configuration Figure 8 presents a variation of the grid finger length and an optimum is found at 760 µm.

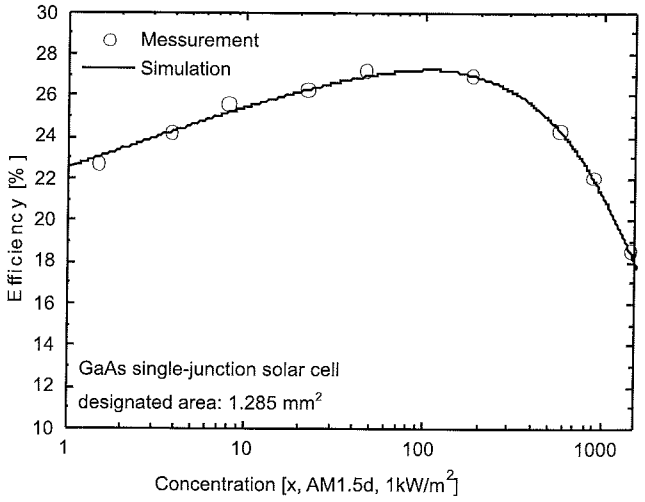

Fig. 6: Correlation between efficiency and concentration of a GaAs single-junction solar cell with an $Al_{0.35}Ga_{0.16}In_{0.49}P$ window layer.

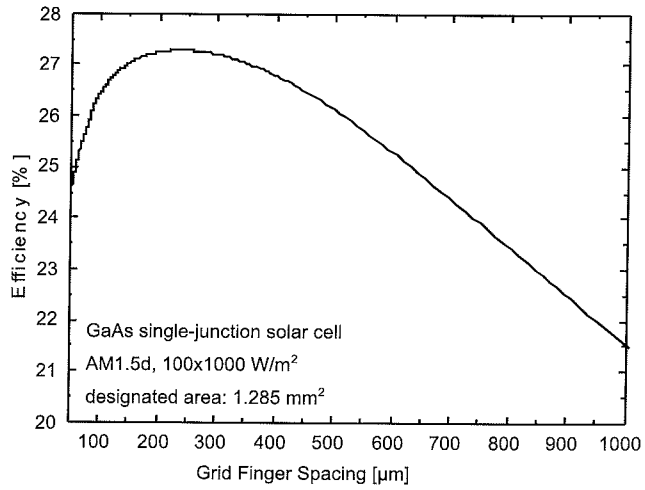

Fig. 7: Calculated GaAs solar cell efficiency as a function of the grid finger spacing.

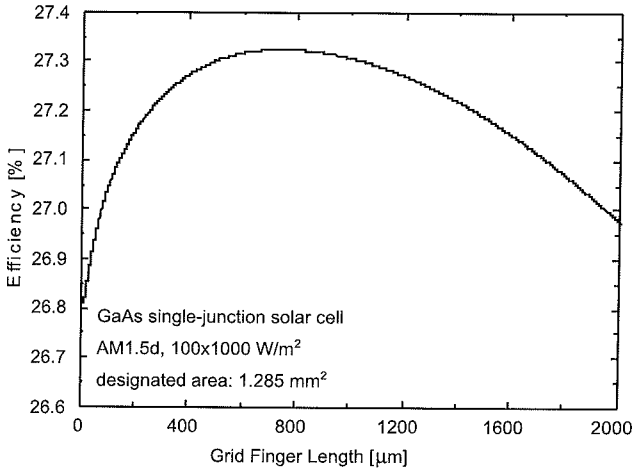

Fig. 8: Calculated efficiency as a function of the grid finger length for a GaAs solar cell.

3 Experimental realisation

After showing the current status of our modelling activities, this section focuses on the experimental realization. Although many different cell concepts are under investigation and show promising results, we are concentrating on a metamorphic triple-junction solar cell, which recently achieved an efficiency of 41.1% at 454 suns /1,2/. The fill factor and efficiency versus concentration ratio are shown in Figure 9. In the following a short description of the improvements that were made to achieve this record efficiency is given. More details about this topic were presented in Ref. /1/.

One of the key factors for the success of the metamorphic triple-junction solar cell is its nearly optimal band gap combination as indicated by the ideal efficiency calculations (Figure 1). Starting from the lattice-matched configuration (LM), the indium content in the top and middle subcells were gradually increased leading to the metamorphic configuration (MM2). In this configuration the $Ga_{0.35}In_{0.65}P$ and the $Ga_{0.83}In_{0.17}As$ subcells are grown lattice-matched to each other, but mismatched to the Ge substrate. Hence, the calculation of ideal efficiencies provided a valuable guidance during the strategical decisions of which configuration to head for.

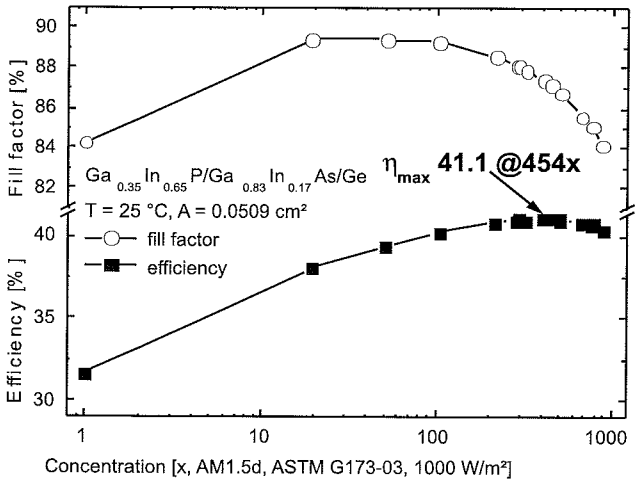

Fig. 9: Progress of fill factor and efficiency of a metamorphic $Ga_{0.35}In_{0.65}P/Ga_{0.83}In_{0.17}As/Ge$ triple-junction solar cell versus concentration level (after Ref. /1/).

However, the main assumption for the calculation of ideal efficiencies is that perfect solar cells are realised with none but the physically inevitable losses. Of particular importance is a perfect material quality, which makes it possible to neglect non-radiative recombination. Obviously in reality this assumption is rather difficult to be met. This is particularly true for metamorphic concepts as the lattice-mismatch between the subcells usually induces a high number of defects in the active solar cell layers. We overcame this limitation through the development of a novel buffer layer structure consisting of seven GaInAs layers with stepwise increasing indium content. Misfit dislocations are confined into this structural element leading to dislocation densities in the active layers of the solar cell below 10^6 cm^{-2}.

Another important factor is the optimal structure, in particular the thicknesses and doping levels of its semiconductor layers. As described above in Section 2.2 the determination of the optimal design could be facilitated through the use of semiconductor simulation environments. Although the numerical models are available the predictive capabilities of the simulation are still particularly limited for metamorphic structures due to the lack of material data. This is caused by the fact that many experimental methods for the measurement of important material data, like spectral ellipsometry or Hall measurements, require simple sample structures. Yet, such samples are difficult to realise for metamorphic materials due to the necessity of a metamorphic buffer structure. Thus, the model-based optimization of the semiconductor layers of metamorphic structures is – in contrast to lattice-matched structures – still limited to rather rough guidelines. The structure of the metamorphic triple-junction solar cell discussed here was hence optimized in a long-term experimental procedure and is certainly not ideal.

Concerning the semiconductor layer structure one of the key factors for the high performance of our metamorphic triple-junction solar cell is the tunnel diode, which achieves very high maximum tunnel current densities in the range of 15 to 25 A/cm^2. It consists of a p-doped AlGaInAs layer and an n-doped GaInP layer. Due to optimized lattice-match to the surrounding layers the generation of dislocations is avoided /1,28/.

Finally, another key factor for the structure was the optimal grid layout, which was optimized with the network model described in Section 2.3. A central factor for the grid design is the intended concentration ratio. As current concentrator systems use different concentration ratios several grids were designed and processed. Such a fine optimization and adjustment of the complex grid structure is hardly possible with only experimental investigation. This example shows that an optimised interaction between theoretical and experimental efforts is absolutely essential for the development and the realization of highest efficient solar cells.

3 Conclusions

In this work the current status and the newest results of the modelling activities for III-V multi-junction solar cells at Fraunhofer ISE are presented. It is shown that ideal efficiency calculations give a valuable guideline for the decision on which band gap combinations to realize. For triple-junction solar cells the band gap configuration of the metamorphic $Ga_{0.35}In_{0.65}P/Ga_{0.83}In_{0.17}As/Ge$ structure comes close to the global optimum. The analysis and optimization of the semiconductor layer structure can be greatly enhanced through simulations with semiconductor simulation

environments. Good modelling results have been achieved for lattice-matched single- and dual-junction solar cell structures. However, the capabilities for metamorphic structures are limited due to the lack of suitable material parameters. The third modelling approach described is network simulation for the optimization of the grid layout. This approach is highly predictive and is successfully applied for the design of contact grids for different cell structures and various illumination conditions. Concerning the experimental realization, the key factors leading to the design of a metamorphic triple-junction solar cell with an efficiency of 41.1 % at 454-fold concentration are highlighted. It is shown that numerical modelling techniques are now well established and supporting the design process of multi-junction solar cells.

Acknowledgments

Simon Philipps, Wolfgang Guter and Elke Welser gratefully acknowledge the scholarship support by the German Federal Environmental Foundation. Simon Philipps is also grateful for the ideational support of the German National Academic Foundation. This work was supported by the European Commission through the funding of the project FULLSPECTRUM (Ref. N: SES6-CT-2003-502620) and by the European Space Agency ESA-ESTEC through contract RFQ 3-11296/07/NL/GLC. The authors are responsible for the content of this paper.

References

/1/ W. Guter, J. Schöne, S. P. Philipps, M. Steiner, G. Siefer, A. Wekkeli, E. Welser, E. Oliva, A. W. Bett, F. Dimroth, "Current-matched triple-junction solar cell reaching 41.1% conversion efficiency under concentrated sunlight", Applied Physics Letters vol. 94, no. 22, pp. 223504/1, 2009.

/2/ M. A. Green, K. Emery, Y. Hishikawa, W. Warta, "Solar Cell Efficiency Tables (Version 34)", Progress in Photovoltaics: Research and Applications, vol. 17, no. 5, pp. 320-326, 2009.

/3/ S. R. Kurtz, D. Myers, W. E. McMahon, J. Geisz, M. Steiner, "A Comparison of Theoretical Efficiencies of Multi-Junction Concentrator Solar Cells", Progress in Photovoltaics: Research and Applications, vol. 16, no. 6, pp. 537-546, 2008.

/4/ G. Létay, M. Hermle, A. W. Bett, "Simulating Single-junction GaAs Solar Cells Including Photon Recycling", Progress in Photovoltaics: Research and Applications, vol. 14, no. 8, pp. 683-696, 2006.

/5/ Z. Q. Li, Y. G. Xiao, Z. M. S. Li, "Modeling of multi-junction solar cells by Crosslight APSYS", High and Low Concentration for Solar Electric Applications, vol. 6339, pp. 633909-15, 2006.

/6/ M. Baudrit, C. Algora, "Modeling of GaInP/GaAs Dual-Junction Solar Cells including Tunnel Junction", Proceedings of the 33rd IEEE PVSC, San Diego, 2008.

/7/ S. Michael, "A novel approach for the modeling of advanced photovoltaic devices using the SILVACO/ATLAS virtual wafer fabrication tools", Solar Energy Materials and Solar Cells, vol. 87, no. 1-4, pp. 771-784, 2005.

/8/ S. P. Philipps, M. Hermle, G. Létay, F. Dimroth, B. M. George, A. W. Bett, "Calibrated Numerical Model of a GaInP-GaAs Dual-Junction Solar Cell", physica status solidi (RRL) - Rapid Research Letters, vol. 2, no. 4, pp. 166-168, 2008.

/9/ K. Nishioka, T. Takamoto, W. Nakajima, T. Agui, M. Kaneiwa, Y. Uraoka, T. Fuyuki, "Analysis of triple-junction solar cell under concentration by SPICE", Proceedings of the 3rd World Conference on Photovoltaic Energy Conversion, Osaka, Japan, 2003.

/10/ B. Galiana, C. Algora, I. Rey Stolle, I. G. Vara, "A 3-D model for concentrator solar cells based on distributed circuit units", IEEE Transactions on Electron Devices, vol. 52, no. 12, pp. 2552-2558, 2005.

/11/ M. Burgelman, J. Verschraegen, S. Degrave, P. Nollet, "Modeling Thin-film PV Devices", Progress in Photovoltaics: Research and Applications, vol. 12, no. 2-3, pp. 143-153, 2004.

/12/ A. S. Gudovskikh, N. A. Kaluzhniy, V. M. Lantratov, S. A. Mintairov, M. Z. Shvarts, V. M. Andreev, "Numerical modelling of GaInP solar cells with AlInP and AlGaAs windows", Thin Solid Films, vol. 516, no. 20, pp. 6739-6743, 2008.

/13/ J. Plá, M. Barrera, F. Rubinelli, "The influence of the InGaP window layer on the optical and electrical performance of GaAs solar cells", Semiconductor Science and Technology, vol. 22, no. 10, pp. 1122-1130, 2007.

/14/ S. Sato, T. Ohshima, M. Imaizumi, "Modeling of degradation behavior of InGaP/GaAs/Ge triple-junction space solar cell exposed to charged particles", Journal of Applied Physics, vol. 105, no. 4, pp. 044504, 2009.

/15/ Linear Technology Corporation, *Switcher CAD III/LT Spice*, 2007.

/16/ G. Létay, A. W. Bett, "EtaOpt - a Program for Calculating Limiting Efficiency and Optimum Bandgap Structure for Multi-Bandgap Solar Cells and TPV Cells", Proceedings of the 17th European Photovoltaic Solar Energy Conference, Munich, Germany, pp. 178-181, 2001.

/17/ W. Shockley, H. J. Queisser, "Detailed balance limit of efficiency of p-n junction solar cells", Journal of Applied Physics, vol. 32, no. 3, pp. 510-519, 1961.

/18/ R. R. King, D. C. Law, K. M. Edmondson, C. M. Fetzer, G. S. Kinsey, H. Yoon, R. A. Sherif, N. H. Karam, "40% efficient metamorphic GaInP/GaInAs/Ge multijunction solar cells", Applied Physics Letters, vol. 90, no. 18, pp. 183516, 2007.

/19/ F. Dimroth, "High-Efficiency Solar Cells from III-V Compound Semiconductors", Physica Status Solidi C, vol. 3, no. 3, pp. 373-379, 2006.

/20/ M. Yamaguchi, T. Takamoto, K. Araki, "Super high-efficiency multi-junction and concentrator solar cells", Solar Energy Materials and Solar Cells, vol. 90, no. 18-19, pp. 3068-3077, 2006.

/21/ J. F. Geisz, D. J. Friedman, J. S. Ward, A. Duda, W. J. Olavarria, T. E. Moriarty, J. T. Kiehl, M. J. Romero, A. G. Norman, K. M. Jones, "40.8% efficient inverted triple-junction solar cell with two independently metamorphic junctions", Applied Physics Letters, vol. 93, no. 12, pp. 123505/1, 2008.

/22/ Synopsys, "Sentaurus Device User´s Manual Release: A-2007.12", Synopsys Inc., Zurich, Switzerland, www.synopsys.com, 2008.

/23/ M. Baudrit, C. Algora, I. Rey-Stolle, I. García, B. Galiana, "Numerical analysis of GaInP solar cells: toward advanced photovoltaic devices modeling", Proceedings of the 5th International Conference on Numerical Simulation of Optoelectronic Devices, Berlin, Germany, pp. 41-42, 2005.

/24/ M. Hermle, G. Létay, S. P. Philipps, A. W. Bett, "Numerical Simulation of Tunnel Diodes for Multi-Junction Solar Cells", Progress in Photovoltaics: Research and Applications, vol. 16, no. 5, pp. 409-418, 2008.

/25/ S. P. Philipps, M. Hermle, G. Létay, W. Guter, B. M. George, F. Dimroth, A. W. Bett, "Numerical Simulation and Modeling of III-V Multi-Junction Solar Cells", 23rd European Photovoltaic Solar Energy Conference and Exhibition, Valencia, Spain, 2008.

/26/ M. Steiner, S. P. Philipps, M. Hermle, F. Dimroth, A. W. Bett, "Front Contact Grid Optimization of III-V solar cells with SPICE network simulation", Proceedings of the 24th European Photo-

voltaic Solar Energy Conference, Hamburg, Germany, to be published, 2009.

/27/ G. Siefer, C. Baur, M. Meusel, F. Dimroth, A. W. Bett, W. Warta, "Influence of the simulator spectrum on the calibration of multi-junction solar cells under concentration", Proceedings of the 29th IEEE Photovoltaics Specialists Conference, New Orleans, Louisiana, USA, pp. 836-839, 2002.

/28/ W. Guter, F. Dimroth, J. Schöne, S. P. Philipps, A. W. Bett, "Investigation and Development of III-V Triple-Junction Concentrator Solar Cells", Proceedings of the 22nd European Photovoltaic Solar Energy Conference and Exhibition, Milan, Italy, pp. 122-125, 2007.

S. P. Philipps, W. Guter, M. Steiner, E. Oliva, G. Siefer, E. Welser, B. M. George, M. Hermle, F. Dimroth, A. W. Bett
Fraunhofer Institute for Solar Energy Systems ISE, Heidenhofstr. 2, 79110 Freiburg, Germany, simon.philipps@ise.fraunhofer.de, phone: +49 761 4588 5332, fax: +49 761 4588 9250

Prispelo (Arrived): 15.08.2009 *Sprejeto (Accepted): 09.10.2009*

PROGRESS IN UNDERSTANDING THE INTERMEDIATE BAND SOLAR CELL

Antonio Luque and Antonio Martí

Instituto de Energía Solar, Universidad Politécnica de Madrid, Espana

Key words: intermediate band gap, high efficiency solar cell

Abstract: High efficiency is intended by electron-hole generation with sub band gap photons while the voltage is ruled by the band gap. Most present cells have small current enhancement and some voltage loss. The reasons are described.

Napredek v razumevanju sončnih celic z vmesnim energijskim pasom

Kjučne besede: vmesni energijski nivoji, sončne celice z visoko učinkovitostjo

Izvleček: Visoko učinkovitost pretvorbe zagotavljajo pari elektron-vrzel, ki jih generirajo fotoni z energijo nižjo od energijske reže, medtem ko je napetost določena z energijsko režo. Večina celic izkazuje majhno povečanje toka, nekatere pa znižanje napetosti. Vzroki so razločeni v članku.

1 Introduction

An Intermediate Band (IB) solar cell is formed /1/ by an IB material situated between two ordinary semiconductors — n- and p-type respectively— that play the role of selective contacts to conduction band (CB) and valence band (VB) electrons. The IB material has a band of states inside the band gap between the CB and the VB. In this way, photons with less energy than the one necessary to pump an electron from the VB to the CB can be absorbed by transitions that pump an electron from the VB to the IB and from the IB to the CB. Thus a full VB→CB electron transition (or electron-hole pair generation) can be completed by means of two photons of energy below the band gap. This mechanism should increase the solar cell current.

While increasing the current the voltage has to be preserved. The voltage in the cells is the difference of the CB and VB quasi Fermi levels (QFL) splitting. In the IB solar cell a third independent QFL must appear for the IB that is isolated from the contacts through two ordinary n- and p-type ordinary semiconductors that play the role of electron and hole selective contacts.

Limiting efficiency of this concept for maximum concentration (the one providing isotropic illumination on the cell with the radiance of the sun's photosphere) is 63% to compare with the Shockley-Queisser limit of 40% for an ordinary cell in the same conditions /2/.

IB GaAs solar were fabricated first /3/ based on this concept using InAs quantum dots (QD) to form the IB by IES (UPM) and the University of Glasgow. Today several more groups have produced similar cells /4-8/. Evidence of the electron-hole formation through the described two-photon mechanism has been produced /9/. Evidence of the three QFL splitting has also been provided /10/. However, the efficiency is not higher than the one of the cells without quantum dots. Bulk ZnTe:O IB solar cells have also been presented /11/ and while the efficiency is still very low the IB behavior is crealy demosntstate and the efficiency of the IB cells is 50% higher than the one of the ZnTe ordinary cells.

2 Current enhancement

The QD IBSC show some current enhancement but it is too small. It is attributed to the small number of QD layers involved, 10 in the first IB solar cells /3/. The obvious conclusion was to fabricate solar cells with more QD layers but this resulted in the production of dislocations /12/ that spoiled the emitter photo-generated current contribution (CB→VB transitions). However the increase of sub-band-gap photon current was achieved. Strain- compensated techniques have been developed first by Hubbard and coworkers /4/ at Rochester Inst. Tech. and NASA Glenn with very good results. Other researchers have also used strain compensating techniques /4-8/. It seems that the deposition of several hundreds of layers without degrading the crystal will be possible. See in Figure 1 the best efficiency so far achieved with and IB solar cell.

However, it seems that the IB→CB photon absorption is very weak. This might be because the aspect of the QD is very flat, reminding a quantum well (QW) and it is know that this transition is forbidden in QWs for photons normal to the surface. The manufacturing of QD with another aspect ratio is desirable. But in any case diffractive methods may bent the rays so breaking the selection rule and at the same time enlarging the ray path length /13/.

But besides, the IB is in most cases not half filled or insufficiently filled because most of groups refuse to dope the IB, probably to keep the quality high. Even with a good photon capture section this will prevent the IB→CB ab-

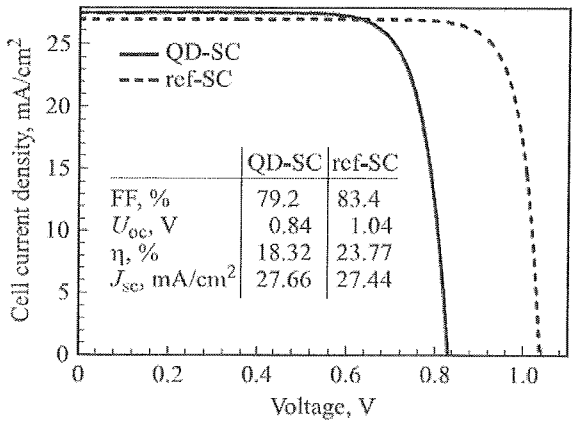

Fig. 1: IV curves of an IB-QD InAs/GaAs solar cell and the reference GaAs solar cell /8/.

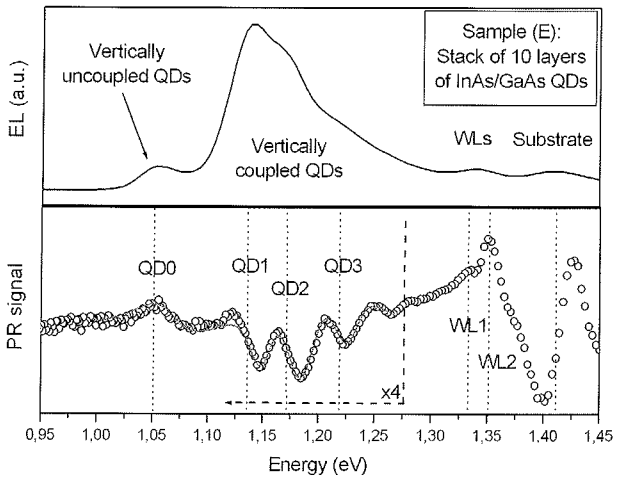

Fig. 2: Electroluminescence and Photoreflectance spectrum of an IB QD solar cell. The first seed layer has one wetting layer and a confined states. The rest of the layers have their wetting layer and three confined levels, each one vertically coupled /14/.

sorption to be produced by lack of electrons. Maybe they observe that the quantum efficiency (QE) is better in undoped samples but again this is misleading because in most cases QE is a one-photon experiment and only tells that the IB and the CB are short-circuited, that is bad.

3 Voltage preservation

A voltage reduction of 100 to 200 mV is usually observed between the QD solar cell and the reference GaAs solar cell. It is mainly due to the reduction of the barrier material band gap caused by:

- The formation of a wetting layer when the QD are grown in the Stranski Krastanov mode. The wetting layer is in reality a quantum well and as such it has not a zero density of states between IB and CB and as such its width has to be considered as a reduction of the barrier material band gap.
- The existence of high quantum number confined states differing in energy less than the optical phonon energy and therefore behaving very much as a continuous band.
- The appearance of a VB offset due to the confined hole states whose excited states also form a continuous in the same terms as above.

Photoreflectance measurements /14/ made in our group show several confined layers that deped on the size and shape of the QDs. This is also confirmed by quantum calculations (by Zunger and coworkers) for the InAs/GaAs case show a reduction of the band gap that at 0°K is of about 300 meV. The reduction observed in the voltage is smaller but is to be expected that it mirrors at least qualitatively the theoretically expected band gap reduction.

But this effect is not negative in itself. It only tells that the bandgap of the barrier material is modified by the addition of QD and thus it is unfair to compare InAs/GaAs cells with GaAs cells. To compare cells of the same badgap it woud be necessary to make the IB cell ain a larger bandgap material like AlGaAs.

But besides this it looks that the IB in this system is strongly connected to the CB. This means that the capture section of CB electrons by the IB is very high /15/. This makes the separation of the three QFL difficult. The main reason for it is the multitude of levels populating the IB-CV interval as seen in Figure 2. But in addition to it the high electric fields present in the cells favor the tunneling of the confined electrons into the CB. We have experimental evidence (in preparation for publication) that the later mechanism has been avoided in recent cells but the fact remains that even the ideal detailed balance calculations tell that the InAs/GaAs QD cell cannot give more efficiency than the GaAs cell at one sun illumination. Thus we believe that a practical QD device has to be made with a larger bandgap barrier material.

4 Bulk material ib cells

IB materials have been found along several paths. The first to be followed that was based on *ab initio* quantum calculations /16/ has recently led to the solvothermal synthesis of $Va_{0.25}In_{1.75}S_3$ /17/ in which the theoretically predicted /18/ three absorption bands have been found. No cell has been done because the synthesis method is not compatible with solar cell manufacturing.

The band anticrossing mechanism /19/ in highly mismatched alloys has led to the discovery of several IB materials as detected by photoreflectance spectroscopy /20, 21/. Recently the first bulk IB solar cell has been produced /11/, of ZnTe:O, where the IB cell is clearly better than the corresponding ZnTe ordinary cell, as shown in Figure 3.

But in reality any deep level impurity might be the precursor of an IB cell. Several new ideas are now in development along this line /22, 23/.

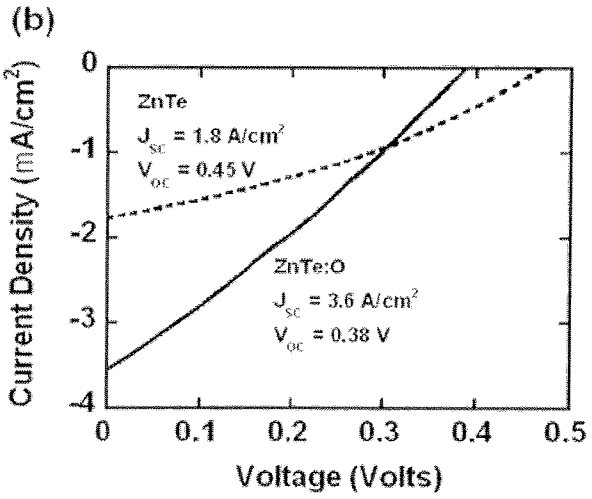

Fig. 3: IV curves of a ZnTe:O IB solar cell and an ordinary ZnTe solar cell. Effciencies are below 1% but 50% higher in the IB solar cell.

4.1 Suppression of the non-radiative recombination

It is well known that deep levels are the origin of SRH non radiative recombination. In bulk materials we believe that the main cause of it is the so called multiphonon emission mechanism /24/ that is associated to the disequilibrium caused when the electric charge an extended electron in the CB or in the VB makes a transition to a localized state with the charge localized around the impurity in the deep level. The lattice start vibrating heavily and this vibration is subsequently damped by the emission of several phonons. We have anticipated /25/ that if the semiconductor is heavily doped so that the impurity states become extended states in an impurity band thie mechanism cannot be produced and the non radiative recombination mush result suppressed. By ion implantation and pulsed laser melting we have doped heavily wafer of Si with Ti that is known to be a strong lifetime killer. We have found that the lifetime is increased when the implanted dose increases /26/. The experiment result is presented in Figure 4.

It is to be noted that this result is just opposite to the common belief of device physicists: the more the Ti the longer the lifetime. We believe this is an important result and explains why IB behavior is to be different form deep level behavior.

5 Conclusions

Stress production during the QD growth seems to be the main cause for reduction of the cell photo generated current. Indeed this also affect drastically to the voltage. When the stress is controlled the voltage is still reduced due to the shrinkage of the main band gap. This is not to be considered as a drawback in itself. The comparison with GaAs cells is inappropriate. The band gap can be restored by using alloys such as GaAlAs as barrier material.

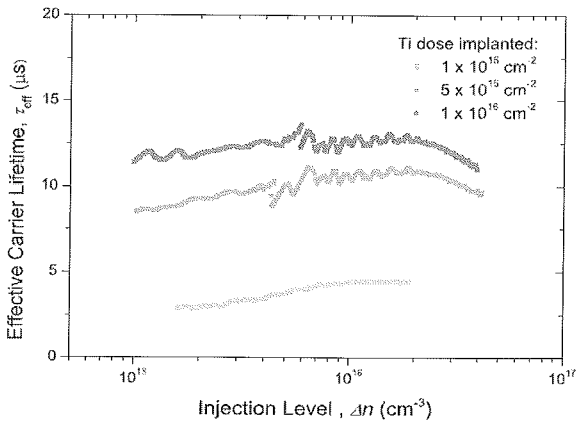

Fig. 4: Lifetime vs. injection level as measured by conductivity decay /27/ in heavily Ti-implanted Si wafers /26/.

The multiple confined lavels seems to provide an easy path to have the IB and the CB thermally connected. This makes difficult the appearance of three quasi Fermi levels and therefore the conservation of the voltage

Doping the IB is essential for the IB→CB photon absorption. Without it the high voltage operation is also impossible. But maybe the shape of the QDs, very close to that of the QWs makes this absorption difficult as it is known that it is forbidden in QWs.

In general, revisiting the optimal materials proposed by us at the beginning /28/ seems now pertinent. QD's should be smaller and their levels more separated from the CB. For it the main bandgap must be higher.

Several bulk IB materials have been found experimentally and many more have been anticipated theoretically. This contrasts to the first predictions of some scientists that considered impossible to find IB materials. IB solar cells have been manufactured although their efficiency is still small.

The different behavior of deep levels and IB in the sense that no SRH recombination is to be expected in the seconds has been anticipated and experimental evidence has been provided.

Over two dozen of groups have published so far in ISI-recorded journals on IB solar cells. Most If the publications are of the last three years and results start to appear copious. We think that soon we shall practical IB solar cells, either in tandem /29/ for operation in concentration, to explore the range of 50% efficiency, or as thin film solar cells more efficient than the present ones and therefore able to compete better in market.

Acknowledgments

This work has been supported by the European Commission within the project FULLSPECTRUM (SES6-CT-2003-502620) and the projects NUMANCIA (S-0505/ENE/000310) funded by the Comunidad de Madrid, and GEN-

ESIS FV (CSD2006-00004) funded by the Spanish National Programme.

References

/1/ A. Luque and A. Martí, "A metallic intermediate band high efficiency solar cell," *Progress in Photovoltaics: Res. Appl.,* vol. 9, pp. 73-86, 2001.

/2/ A. Luque and A. Martí, "Increasing the efficiency of ideal solar cells by photon induced transitions at intermediate levels," *Physical Review Letters,* vol. 78, pp. 5014-5017, 1997.

/3/ A. Luque, A. Martí, C. Stanley, N. López, L. Cuadra, D. Zhou, and A. Mc-Kee, "General equivalent circuit for intermediate band devices: potentials, currents and electroluminescence," *Journal of Applied Physics,* vol. 96, pp. 903-909, 2004.

/4/ S. M. Hubbard, C. D. Cress, C. G. Bailey, R. P. Raffaelle, S. G. Bailey, and D. M. Wilt, "Effect of strain compensation on quantum dot enhanced GaAs solar cells," *Applied Physics Letters,* vol. 92, p. 123512, Mar 2008.

/5/ D. Alonso-Alvarez, A. G. Taboada, J. M. Ripalda, B. Alen, Y. Gonzalez, L. Gonzalez, J. M. Garcia, F. Briones, A. Marti, A. Luque, A. M. Sanchez, and S. I. Molina, "Carrier recombination effects in strain compensated quantum dot stacks embedded in solar cells," *Applied Physics Letters,* vol. 93, p. 123114, Sep 2008.

/6/ V. Popescu, G. Bester, M. C. Hanna, A. G. Norman, and A. Zunger, "Theoretical and experimental examination of the intermediate-band concept for strain-balanced (In,Ga)As/Ga(As,P) quantum dot solar cells," *Physical Review B,* vol. 78, p. 205321, 2008.

/7/ R. Oshima, A. Takata, and Y. Okada, "Strain-compensated InAs/GaNAs quantum dots for use in high-efficiency solar cells," *Applied Physics Letters,* vol. 93, p. 083111, 2008.

/8/ С. А. Блохин, А. В. Сахаров, А. М. Надточий, А. С. Паюсов, М. В. Максимов, Н. Н. Леденцов, А. Р. Ковш, С. С. Михрин, В. М. Лантратов, С. А. Минтаи-ров, Н. А. Калюжный, and М. З. Шварц, "Фотоэлектрические преобразователи AlGaAs/GaAs с массивом квантовых точек InGaAs," Физика и техника полупроводников, vol. 43, pp. 537-542, 2009.

/9/ A. Marti, E. Antolin, C. R. Stanley, C. D. Farmer, N. Lopez, P. Diaz, E. Canovas, P. G. Linares, and A. Luque, "Production of Photocurrent due to Intermediate-to-Conduction-Band Transitions: A Demonstration of a Key Operating Principle of the Intermediate-Band Solar Cell," *Physical Review Letters,* vol. 97, pp. 247701-4, 2006.

/10/ A. Luque, A. Marti, N. Lopez, E. Antolin, E. Canovas, C. Stanley, C. Farmer, L. J. Caballero, L. Cuadra, and J. L. Balenzategui, "Experimental analysis of the quasi-Fermi level split in quantum dot intermediate-band solar cells," *Applied Physics Letters,* vol. 87, pp. 083505-3, 2005.

/11/ W. Wang, A. S. Lin, and J. D. Phillips, "Intermediate-Band Photovoltaic Solar Cell Based on ZnTe:O," *Applied Physics Letters,* vol. 95, p. 011103, 2009.

/12/ A. Marti, N. Lopez, E. Antolin, E. Canovas, A. Luque, C. R. Stanley, C. D. Farmer, and P. Diaz, "Emitter degradation in quantum dot intermediate band solar cells," *Applied Physics Letters,* vol. 90, pp. 233510-3, 2007.

/13/ I. Tobias, A. Luque, and A. Marti, "Light intensity enhancement by diffracting structures in solar cells," *Journal of Applied Physics,* vol. 104, p. 034502, Aug 2008.

/14/ E. Cánovas, A. Martí, N. López, E. Antolín, P. G. Linares, C. D. Farmer, C. R. Stanley, and A. Luque, "Application of the photoreflectance technique to the characterization of quantum dot intermediate band materials for solar cells," *Thin Solid Films,* vol. 516, pp. 6943-6947, 2008.

/15/ A. Luque, A. Martí, N. López, E. Antolín, E. Cánovas, C. R. Stanley, C. Farmer, and P. Díaz, "Operation of the intermediate band solar cell under nonideal space charge region conditions and half filling of the intermediate band," *Journal of Applied Physics,* vol. 99, p. 094503, 2006.

/16/ P. Wahnón and C. Tablero, "Ab-initio electronic structure calculations for metallic intermediate band formation in photovoltaic materials," *Physical Review B,* vol. 65, p. 155115, 2002.

/17/ R. Lucena, I. Aguilera, P. Palacios, P. Wahnon, and J. C. Conesa, "Synthesis and Spectral Properties of Nanocrystalline V-Substituted In2S3, a Novel Material for More Efficient Use of Solar Radiation," *Chemistry of Materials,* vol. 20, pp. 5125-5127, Aug 2008.

/18/ P. Palacios, I. Aguilera, K. Sanchez, J. C. Conesa, and P. Wahnon, "Transition-metal-substituted indium thiospinels as novel intermediate-band materials: Prediction and understanding of their electronic properties," *Physical Review Letters,* vol. 101, p. 046403 Jul 2008.

/19/ W. Walukiewicz, W. Shan, K. M. Yu, J. W. Ager, E. E. Haller, I. Miotkowski, M. J. Seong, H. Alawadhi, and A. K. Ramdas, "Interaction of localized electronic states with the conduction band: Band anticrossing in II-VI semiconductor ternaries," *Physical Review Letters,* vol. 85, pp. 1552-1555, Aug 2000.

/20/ K. M. Yu, W. Walukiewicz, J. Wu, W. Shan, J. W. Beeman, M. A. Scarpulla, O. D. Dubon, and P. Becla, "Diluted II-VI Oxide Semiconductors with Multiple Band Gaps," *Physical Review Letters,* vol. 91, pp. 246403-4, 2003.

/21/ K. M. Yu, W. Walukiewicz, J. W. Ager, Iii, D. Bour, R. Farshchi, O. D. Dubon, S. X. Li, I. D. Sharp, and E. E. Haller, "Multiband GaNAsP quaternary alloys," *Applied Physics Letters,* vol. 88, pp. 092110-3, 2006.

/22/ A. Marti, D. Fuertes-Marron, and A. Luque, "Evaluation of the efficiency potential of intermediate band solar cells based on thin-film chalcopyrite materials," *Journal of Applied Physics,* vol. 103, p. 073706, 2008.

/23/ A. Marti, C. Tablero, E. Antolin, A. Luque, R. P. Campion, S. V. Novikov, and C. T. Foxon, "Potential of Mn doped In1-xGaxN for implementing intermediate band solar cells," *Solar Energy Materials and Solar Cells,* vol. 93, pp. 641-644, May 2009.

/24/ C. H. Henry and D. V. Lang, "Nonradiative Capture and Recombination by Multiphonon Emission in Gaas and Gap," *Physical Review B,* vol. 15, pp. 989-1016, 1977.

/25/ A. Luque, A. Martí, E. Antolín, and C.Tablero, "Intermediate bands versus levels in non-radiative recombination," *Physica B,* vol. 382, pp. 320-327, 2006.

/26/ E. Antolin, A. Marti, J. Olea, D. Pastor, G. Gonzalez-Diaz, I. Martil, and A. Luque, "Lifetime recovery in ultrahighly titanium-doped silicon for the implementation of an intermediate band material," *Applied Physics Letters,* vol. 94, p. 042115, 2009.

/27/ R. Lago-Aurrekoetxea, I. Tobias, C. del Canizo, and A. Luque, "Lifetime measurements by photoconductance techniques in wafers immersed in a passivating liquid," *Journal of the Electrochemical Society,* vol. 148, pp. G200-G206, Apr 2001.

/28/ A. Martí, L. Cuadra, and A. Luque, "Design constraints ofthe quantum-dot intermediate band solar cell," *Physica E,* vol. 14, pp. 150–157, 2002.

/29/ E. Antolín, A. Martí, and A. Luque, "Energy conversion efficiency limit of series connected intermediate band solar cells," in *Proc. of the 21st European Photovoltaic Solar Energy Conference*, J. Poortmans, H. Ossenbrink, E. Dunlop, and P. Helm, Eds. Munich: WIP-Renewable Energies, 2006, pp. 412-415.

Antonio Luque and Antonio Martí
Instituto de Energía Solar,
Universidad Politécnica de Madrid

Prispelo (Arrived): 15.08.2009 *Sprejeto (Accepted): 09.10.2009*

EXPLOITING SOLAR ENERGY WITH PHOTOVOLTAICS

Jože Rakovec

Faculty of Mathematics and Physics, University of Ljubljana, Ljubljana, Slovenia

Key words: solar irradiation, Slovenia, photovoltaics

Abstract: Energy balance of a solar panel is considered in relation to its efficiency. The monthly, seasonal and yearly means of solar radiance exposures are presented in a form of geo-referenced maps for whole Slovenia with a spatial resolution 100 m x 100 m, as well as the diagrams of the optimal tilts and orientation of solar collectors for selected places in Slovenia. In rough relief, not only the whole landscape is divided into sunny and shady parts, but also different sky-view factors influence strongly the diffuse part of radiance exposure. The trend of increasing global solar radiance exposure during the last few decades can partly be explained with the trend of the reduced fog occurrence over Slovenia.

Fotonapetostno izkoriščanje sončne energije

Kjučne besede: sončno obsevanje, Slovenija, fotovoltaika

Izvleček: Energijska bilanca fotonapetostnega modula je pogojena tudi z njegovim izkoristkom. Mesečna, sezonska in letna povprečja sončnega obsevanja so predstavljena na geografski karti z resolucijo 100 m x 100 m za celotno Slovenijo. Prav tako so podani diagrami optimalnega naklona in orientacije fotonapetostnih modulov za izbrane kraje v Sloveniji. Na razgibanem terenu pokrajina ni razdeljena samo na senčni in osončen del temveč tudi glede na različne vidne kote neba, ki močno vplivajo na difuzni del obsevanja. Trende povečevanja sončnega obsevanja v zadnji dekadi lahko razložimo delno tudi z zmanjšanjem pojava megle v Sloveniji.

1 Introduction

The natural resource for exploiting solar energy is of course solar irradiance that differs from place to place due to astronomical and weather related factors. While astronomical part can be well described with analytical equations, the meteorological part should be determined with a help of the measured data as well as using the results of meteorological models. The most important is of course the solar irradiance (power density), or radiance exposure (energy density, accumulated in a certain time, for example in a day). The next most important is air temperature, affecting the energy balance of solar collectors, followed by other parameters that influence heat exchange between collectors and their environment, like wind, precipitation etc., resulting in temperature of collector. Temperature is important as efficiency of PV cells diminishes with temperature.

In this paper are thus presented the factors of energy balance of a solar panel, the methodology for obtaining geo-referenced solar radiance exposures in a horizontal resolution of 100 m x 100 m, and the optimal tilts and orientations of surfaces with the highest radiation exposures.

2 The data

2.1 Solar energy data

Solar energy is not measured for a long period at many meteorological stations in Slovenia since most of the pyranometers, measuring global solar irradiation, were installed only in the last ten or fifteen years. Therefore, the time period for climatology of solar radiance exposures do not span over the 30-year period, which comprises the climatologically established standard that ensures the desired stability and representativeness of the measured data. Namely, if we want to consider the 30-year period we would have to hold back on our study and the publishing of results for the next 15 years. Due to the requirements of such data, the study was only performed on 10-year-long data sets.

As the exploitation of solar energy depends on the proportion between the direct and the diffuse part of irradiance, it is important to know both. The relief of Slovenia is rough and so not only that the whole landscape is divided into some parts that are more exposed to the sun and other more shady ones; the relief is also significant for the diffuse part of radiation. The diffuse radiation from the sky is reduced by the sky-view factor, which is the visible proportion of bright sky that also contributes an important part to insolation. The direct part of quasi-global radiance depends mostly on the incidence angle, which is defined by astronomical and surface parameters, as well as the horizon of the surrounding relief. The obstacles on horizon influence the effective possible duration of solar radiation. All these influences were included in our own model /1/ for computing quasi-global solar irradiance and radiance exposure with a spatial resolution of 100 m x 100 m (based on a digital relief model of Slovenia, © Surveying and Mapping Authority of the Republic of Slovenia).

2.2 Other meteorological data, influencing the efficiency of the PV panel

In this subsection we are going to explain how the environmental data influence efficiency of the PV panel. It is known that efficiency diminishes with the increasing temperature

T /e.g. 2/. The temperature of cells or a whole panel as a bulk is the result of the energy exchange between the panel and its environment. The first are the conduction and the convection, depending on panels and on environmental temperature, with exchange coefficients that depend also on wind and turbulence. Next is the infrared radiation leaving the panel (depending on 4^{th} power of panels temperature) and infrared radiation from the environment to the panel, depending on 4^{th} power of temperature of the environment (above the panel is the air having in clear sky conditions the bulk emissivity of approx. 0.7). In addition, eventual precipitation or dew has energetic consequences via the latent heat of evaporation. Therefore, for a detailed consideration of factors of panel's efficiency besides the solar irradiance also these heat exchanges should be taken into account.

3 Global and quasi-global solar radiance exposures

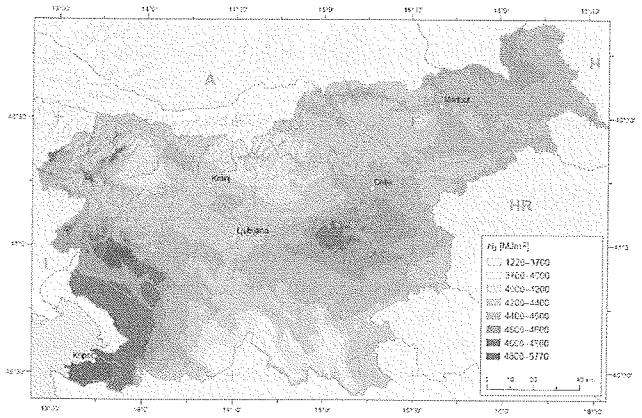

Fig. 1: Yearly mean of the global radiant exposure for Slovenia /1/.

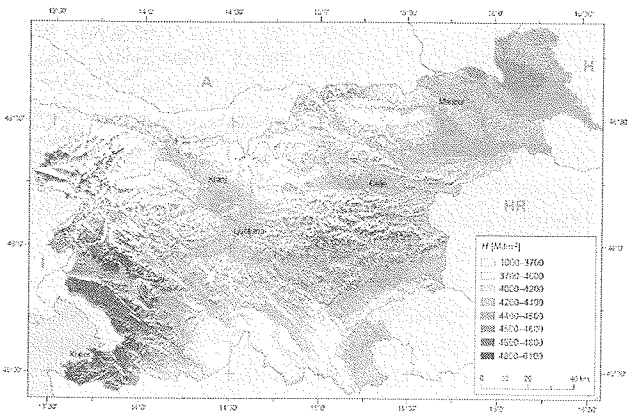

Fig. 2: Yearly mean of the quasi- global radiant exposure for Slovenia /1/.

Monthly charts of the global (on horizontal receiving surface) and quasi-global solar radiant exposure (of differently tilted and oriented surfaces) were computed, as well as seasonal and yearly charts. As two examples we show here the yearly chart of the global (in a 1 km x 1 km horizontal resolution; Fig. 1), and the quasi-global exposures (in a 100 m x 100 m horizontal resolution; Fig. 2) for Slovenia. The sunny and shady slopes are evident at first glance. The radiant exposure could even be some 20 % higher on the sunny slopes in comparison with the global exposure of horizontal surfaces. The shady slopes differ from the horizontal areas even more (even by 70 %). This asymmetry is mainly caused by the effect of the relief on the direct radiation - shady slopes experience a less favourable incidence angle of the sun and are often in the shade (when they only receive a diffuse part of radiation), while the sunny slopes are only influenced by a greater inclination angle of the sun, while in general they are not shadowed.

4 The optimum orientation and tilt

The orientation and slope of a collector can contribute an important increase to the energy collected in the exploitation of solar energy. The primary factor of sensible exploitation is, of course, the placement of the collector in a sunny place in order to prevent shadows from obstacles in the nearby and more distant vicinity. Then the optimal inclination and orientation has to be established: one can assume that the collector should be oriented towards the south and that the summer inclination (with the sun high in the sky) should be smaller than the winter inclination. However, a careful analysis also offers some less expected and even surprising results (Fig. 3).

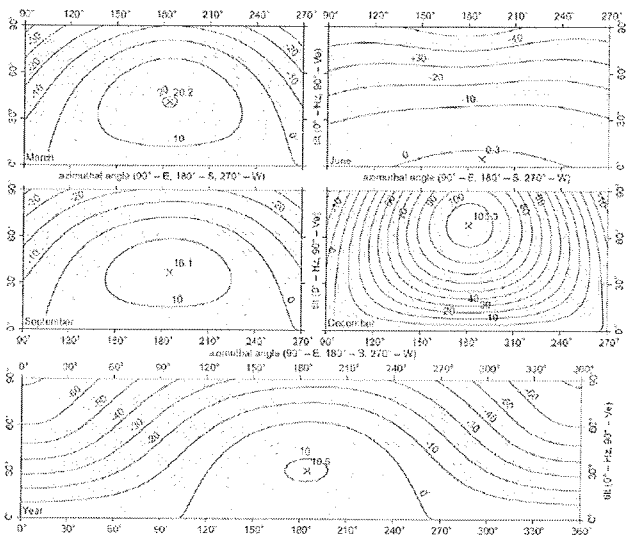

Fig. 3: Contour plots of relative PV array energy yield regarding the horizontal surface as a function of fixed orientation and tilt for March, June, September, December and the whole year for Portorož in the Mediterranean part of Slovenia /3/.

For example, mainly during the cold part of the year the basins and plains of the lowlands are often foggy or covered by low stratus cloudiness that clears only late in the morning or even in the afternoon. An orientation slightly to

the West provides a better incidence angle for the stronger afternoon direct radiance exposure. There are regional differences in optimal inclination: the optimal value in the Mediterranean area is, for instance, higher than in the northeastern area. In June, when the towards South tilted collectors do not receive direct irradiance in morning and evening hours, when the sun is not yet, or no more on the southern part of the sky, tilting the collector is not very appropriate as regards the daily sum of radiant exposure.

The above consideration is general - considering only the solar radiance exposure of the receiving surfaces. Especially with PV panels, another factor should be taken into account, being connected with the dependence of its efficiency on temperature. In morning hours, panels are normally cold and thus their efficiency is higher than in afternoon hours when the panels may warm up to 70 °C. With such an increase of the panel's temperature its efficiency drops in outdoors conditions from over 11 % down to some 10 % - relatively that means for one tenth; Figure 4, /4/. This degrease in efficiency prevails over the slightly higher irradiances in afternoon hours. Therefore, specifically for PV panels orientation slightly towards east may perform better.

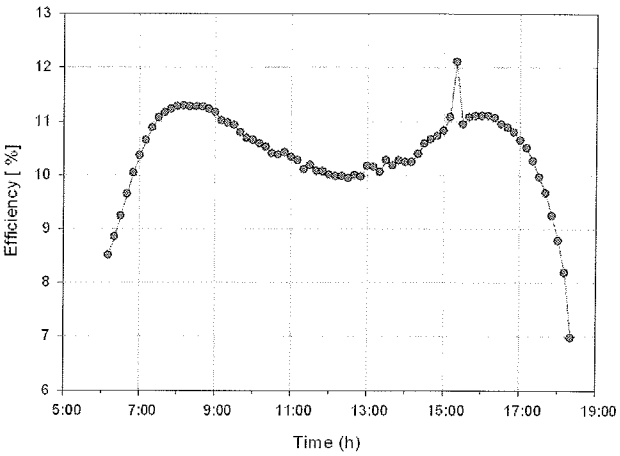

Fig. 4: PV panel efficiency during the clear sky day /4/

5 Trend in last decades

The trend of increasing global solar radiance exposure (Fig. 5) can partly be explained by the trend of the reduced fog occurrence over Slovenia /5/, yielding to the increase in solar energy seen during the last few decades.

5 Conclusions

The results of our present study can be compared with the ESRA - the European Solar Radiation Atlas /6/, as well as with a study for Slovenia from some decades ago /7/. The comparison with the ESRA shows that in December almost the whole of Slovenia is in the class 2.7-3.6 MJ/m^2 daily, except for the Julian Alps that are in the class 3.6-4.5 MJ/m^2 daily - our results show more details and for the basin the interval 2.3-2.9 MJ/m^2, the majority in an interval 2.9-

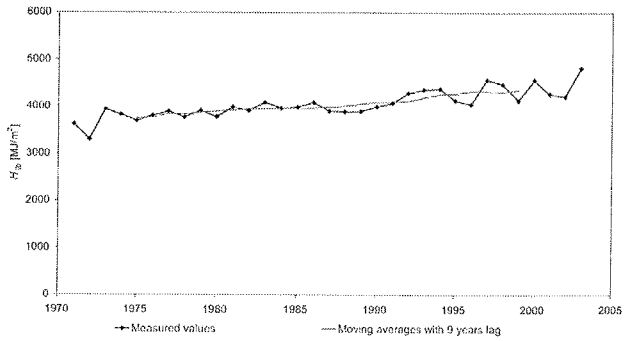

Fig. 5: Trend of solar global radiant exposure for Ljubljana in last decades /1/.

3.9 MJ/m^2, and with some maxima (mainly in the mountains) over 5 MJ/m^2 daily. In June, ESRA global solar radiance exposure in Slovenia is in four classes: the narrow coastal part 20.7-21.6 MJ/m^2, the rest of the Mediterranean part of the country 19.8-20.7 MJ/m^2, a belt from the Julian Alps to the SE and to the NE of the country with 18.9-19.8 MJ/m2, and the rest with 18.0-18.9 MJ/m^2 daily. Our results range from 5.8-24 MJ/m^2. So both of the results largely agree to a certain extent - but our study provides much more details.

Acknowledgements

Acknowledgements to Dr. Damijana Kastelec and to Dr. Klemen Zakšek, the coauthors of publication /1/.

References

/1/ Kastelec D, Rakovec J, Zakšek K. Sončna energija v Sloveniji (Solar energy in Slovenia). Ljubljana (Sl): Založba ZRC SAZU, 2009.

/2/ Carlson, DE, Lin G, Ganguly G. Temperature dependence of amorphous silicon solar cell PV parameters. IEEE Phot Spec C 2000; 28; 707-712.

/3/ Rakovec J, Zakšek K. Sončni obsevi različno nagnjenih in različno orientiranih površin (Solar radiance exposures of differently tilted and differently oriented surfaces). EGES 2008; 2: 93-95 and 3: 65-69.

/4/ J. Kurnik, M. Jankovec, K. Brecl, M. Topič, 2008: Development Of Outdoor Photovoltaic Module Monitoring System. Informacije MIDEM 38, 75-80.

/5/ Petkovšek Z., 1996: Urban climate change on a fog case. Proc. 14th Int. Cong. Biometeorol, 1-8 Sept 1996, Ljubljana, 306-310.

/6/ ESRA, 2000 - Schramer, K. and J. Greif, 2000: The European Solar Radiation Atlas. Ecole des Mines de Paris. Vol. 2: xii+296 pp.

/7/ Hočevar, A. in sod., 1980: Razporeditev potenciala sončeve energije v Sloveniji. VDO Biotehniška fakulteta, VTOZD za agronomijo, (Ljubljana), 69 str.

Jože Rakovec
Faculty of Mathematics and Physics,
University of Ljubljana
joze.rakovec@fmf.uni-lj.si

Prispelo (Arrived): 15.08.2009 *Sprejeto (Accepted): 09.10.2009*

HIGH PENETRATION OF PHOTOVOLTAIC SYSTEMS IN ELECTRICITY NETWORKS

[1]Hubert Fechner, [2]Christoph Mayr

[1]University of Applied Sciences Technikum Vienna, Austria
[2]Austrian Institute of Technology, Vienna, Austria

Key words: PV systems, electricity networks, smart grids

Abstract: While the global photovoltaic market is extremely growing and this technology is more and more seen as important future energy supply which will significantly contribute to the electricity generation, current electricity grids are not yet designed to integrate a steadily increasing penetration of photovoltaic generation. This manuscript discusses the main technical challenges as well as the currently ongoing international activities in this field in order to make the electricity grids smarter with a focus on inverter technology as key element in this process.

Visoka stopnja vključevanja fotonapetostnih sistemov v električno omrežje

Kjučne besede: PV sistemi, električna omrežja, pametna omrežja

Izvleček: Medtem, ko globalni trg fotovoltaike ekstremno narašča in fotovoltaika izgleda kot pomemben vir energije v prihodnosti, ki bo pomembno vplivala na proizvodnjo električne energije, električno omrežje ni načrtovano tako, da bi bilo pripravljeno na priključevanje vedno večjega števila fotonapetostnih elektrarn. Članek opisuje tehnične izzive in trenutne mednarodne aktivnosti na tem področju, kako narediti električna omrežja pametnejša. Poudarek je na tehnologiji razsmernikov kot ključnih gradnikov v procesu vključevanja.

1 Introduction

During the last 10 years, the global development of photovoltaic (PV) increased with higher growth rates than ambitious scenarios could foresee, mainly due to ambitious programs in two countries, Germany and Japan.

In the year 2008, for the first time a growth of the annual market of more than 100% was evident as in a number of additional countries support programs began to take effect. In total more than 14 GW are nowadays installed worldwide, most of them grid connected.

Main drivers are the outstanding features of this solar technology like availability of raw material (silicon as second most frequent element on the earth) the wide acceptance of application - even as architectural element in the design of buildings - as well as the clear future perspective of further increasing efficiencies and decreasing prices.

2 PV until 2020

The European Photovoltaic Industry Association as well as other institutions and national aims see market shares of up to 12% PV of the total electric power generation until 2020 achievable. /1/ /2/

The frame conditions to achieve this goal are:

- Cost competitiveness achieved mainly by larger production facilities, improved manufacturing and automatisation, and technological progress like increased efficiencies.
- Market deployment taking into account the added value of PV beyond energy like meeting the peak demand, reducing the burden of environmental cost, reduced fuel price risk, representing a green image and many more./3/
- Policy frameworks which need to be supportive by unbureaucratic feed-in tariffs or other measures until the cost competitiveness is given (grid parity).
- Interaction with other renewable generation in order to meet the whole requirements of the future electricity system mainly by renewable energy generation.
- The supply chain to bring up multi Gigawatt productions for an annual market of up to 160 GW until 2020. The availability of materials, the production capacities and the education needs to follow these strong scenarios of market development.
- Although mainly due to the daytime generation characteristics of PV, most electricity networks can absorb much more PV generation than other fluctuating production, the system integration of huge amounts of PV into the electricity networks needs specific requirements which will be discussed in more detail in the following chapters.

3 Challenges for electricity networks

While photovoltaic as distributed generation from renewable energy resources is seen as key element of future energy supply, current electricity grids are not designed to integrate a steadily increasing share of distributed genera-

tors. The hierarchical network topology was designed for unidirectional power flows and passive operation.

Photovoltaics, even though only currently contributing to less than one percent of the power generation in the overall electricity networks of countries show traditionally a very uneven appearance. This might lead to challenges which firstly appear only in some parts of the network mainly depending on the local condition of the grid.

Overvoltage:

Local distribution networks soon can be fed by solar power to an amount which pushes the local voltage level beyond its limits laid down e.g. in the EN 50160 standards. The overvoltage concern is mostly the top priority challenge in PV interconnection. Overvoltage problems are more likely to occur on rural grid, where the line impedance is higher and the load is relatively low. One solution to overcome this problem is currently used in Japan, where inverters reduce the active output power when a certain voltage threshold is exceeded. However, with this approach, the owner of the PV system is facing disadvantages with reduced income from his PV generation. /4/

The following graph shows the change of a local distribution network from typical passive networks with load only to active networks with bidirectional power flow due to distributed generation in the low (and medium) voltage level.

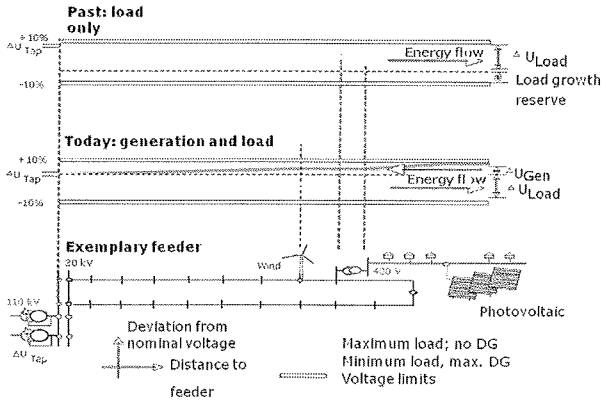

Fig. 1: Transition from passive to active distribution networks /5/

Harmonics:

While the impact of harmonics was a high concern in the beginning of PV grid interconnection, it is now extremely small with the recent advancements in power electronics and other technologies. Meanwhile, modern inverters are even capable to filter harmonics out of the grid, which are caused by various consumer applications.

Safety:

Unintentional islanding in distribution networks due to the presence of PV generation is one of the major safety concerns for the grid interconnection of generators. Although the possibility of unintended islanding operations is very small, the probability to encounter an island is not negligible. The risks involved if unintended islanding does occur are great.

Protection methods to the standard voltage and frequency monitoring are required in order to detect a loss of mains at the generator and ensure the safety of customers and maintenance personnel.

There are significant differences between national interconnection requirements in the recognition of the problem's importance which causes troubles mainly for international inverter manufacturers. /6/

Further aspects:

Beside concerns of the impact to the general voltage level, the behavior during grid faults like voltage sags /7/ and other grid interaction (reactive power, voltage unbalance,...) have to be taken into account at high levels of PV penetration in local grid situations.

Stability problems might occur if simultaneous loss of a large number of distributed PV-generation in higher level networks happens. Therefore, inverters must be able to provide a coordinated and/or local grid management, also to not disconnect at the first occurrence of a grid disturbance.

In order to avoid excessively expensive grid reinforcements, new solutions for active grid operation will be necessary.

The development of photovoltaic inverters, from simple conversion of direct current into the alternating current of the public grid with highest efficiency under sometimes frequently changing solar conditions ("maximum power point tracking", MPPT) to multifunctional inverters now able to support the local grid situation is indeed remarkable:

The new generation of high quality inverters is now capable to actively contribute to grid stability by power and frequency control, reactive power management, coordinated voltage control as well as by a sophisticated fault ride through capability. Power quality is addressed mainly by the already mentioned filtering of harmonics as well as compensation of voltage unbalance in three phase network. An additional function will be to contribute to the short circuit current.

Germany, one of the leading countries in photovoltaic has recently issued the Interconnection requirements for generators connected to the Medium Voltage Network based on the Transmission Code 2007 (TC 2007). This document might show the way of PV interconnection in the future and further encourages or rather makes high demands on the inverter manufacturers to develop innovative products.

4 Positive effects for the electricity networks

Predominantly, the supply profile of PV systems fits well to most of the load profiles in industrial countries with a load peak around noon. The currently increasing application of air conditioning systems leads to the fact that these peaks are getting even higher and higher. The energy demand for Air-conditioning corresponds quite well with the solar irradiation which is directly linked to the power generation of grid connected PV systems.

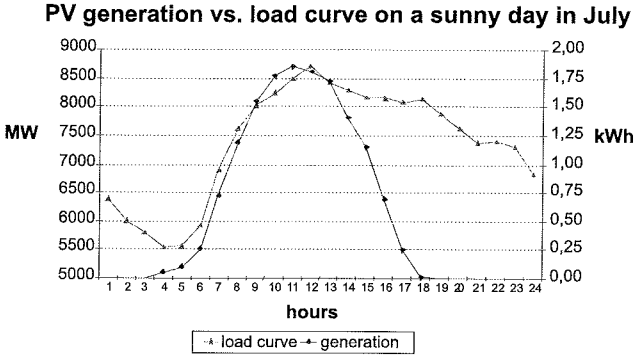

Fig. 2: PV generation versus typical load /2/

Besides matching some peak load situations quite well, there could be some other positive effects for the electricity networks:

- Reduction of network losses due to more local generation and therefore decreased power transmission
- More transmission capacity opens space for other transmission services
- Active network services from multifunctional photovoltaic inverters can support the local network management

However, most of these functionalities will only be effective in high penetration scenarios. /8/

5 Key requirements for electricity networks in order to cope with high penetration of PV

Beside multifunctional inverters as the main link to the electricity network, there are several further requirements for the networks in order to be well prepared for a high penetration photovoltaic scenario:

- The European Technology Platform Smart Grids estimates that until 2030 investments in European electricity networks of approximately 500 Billion Euro will be necessary. In this context, the replacement of old infrastructure needs to be innovative to maximize capacity and functionality for high penetration of photovoltaics and other distributed generation.

Especially the distribution networks will require major communication infrastructure improvements to better make use of the fluctuating generation from photovoltaics by allowing active demand participation.

This "empowering of the customers" comprises the choice of managing the cost and the peak demand by e.g. different tariffs (Time of use, peak pricing,...) communicating programs (e.g. intelligent heating systems), as well as various energy information systems that eases energy saving. Smart metering might play an important role in this context.

- Forecasting programs will allow better PV generation prediction and help to optimize the total power management.
- The use of storage capacities might further help to integrate large amount of PV into the electricity system. The intensive E-mobility discussion we are currently facing with the probability of the future appearance of huge battery capacities need to be more closely linked to the requirements of PV generation.

6 Currently ongoing activities

The International Energy Agency (IEA) has recently started an initiative dealing with "High penetration of photovoltaic systems in electricity networks" within the "Photovoltaic Power System Program" (IEA-PVPS). The new task is currently under development and will bring together experienced researchers, industry and network operators from all countries which show a good development in the penetration of grid connected photovoltaic.

The main topics which are dealt within this new activity are

- PV generation in correlation to energy demand focusing on the consumer behavior to be better linked to the generation profile
- The effects on PV generation to the local grid as well as to the general electricity system
- Smart inverter technology dealing with requirements for inverters at high PV penetration as well as
- Economics and needs in Standardization and Regulation

Modeling and simulation are tackled in this global research initiative as well.

Other activities like the IEA ENARD Implementing agreement (Electricity Networks, Analysis, Research and Development) are dealing with renewable energy integration in distribution networks more generally (ENARD Annex II – DG System Integration into Distribution Networks) or European research projects like: META PV or PV UPSCALE.

In the United States, the Solar Energy Technology Program (SETP), within the Department of Energy Office, conducts research, development, demonstration and deployment activities to accelerate widespread commercializa-

tion of clean solar energy technologies (PV and concentrating solar power /CSP/) across America. Systems integration has placed high importance on working with utilities, industry, and other stakeholders to develop the technologies and methods enabling the widespread deployment of distributed PV technologies, including storage systems, advanced power electronics, and controls, into the U.S. electricity grid.

6 Conclusion

PV in high penetration as significant source of electricity production might appear most probably in the next decade.

However some challenges in interacting with the electricity network needs still to be addressed.

New inverter technology offers a wide range of services dedicated to an unproblematic interoperation of photovoltaic systems with the electricity network.

Generally, the technical solutions seems not to be the main barriers for high penetration of PV, but standardization, regulation as well as new market models needs to be developed. The necessary refurbishment of the European electricity network in the upcoming years should take into account the needs and requirements due to decentralized generation, predominantly by the integration of communication technologies.

International collaboration is already established in order to ease the way and derive benefit from first experiences already made in other countries and regions.

References

/1/ Set for 2020 - Solar photovoltaic electricity, a mainstream power source in Europe by 2020, European Photovoltaic Industry association, 2009

/2/ H.Fechner et. al., Austrian PV Technology Roadmap, Austrian Ministry of Transport, Technology and Innovation 2009

/3/ Demet Suna, Reinhard Haas and Assun Lopez Polo, Analysis of PV System's Values beyond energy, IEA PVPS Task 10, Report IEA-PVPS T10-02:2008, March 2008

/4/ Overcoming PV grid issues in urban areas an IEA PVPS Task 10 Urban Scale PV report, September 2009

/5/ Helfried Brunner, arsenal research - Austrian Institute of Technology and Wolfgang Prüggler, Energy Economics Group TU Wien, 2008

/6/ Brundlinger, R., Bletterie, B., arsenal research, Unintentional islanding in distribution grids with a high penetration of inverter-based DG: Probability for islanding and protection methods, Powtech 2005, St.Petersburg

/7/ B. Bletterie, R. Bründlinger, H. Fechner; "Sensitivity of photovoltaic inverters to voltage sags - test results for a set of commercial products"; 18. International Conference on Electricity Distribution, 06.-09.06.2005, Turin, Italy

/8/ M. Braun, T. Degner, T. Glotzbach, Y.-M. Saint-Drenan, Wertigkeit von PV-Strom, Nutzen durch Substitution des konventionellen Kraftwerkparks und verbrauchsnahe Erzeugung, Institut für Solare Energieversorgungstechnik (ISET) e.V., Kassel 2008

Hubert Fechner, University of Applied Sciences
Technikum Vienna, Austria
Giefinggasse 6, A-1210 Vienna,
E-mail: hubert.fechner@technikum-wien.at
Ph: ++43-1-333-4077-572

Christoph Mayr, Austrian Institute of Technology,
Giefinggasse 2, A-1210 Vienna,
Ph: ++43-50550-6633
E-mail: christoph.mayr@ait.ac.at

Prispelo (Arrived): 15.08.2009 *Sprejeto (Accepted): 09.10.2009*

IMPACT OF GRAIN BOUNDARIES ON THIN-FILM PHOTOVOLTAICS

James R. Sites

Physics Department, Colorado State University, Fort Collins, USA

Key words: grain boundaries, CIGS, CdTe Solar cells, rekombinations

Abstract: Grain boundaries in CIGS and CdTe appear to have radically different impact on the solar-cell voltage and fill factor. The proposed explanation is that the valence-band energy in the vicinity of CIGS grain boundaries is shifted downwards, hence keeping the holes in the p-material away from the grain boundaries and potential recombination. Such grain boundaries appear to be an anomalous situation, which would not apply to CdTe and other thin-film polycrystalline materials. The suggestion to avoid grain-boundary recombination in CdTe cells is to construct a fully depleted absorber with an electron reflector layer at its rear surface.

Vpliv mej med zrni na tankoplastno fotovoltaiko

Kjučne besede: meje zrn, rekombinacije, CIGS, CdTe sončne celice

Izvleček: Meje kristalnih zrn v polikristalnih CIGS ali CdTe sončnih celicah izkazujejo popolnoma različen vpliv na napetost odprtih sponk in polnilni faktor. Članek utemeljuje razlike z razlago, da je energija valenčnega pasu v bližini mej zrn CIGSa znižana, kar zadržuje vrzeli v p-materialu proč od mej zrn in potencialnih rekombinacij. Takšna sprememba energije valenčnega pasu izgleda neobičajna in se ne pojavlja v CdTe in ostalih polikristalnih tankoplastnih materialih. Da bi se izognili rekombinacijam na mejah zrn v CdTe je potrebno zgraditi popolnoma osiromašeno absorpcijsko plast z elektronsko odbojno plastjo za proste elektrone na zadnji strani.

1 Introduction

Thin-film polycrystalline solar cells have a typical grain, or crystallite, size the order of 1 μm. This means that approximately 1% of their atoms are located on a grain surface, and the likely possibility of extraneous electron states suggests that photovoltaic performance may be seriously compromised. In practice, however, the record-performance $Cu(In,Ga)Se_2$ (CIGS) solar cells have shown voltages very close to their crystalline counterparts, diode quality factors suggestive of minimal junction recombination, and efficiencies of near 20% /1/. In contrast, the other leading thin-film material, CdTe, has a record voltage well below that of similar band-gap crystalline cells, a diode-quality factor dominated by recombination, and an efficiency of 16.5% /2/.

If one looks at SEM cross-sections of CIGS and CdTe cells, their micron-scale structure appears remarkably similar. However, instead of the record CdTe efficiency being 3% larger than CIGS, as the two band gaps would predict, it is more than 3% smaller. This difference is dramatically illustrated in Fig. 1, where the voltage deficit for the CdTe cell is 200 mV greater than that for CIGS and the primary cause of the difference in efficiency.

The purpose of this presentation is to explore what one might expect for thin-film polycrystalline solar cells, to explain why there is such a dramatic difference between results to date with CIGS and CdTe, and suggest a strategy for eliminating that difference.

2 CIGS: the anomoly

The large voltages achieved by CIGS solar cells suggest that the grain boundaries (GB) have only a minimal effect on their voltage and fill factor. More quantitatively, one can calculate the upper limit of grain-boundary recombination velocity (S_{gb}) that would allow the voltage and fill-factor and fill-factor achieved in Ref. /1/. That value would be the order of 10^3 cm/s /3/, which would imply that only about 0.01% of the carriers entering the diode depletion region contribute to the cell's forward current through recombination. That fraction is implausibly low, especially since the comparable S_{gb} for the highest efficiency CdTe cells, and by inference other micron-scale-grain materials, must be the order of 10^6 cm/s. A possible explanation is that the carriers (holes) are blocked by an internal potential from reaching the CIGS grain boundaries.

One mechanism that might keep the holes from reaching the CIGS GBs is a positive sheet of charge at the GB. This mechanism is appealing, because the internal surfaces in p-type material may be positively charged. However, this mechanism in itself does not explain the high the voltages observed. In fact, a GB with positive charge will allow additional forward-current recombination and result in smaller voltage than for the equivalent neutral GB /3/. Physically, the same potential that assists collection by channeling the photogenerated electrons and holes will in forward bias provide channels for electrons and holes to flow in the opposite direction, allow greater recombination, increase the forward current, and hence reduce V_{OC}.

A more likely explanation for the benign nature of CIGS GBs is reduced valence-band energy in the vicinity of a

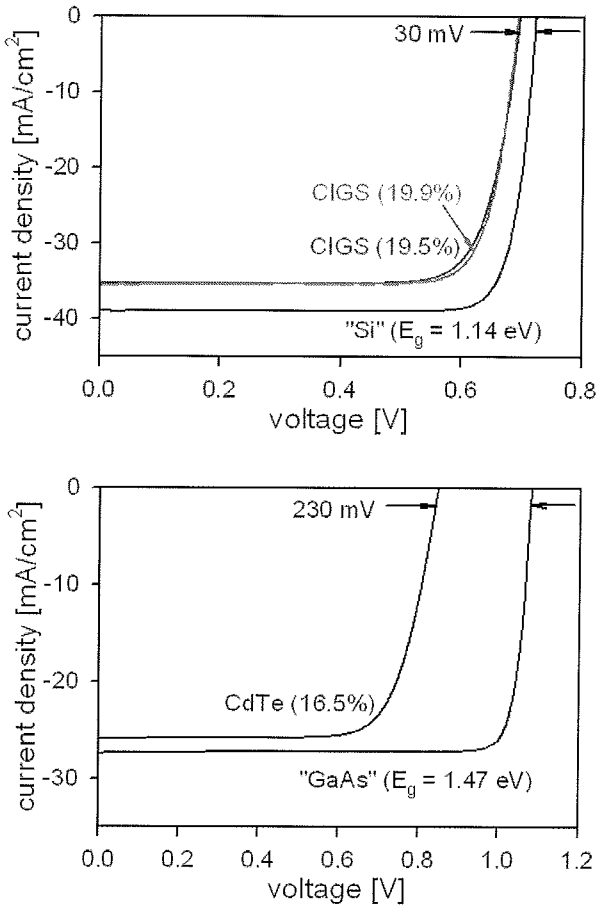

Fig. 1: Current-voltage of record-efficiency CIGS and CdTe cells compared to crystalline cells with small adjustments made for band-gap differences.

GB without an equivalent reduction in the conduction band /3/. This scenario is consistent with theoretical analysis of CIGS surfaces and interfaces, where a copper deficit results in an expanded band gap with a lower valence band /4/. It is also supported by experimental measurements of copper deficiency near GBs in CIGS /5/.

Reduction in the valence band by ΔE_V near a GB and the calculated impact on the J-V curves are shown in Fig. 2. For S_{gb} of both 10^5 and 10^6 cm/s, the voltage and efficiency should approach the values for the GB-free case when ΔE_V is approximately 0.3 eV or larger.

The Fig. 4 curves are reasonably independent of the ΔE_V shape or width, and they are little changed if a modest GB charge is superimposed on the downward expansion of the band gap. Although high voltages and efficiencies experimentally observed with CIGS solar cells could be explained by a very small value of grain-boundary recombination velocity, it seems much more likely that it is the result of the band-gap expansion.

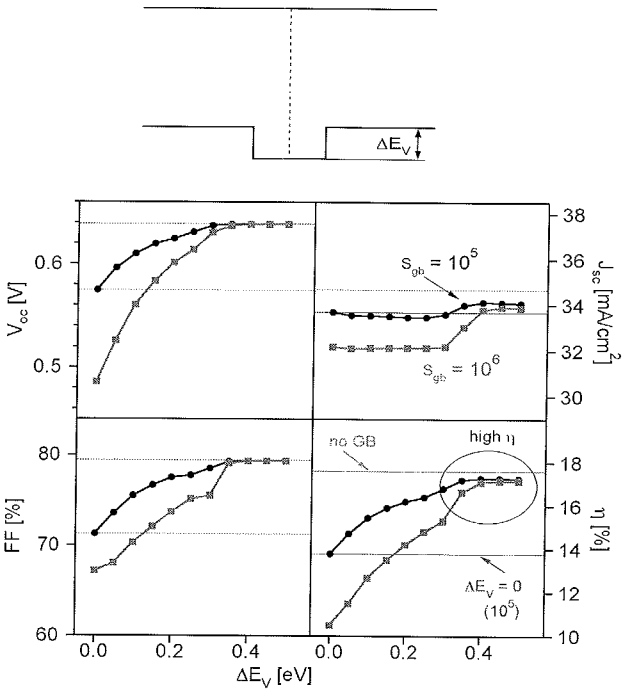

Fig. 2: Current-voltage parameters as a function of valence-band reduction (shown schematically above). The values of S_{gb} are those that would apply if the GB were not shielded by ΔE_V. (From Ref. /3/).

3 CdTe: What can be done?

If thin-film polycrystalline CdTe is the normal situation and has a high GB recombination velocity, is there anything to be done to improve on the voltage and efficiency that has been achieved to date? One strategy would be to substantially reduce the GB defects, increasing both hole density and carrier lifetime (hence reducing S_{gb}), and essentially make the thin-film CdTe similar to crystalline GaAs. This strategy, however would require nearly a three-order-of-magnitude increase in lifetime and two in carrier density, essentially replicating CIGS values. Such increases are probably not realistic.

An alternative possibility is to expand the conduction band at the back of the CdTe layer, perhaps by alloying with Zn or Mg, to introduce an electron reflector that keeps the photogenerated electrons away from the back metallic contact. This situation is illustrated in Fig. 3, where the barrier has allowed the cell to be in larger forward bias before the forward current limits V_{OC}.

For the electron-reflector strategy to be successful, it is necessary for the CdTe to be fully depleted at the operating voltage so that the internal field will compensate for the relatively low carrier lifetime. In this respect, the low carrier density of CdTe cells (~10^{14} cm^3) is advantageous, since the depletion width at zero bias is 1 to 2 μm. To assure the full depletion, however, it would be advisable to keep the CdTe-layer thickness close to 1 μm.

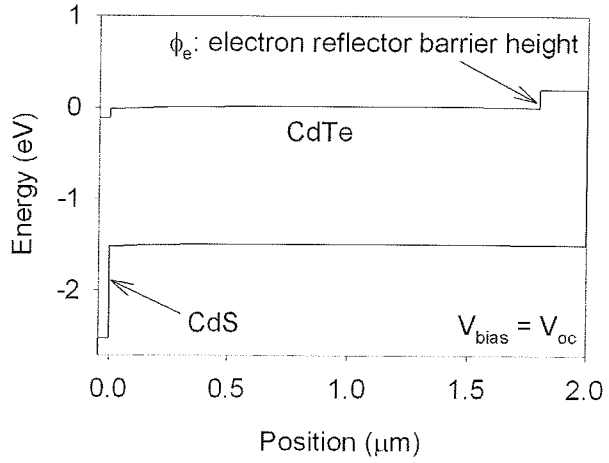

Fig. 3: Schematic of electron-reflector strategy to enhance CdTe voltage and efficiency.

Fig. 4 shows the calculated value of voltage for CdTe cells with and without the electron barrier φ_e. Without it, the voltage for cells with lifetime $\tau \sim 1$ ns is similar to that of today's high-efficiency cells. With the barrier, the voltage should approach that of crystalline material, but further improvement is not predicted for barriers much above 2 eV.

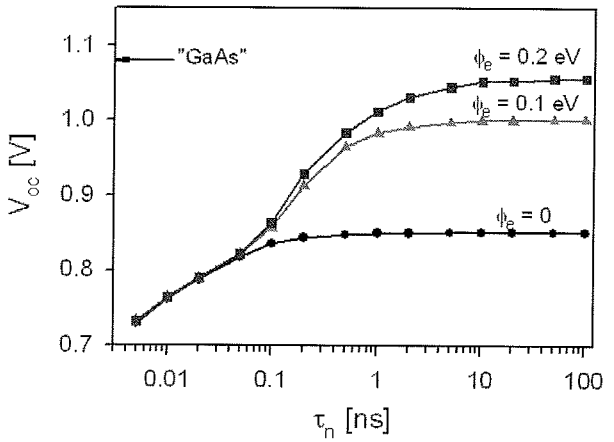

Fig. 4: Calculated CdTe voltage as a function of electron lifetime τ and reflection-barrier height φ_e. From Ref. /6/. Full depletion is assumed.

Although the electron-reflector structure would predict a high voltage, its fill-factor will remain lower than optimal unless the CdTe lifetime is increased somewhat above 1 ns. Nevertheless, it should be possible without the need for a major improvement in the quality of thin-film CdTe to reach one volt and 20% efficiency.

4 Conclusions

The reason for the large difference in voltage deficit, and hence efficiency, between polycrystalline CIGS and CdTe solar cells is that CIGS appears to have a fortuitous reduction in valence band near its grain boundaries that reduces the effective grain-boundary recombination velocity to 1000 cm/s or below. Polycrystalline CdTe does not have this feature, and the CdTe hole density is typically two orders of magnitude below that of CIGS. To significantly increase CdTe voltage, a different device structure based on an electron reflector at the back surface is advised.

Acknowledgments

This work was supported by the U.S. National Renewable Energy Laboratory through its Thin-Film Partnership program. The author is particularly grateful to Dr. Markus Gloeckler, Dr. Jun Pan, and Mr. Kuo-Jui (Ray) Hsiao for their contributions to the work presented here.

References

/1/ I. Repins, M.A. Contreras, B. Egaas, C. DeHart, J. Scharf, C.L. Perkins, B. To, and R. Noufi, "19.9%-Efficient ZnO/CdS/CuInGaSe$_2$ Solar Cell with 81.2% Fill Factor," *Prog. Photovolt: Res. Appl.* **16**, 235 (2008).

/2/ X. Wu, J.C. Keane, R.G. Dhere, C. DeHart, D.S. Albin, A. Duda, T.A. Gessert, S. Asher, D.H. Levi, and P. Sheldon, "16.5% Efficient CdS/CdTe Polycrystalline Thin-Film Solar Cell" *Proceedings of the 17th European Photovoltaic Solar Energy Conference,* (WIP, Munich, 2001) p. 995

/3/ M. Gloeckler, J.R. Sites, and W.K. Metzger, "Grain-Boundary Recombination in Cu(In,Ga)Se$_2$ Solar Cells," J. Appl. Phys. 98, 113704, (2005).

/4/ C. Perrson and A. Zunger, "Anomalous Grain Boundary Physics in Polycrystalline CuInSe$_2$: The Existence of a Hole Barrier," *Phys. Rev. Lett.* **91**, 266401 (2003).

/5/ M.J. Hetzer, Y.M. Strzhemechny, M. Gao, M. Contreras, A. Zunger, and L.J. Brillson, "Direct Observation of Copper Depletion and Potential Changes at Copper Indium Diselenide Grain Boundaries," *Appl. Phys. Lett.* **86**, 162105 (2005).

/6/ J.R. Sites and J. Pan, "Strategies to Increase CdTe Solar-Cell Voltage," *Thin Solid Films* **515**, 6099-6102 (2007).

James R. Sites
Physics Department, Colorado State University, Fort Collins, CO 80523 USA

Prispelo (Arrived): 15.08.2009 *Sprejeto (Accepted): 09.10.2009*

THIN-FILM SILICON SOLAR CELLS: STABILITY AND LIGHT TRAPPING

M. Zeman[1], G. van Elzakker[1], P. Sutta[2], O. Isabella[1], J. Krc[3]

[1]Delft University of Technology, PVMD /DIMES, Delft, Netherlands
[2]University of West Bohemia, NTRC, Plzeň, Czech Republic
[3] University of Ljubljana, Faculty of Electrical Engineering, Ljubljana, Slovenia

Key words: thin film silicon, stability, light trapping

Abstract: Thin-film silicon solar cell technology is one of the promising photovoltaic technologies for delivering low-cost solar electricity. Today the thin-film silicon PV market (402 MW_p produced in 2008) is dominated by amorphous silicon based modules; however it is expected that the tandem amorphous/microcrystalline silicon mo-dules will take over in near future. The properties of silicon films grown from the mixture of hydrogen and silane will be discussed and the solar cell behavior will be presented. In order to increase the absorption in thin absorber layers novel approaches for photon management inside solar cells are developed. In this article i) optimal surface texture of the electrodes for introducing efficient light scattering and ii) development and implementation of optically-active layers for enhanced reflection at the back contact are presented.

Tankoplastne silicijeve sončne celice: Stabilnost in ujetje svetlobe

Kjučne besede: tankoplastni silicij, stabilnost, ujetje svetlobe

Izvleček: Tehnologija tankoplastnega silicija je ena izmed obetajočih tehnologij za proizvodnjo poceni električne energije. Na današnjem trgu fotovoltaike iz tankoplastnega silicija (proizvedenih 402 MW_p v letu 2008) prevladujejo moduli iz amorfnega silicija, dasi se pričakuje, da bodo tandemske strukture amorfni/mikrokristalni silicij prevladovale v bližnji prihodnosti. V članku so obravnavane lastnosti silicijevih plasti narejene iz mešanice vodika in silana ter predstavljeno delovanje sončnih celic. Za povečevanje absorpcije v tanki absorpcijskih plasteh so razvite nove tehnike ujetja fotonov. V članku je predstavljena: i) optimalna teksturizacija elektrod za učinkovito sipanje svetlobe, ii) razvoj in uporaba optično aktivnih plasti za povečanje odbojnosti zadnje plasti.

1 Introduction

In 1975 Walter Spear and Peter LeComber reported that amorphous silicon had semiconducting properties. They demonstrated that the conductivity of amorphous silicon can be manipulated by several orders of magnitude by adding some phosphine or diborane gas to the glow discharge gas mixture /1/. This was a far-reaching discovery since until that time it had generally been thought that amorphous silicon could not be made *n*-type or *p*-type by substitutional doping. In fact, amorphous silicon suitable for electronic applica-tions, where doping is required, is an alloy of silicon and hydrogen. The electronic-grade amorphous silicon is therefore called hydrogenated amorphous silicon (*a*-Si:H).

The successful doping of amorphous silicon created tremendous interest in this material for two reasons. First, the material had several interesting properties that opened up many opportunities for semiconductor device applications. For example, due to the high absorption coefficient of *a*-Si:H in the visible range of the solar spectrum, a 1 mm thick *a*-Si:H layer is sufficient to absorb 90% of the usable solar energy. Second, the glow discharge deposition technique, also referred to as plasma enhanced chemical vapour deposition (PECVD), enabled the production of *a*-Si:H films over a large area (larger than 1 m^2) and at a low temperature (100°C to 400°C). The low processing temperature allows the use of a wide range of low-cost substrates such as a glass sheet, a metal or a polymer foil. The *a*-Si:H is simply doped and alloyed by adding appropriate gases to a source gas, usually silane. These features have made *a*-Si:H a promising candidate for low-cost thin-film solar cells.

The first *a*-Si:H solar cell was made by Carlson and Wronski in 1976 and exhibited an energy conversion efficiency of 2.4% /2/. The University of Neuchâtel introduced a micromorph tandem solar cell in 1994, which comprised an *a*-Si:H top cell and a hydrogenated microcrystalline silicon (μc-Si:H) bottom cell /3/. Thin-film silicon solar cell technology has improved considerably, and today, it is capable of producing solar cells with initial efficiencies exceeding 15% /4/. It has also matured as production technology that delivered modules with a total output power of 402 MW_p in 2008 /5/. Based on the companies' announcements the production capacity of thin-film silicon modules is expected to grow to almost 8 GW in the year 2010. The thin-film silicon PV market is dominated by amorphous silicon based modules; however it is expected that the micromorph tandem modules will take over in near future. Two manufacturing methods for thin film silicon solar cells can be distinguished; the silicon-on-glass approach and the roll-to-roll approach, in which solar cells are deposited on flexible substrates.

A drawback of the *a*-Si:H silicon solar cell technology is a relatively low stabilized efficiency of modules that varies between 5 to 8%. A challenge of this technology is to suppress the light-induced degradation of amorphous silicon solar cells. A widely used method for obtaining more stable *a*-Si:H material is based on applying hydrogen dilution of silane during its growth. In this article the properties of silicon films grown from the mixture of hydrogen and silane are discussed and the performance of solar cells with hydrogen diluted absorber layers is presented.

An efficient utilization of the sun spectrum is a key issue in the field of thin-film silicon solar cell technology. The tandem approach employing the combination of amorphous silicon and microcrystalline silicon absorber layers offers an improved performance of the modules reaching efficiencies above 10%. The tandem approach allows using thinner absorber layers in the component cells that contributes to a suppression of light induced degradation of *a*-Si:H component cell. When applying thinner absorber layers photon management becomes very important for increasing the absorption in the absorber layers. In this article two novel approaches for photon management are discussed: i) optimal surface texture of the substrates for introducing efficient light scattering and ii) development and implementation of optically-active layers based on 1-D photonic crystals for enhanced reflection at the back contact.

2 Improved stability of *a*-Si:H films

It has been demonstrated that solar cells with *a*-Si:H absorber layers prepared from silane diluted with hydrogen in plasma-enhanced chemical vapor deposition (PECVD) showed less degradation during light exposure than solar cells with undiluted absorbers /6,7/. This *a*-Si:H material is referred to as protocrystalline silicon (pc-Si:H) due to the fact that it will eventually evolve from the amorphous to microcrystalline phase when grown to a sufficient thickness /8,9/.

2.1 Experimental details

Individual hydrogenated silicon films and solar-cell absorber layers were deposited under the following deposition conditions; an rf-power of 4 W, a silane (SiH_4) flow of 5 sccm, a substrate temperature of 180°C. The hydrogen dilution is expressed by the dilution ratio R, which is defined as $R=/H_2///SiH_4/$. The dilution was varied between R > 0 and R = 40. An undiluted reference film (R = 0) was grown at a different pressure of 0.7 mbar and a SiH_4 flow of 40 sccm. The thickness of all films was ~ 300 nm, which corresponds to the thickness of the absorber layer in solar cells. In order to obtained 300 nm thick pc-Si:H films at all R the chamber pressure of 2.6 mbar was used. The individual films were deposited on Corning Eagle 2000 type glass substrates and on crystalline silicon (c-Si) substrates coated with a 20 nm thick *a*-Si:H layer grown from pure silane.

Single junction p-i-n solar cells were deposited on Asahi U-type substrates using the above described films as the absorber layers. The solar cells have the following structure: p-type *a*-SiC:H layer (10 nm)/*a*-SiC:H buffer layer/ intrinsic absorber layer (300 nm)/n-type *a*-Si:H layer (20 nm). The back contact consists of 300 nm aluminum. The external parameters of the solar cells (efficiency ç, fill factor *ff*, short-circuit current density J_{SC}, open-circuit voltage V_{OC}) were determined from I-V measurements using an Oriel Corporation solar simulator. The solar cells were degraded at a constant temperature of 50 şC with halogen lamps using a power density of 100 mW/cm^2.

The structural properties of the films were studied by X-ray diffraction (XRD) analysis using an automatic powder diffractometer X'pert Pro in asymmetric goniometer configurations with CuK-alpha radiation (lambda = 0.154 nm).

2.2 Structural properties of *a*-Si:H films

The XRD technique was used to study the influence of hydrogen dilution of silane on the structural properties of pc-Si:H films. In particular the narrowing of the first scattering peak (FSP) in the XRD spectra was investigated since this parameter is used as an indication of an improved medium range order (MRO). Figure 1 shows the FSP of the pc-Si:H film prepared at R=20. The procedure to obtain this XRD pattern is described elsewhere /10/.It was found that the FSP peak of all films of the dilution series could be fitted with a large-area peak centered around 27.5 degrees and a smaller peak centered around 32.5 degrees. In figure 1 the XRD patterns for crystalline silicon (Si) and crystalline silicon hydride (Si_4H) standards are included.. Comparing the standards to the measured XRD patterns we find a striking match between the position of the two Pearson VII functions and the silicon hydride lines, while the silicon (111) line clearly does not correspond to the center position at 27.5 degrees. Given the controversy regarding the origin of the *a*-Si:H FSP /11/, this result provides an interesting new interpretation of the ordered domains in the amorphous matrix. A good agreement between the position of the peaks of the measured lines and the standard XRD patterns of the silicon hydride provides evidence that the diffracting signal comes mainly from ordered domains of a tetragonal silicon-hydride /12/ and not from ordered domains of silicon.

The dominant peak at 27.5 degrees was used for the further analysis of the structural properties. Figure 2 shows the FWHM values of this peak as a function of R. The figure demonstrates that the FWHM decreases with increasing R from 0 to 20, and remains nearly constant when R is further increased from R = 20 to R = 40. This confirms previous reports about the narrowing of the FSP /10/, but shows for the first time that this effect saturates for a certain value of R.

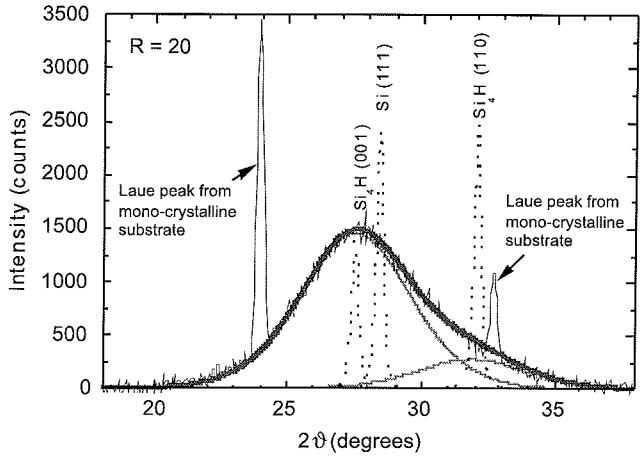

Fig. 1: XRD patterns of the FSP measured on a 300 nm thick pc-Si:H film deposited at R=20 on a c-Si substrate. Also shown are the XRD lines for crystalline Si and Si_4H standards.

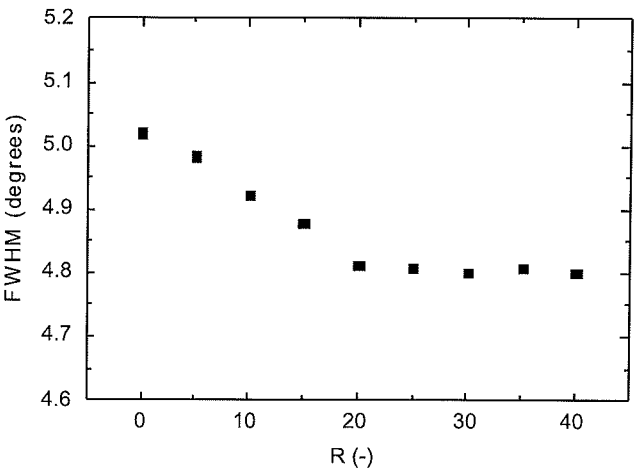

Fig. 2: FWHM values of the FSP as a function of R of the pc-Si:H films deposited on a c-Si substrate.

2.3 Degradation behavior of *a*-Si:H solar cells

The *a*-Si:H films prepared from hydrogen diluted silane were implemented as absorber layers in *p-i-n* solar cells. The solar cells were subjected to a degradation experiment. Figure 3 shows the evolution of the solar cell efficiency with the exposure time. In Fig. 3 the efficiency is normalized to the initial value before degradation. The degradation experiment confirms that the cells with absorber layers deposited using hydrogen dilution are more stable to light exposure. A clear reduction of the degradation is already observed when the dilution ratio is increased from R = 0 to R = 10 and the degradation is further suppressed when R is increased to 20. However, solar cells with absorber layers prepared at R > 20 exhibit similar degradation behavior as the cell with the absorber layer prepared at R = 20. The efficiency of the solar cells with absorber layers prepared at R ≥ 20 stabilizes at around 88% of their initial efficiency.

The similar degradation behavior of solar cells with absorber layers deposited at R ≥ 20 indicates that there is a correlation with the structural properties observed for the individual films. The saturation of the FWHM value of the FSP for pc-Si:H films prepared at R ≥ 20 is a strong indication that the structural order has achieved an optimal state in these films. The improved structural order contributes to suppressing the light induced degradation by de creasing the amount of weak Si-Si bonds which are removed by hydrogen etching of the growing surface /13/.

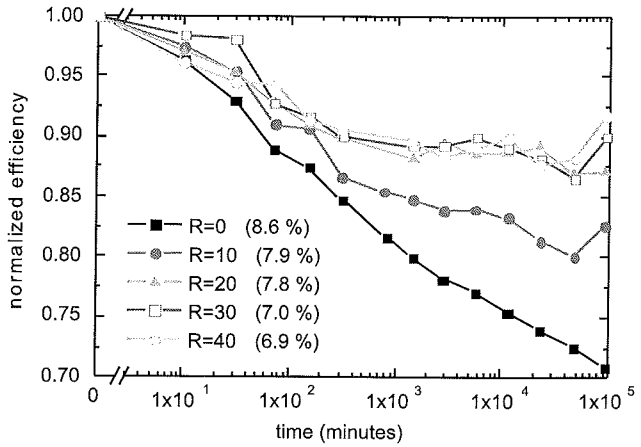

Fig. 3: Normalized η of diluted a-Si:H solar cells as a function of illumination time. The initial values of η are given in brackets.

However, the improved structural order in amorphous films still does not prevent the occurrence of the degradation. The mechanisms that initiate the degradation have to be further investigated in order to fully prevent it.

3 Advanced light trapping

At present, further development and implementation of efficient light trapping is considered the most important research area in the field of thin-films silicon solar cells. Light-trapping techniques help to capture light in the desired parts of a solar cell, which are the absorber layers, and prevent it from escaping. Efficient light trapping in thin-films silicon solar cells is based on scattering of light at rough interfaces and the employment of high-reflective back contacts and refractive-index matching layers in order to manipulate reflection in the cell. Scattering of light at rough interfaces results in a longer average optical path through the absorber layers. Repeated reflection at the back and front contacts causes multiple passes of light through the absorber layer. These processes determine an efficient light confinement that substantially enhances light absorption in the absorber layer and increases the photocurrent of the solar cell. In the case of tandem devices, the challenge of light scattering is to optimize the absorption for the top and the bottom cells. Any pass of light from the front to the back contact of the cell is accompanied by an absorption loss in the metallic back contact.

Minimizing optical losses at the back side of the solar cells has become an important issue and in this sense engineering of dielectric (theoretically absorption-free) back reflectors is a key topic.

In this article three novel light-trapping techniques for manipulating light inside solar cells are presented. The first technique deals with the manipulation of light scattering at rough interfaces inside a solar cell. The surface texture of these rough interfaces is so designed that light is scattered into (pre) selected angles. We shall refer to this approach as the **angle-selective** management of scattered light at surface-textured interfaces. The second technique treats the **modulated surface textures**, which are a combination of large and small surface features of substrate carriers. The modulated surface-texture substrates allow light scattering in a broader range of wavelengths. The third technique deals with the manipulation of reflection and transmission at a particular interface inside a solar cell. This specially designed *optical interface* results in a **wavelength-selective** management of (high) reflection or transmission of light. In this article the periodically-designed surface textures, such as periodic gratings, are representatives of the first technique, textured glass substrates coated with an etched aluminum-doped zinc oxide (AZO) are examples of the modulated surface textures, and the one-dimensional (1-D) photonic-crystal-like (PC) structures are introduced as the *optical interfaces* for the realization of the third technique.

3.1 1-D periodic diffraction gratings

Diffraction gratings were introduced into thin-film solar cells in order to achieve better control of light scattering inside the cells. The switch from randomly-textured surfaces to 1-D periodic gratings allows to suppress the total reflection in the wavelength region of interest and to scatter light into (pre) selected angles by manipulating geometrical parameters *P* and *h* of the gratings /3//7/. Figure 4 shows the surface morphology of a periodic grating patterned in a lacquer on glass substrate that was characterized by Atomic Force Microscopy (AFM).

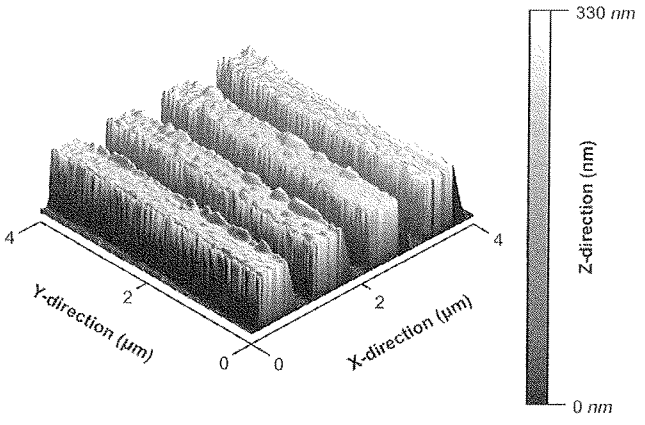

Fig. 4: 3D-view of a grating with P = *1000 nm and* h = *300 nm.*

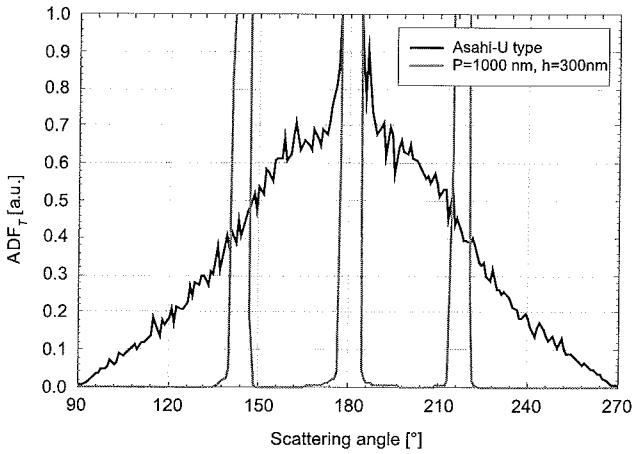

Fig. 5: ADF_T *(at 633 nm) of Asahi-U type substrate and grating (*P = *1000 nm and* h = *300 nm).*

The understanding of scattering properties of 1-D gratings is important in order to make a right choice of the *P* and *h* for the use in a particular solar cell. The scattering properties are described by the angular distribution function (*ADF*) and the haze in transmission for 1-D grating. In Figure 5 the ADF_T of the 1-D periodic grating and of the Asahi-U type substrate are shown. The measurement confirmed that light was scattered into selected angles from the 1-D periodic gratings according to the diffraction grating equation:

$$\varphi_{scatt} = \arcsin\left[\frac{m\lambda}{nP} - \sin(\varphi_{inc})\right] \qquad (1)$$

Furthermore Fig. 5 demonstrates the fundamental difference in the *ADF* between randomly surface-textured substrate, such as Asahi-U type substrate, and 1-D periodic gratings. In case of randomly surface-textured substrates the *ADF* is a continuous function of the scattering angle, while in case of periodic gratings the light is scattered into discrete angles.

The haze in transmission of 1-D gratings that had different *P* and constant *h* is shown in Fig. 6. Also for this scattering parameter the geometrical features *P* and *h* play an important role, as the value of *P* represents the threshold for scattering the light (according to Equation 1, for $\lambda > P$ diffraction modes are not allowed, therefore only specular component may be transmitted) and *h* is directly related to the value of the haze (for *h* aiming to zero the 1-D grating approximates a flat surface) /14/.

Although some theoretical questions regarding 1-D gratings are still open, such as the relationship between the intensity of diffraction modes and *h* and knowledge of the scattering properties in different media than glass/air, 1-D gratings have been already successfully used as scattering surfaces in thin-film silicon solar cells in both superstrate /14/ and substrate configuration /15/.

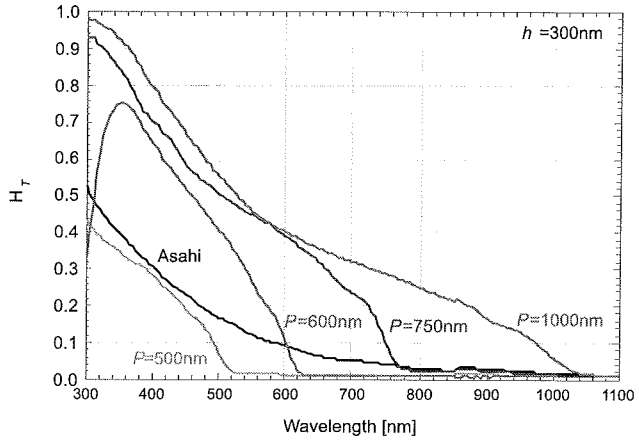

Fig. 6: Haze in transmission of gratings with different period and constant height (h = 300 nm). Asahi-U type is present as reference for randomly-textured surfaces (exponential decay).

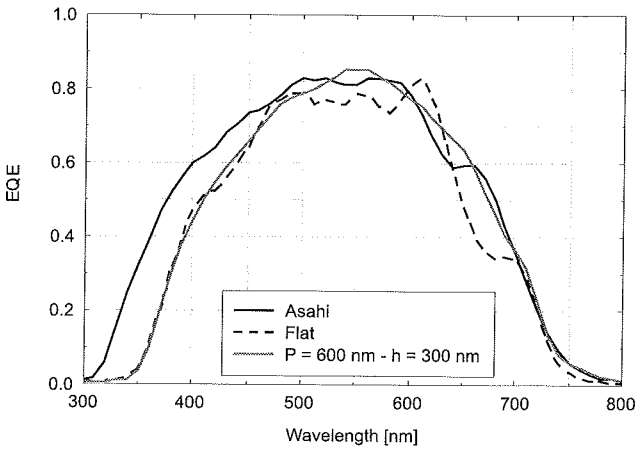

Fig. 7: The EQE of the compared solar cells.

3.1.1 Solar cell on 1-D periodic grating

As an example of the scattering potential of 1-D periodic surface texture in solar-cell technology, a *p-i-n* thin-film *a*-Si:H solar cell deposited on glass with 1-D periodic grating (*P* = 600nm and *h* = 300 nm) is presented. A 1000 nm thick ZnO:Al layer as the front contact was deposited on the textured glass substrate using the RF magnetron sputtering. The solar cell was fabricated using rf-PECVD deposition technique and its structure was: glass / fron ZnO:Al / p-layer (mc-Si:H) / p-layer (*a*-SiC:H) / buffer layer (*a*-SiC:H) / i-layer (*a*-Si:H) / n-layer (*a*-Si:H) / Ag / Al. The change of the surface roughness was evaluated using AFM after the deposition of each layer. The initial periodicity was preserved up till the back contact, although the height of the periodic structure decreased after the deposition of each subsequent layer. The external parameters of the solar cell are reported in Table 1 and compared with those of solar cells deposited on Asahi-U type and flat ZnO:Al as references. In Figure 7 the external quantum efficiency (*EQE*) of the compared solar cells is reported.

Table 1: Initial external parameters of solar cells.

Texture	V_{OC} [V]	J_{SC} [mA/m^2]	FF	η [%]
Asahi-U	0.845	-15.2	0.708	9.09
Flat	0.849	-13.4	0.641	7.29
*P*600 x *h*300	0.833	-14.8	0.707	8.7

The difference in J_{SC} between the solar cells deposited on the 1-D grating and the Asahi-U type substrate can be mainly explained by the higher absorption in the short wavelength region in the ZnO:Al compared to the SnO_2:F front contacts. For wavelengths above 500 nm, the *EQE* of the solar cell deposited on the grating is higher than the *EQE* of the solar cell deposited on the flat substrate. Due to anti-reflective and scattering effects, the *EQE* in this wavelength region is similar to Asahi-U reference.

This result indicates that 1-D periodic gratings are suitable substrates for improved light management in thin-film silicon solar cells. 1-D gratings were fabricated in several combinations of period and height on glass substrates and use as substrates for *a*-Si:H solar cells. High performance was obtained in solar cells with diffraction grating substrates having P = 600 nm and h = 300 nm. The J_{SC} of this solar cell increased by 14.2% relative to the J_{SC} of the solar cell with flat interfaces.

3.2 Modulated surface textures

The term modulated texture refers to a surface morphology that combines two types of textures with different statistical (vertical and lateral) surface parameters. This concept aims at enhanced light scattering in a broader wavelength range combining large and small surface features. This approach is an interesting choice for surface texturing in tandem thin-film silicon solar cells. In this article one example of modulated surface texture is presented: a combination of (large) random and (small) random textures. The different textures were introduced at different interfaces of the substrate, namely large random features were introduced at the glass / ZnO:Al interface and small random features were created at the ZnO:Al / air interface. The large random surface texture was obtained by treating flat Corning Eagle 2000^{TM} glass in a compound solution composed of HF and H_3PO_4 for 35 minutes. A 1 mm thick ZnO:Al film was sputtered on top of the rough glass surface. The modulated surface texture was obtained by wet-etching of the ZnO layer for 40".

3.2.1 Analysis of the modulated textures

The AFM was intensively used to evaluate the development of the modulated textures since it delivered highly detailed images and statistical information of the surface. An initial decrease in the surface roughness was measured after the deposition of the ZnO:Al mainly due to the smoothening effect. After the etching of the ZnO:Al layer the surface roughness increased resulting in the superimposition of the large and small features on the same surface. The im-

age of the modulated surface texture on etched glass in Fig. 8 shows clearly the combination of large features (away from each other in the order of microns) with smaller holes and craters (fingerprint of the etched AZO 40").

A simple and comprehensive means to represent the surface modulation is the spatial-frequency surface representation /16/. Using this representation the discrete lateral features that dominate the vertical surface roughness can be evaluated. It also helps to understand why surface profiles with similar mean-square-root surface roughness may have different scattering behavior. When comparing the spatial-frequency surface representations of the etched glass and its modulated version (etched glass + etched AZO) one can observe in both cases the broad peak at low spatial-frequency components that correspond to the large features. In the case of modulated surface texture the high spatial-frequency components (small holes and craters) are present in the spatial-frequency representation that are a consequence of the etching of ZnO:Al layer.

The haze parameter of the modulated surface textures is presented in Fig. 9. The initial textured surface exhibited low scattering level due to the large features. The surface covered with the ZnO:Al showed a similar behavior as the bare surface. Regarding the modulated textures, the haze values were boosted because of the etching step that provided additional rough features.

3.2.2 Solar cells on modulated surface textures

Single junction *a*-Si:H *p-i-n* solar cells were deposited by rf-PECVD on the modulated surface-textured susbtrates. The back contact consisted of a thin layer of ZnO:Al (80 nm) and silver. An overview of the initial external parameters is reported in Table 2. The *EQE* of the *a*-Si:H cells deposited on the modulated surface-textured substrate is shown in Figure 10.

The spectral response of the solar cells deposited on modulated surface textures was improved in the short wavelength region with respect to the solar cells deposited either on AZO 40" substrate or on etched glass covered by the ZnO:Al layer. This enhancement results partly from the different thickness of the ZnO:Al layer before and after etching and partly on the anti-reflecting (AR) effect of the modulated surface texture.

Table 2: Initial external parameters of solar cells deposited on modulated surface textures.

Texture	V_{oc} [V]	J_{sc} [mA/cm^2]	FF	η [%]
Etched glass/AZO 40"	0.874	17.8	0.639	9.97

The high surface roughness of the modulated texture and its corresponding spectral-frequency distribution, which affects the scattering and AR properties, led to the high *EQE* in the long wavelengths region. This result demonstrates the potential of modulated surface-textured substrates for enhancing the absorption of light in the absorber layers of thin-film silicon solar cells.

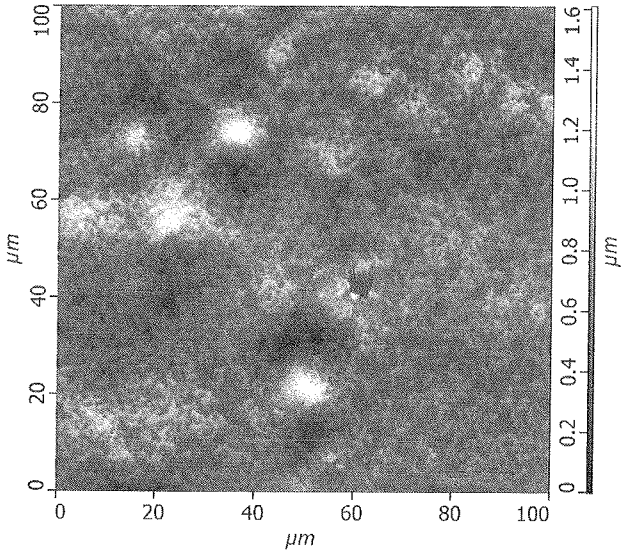

Fig. 8: Top view of the modulated surface texture on etched glass.

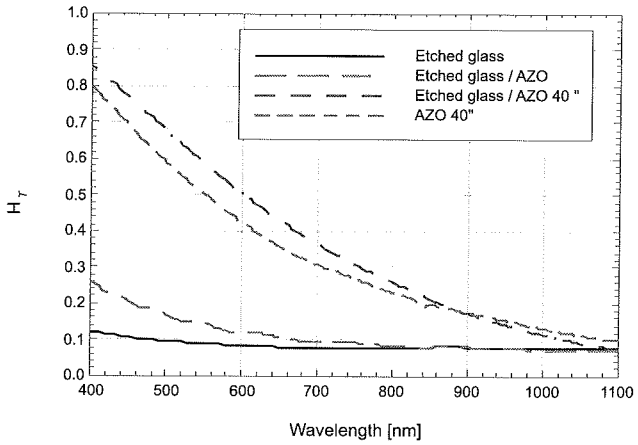

Fig. 9: Haze parameter in transmission of the substrates with the texture types (b).

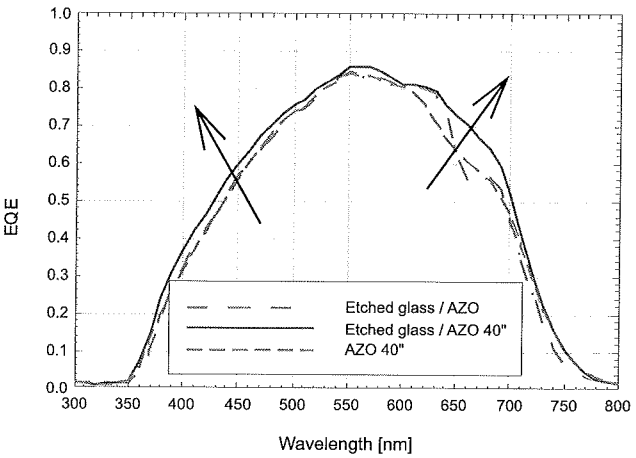

Fig. 10: EQE of the solar cells deposited on different surface-textured substrates.

3.3 1-D photonic-crystal-like structures as distributed Bragg reflector

Optical losses can occur at the metallic back contact of thin-film silicon solar cells because the surface-textured silver back reflectors suffer from undesired plasmon absorption /17/. In order to minimize such losses in single or tandem silicon solar cells an optimal approach for engineering a high-quality back reflector is desired. The design of such back reflector has to result in a high reflectance at the back contact in the solar cell in a broad and tunable wavelength region. These design specifications match the behavior of 1-D PC in the role of distributed Bragg reflector (DBR). 1-D PC is a multilayer structure in which two layers with different optical properties (refractive indexes) are periodically alternated. When light propagates through this structure, constructive and deconstructive interferences arise, resulting in the wavelength-selective reflectance or transmittance behavior. It has been demonstrated that periodically repeated stacks of *a*-Si:H and *a*-SiN_x:H (deposited using rf-PECVD at 235 °C) on glass exhibit a highly-reflective behavior in a broad range of wavelengths /18/. Operational 1-D PCs were fabricated on thin-film silicon compatible substrates (glass / etched ZnO:Al) and at compatible temperature < 180 °C /19/. The effects of the deposition temperature, the different substrate (from flat glass to glass/etched ZnO:Al), and the angle of incidence on the optical properties of 1-D PCs were determined. The high reflectance (80-90%) achieved in a broad wavelength region of 400 nm was in good agreement with the simulations of these structures.

3.3.1 Solar cells with DBR

Three pairs of layers of *a*-Si:H and *a*-SiN_x:H were used to fabricate an 1-D PC operational as the DBR. The schematic structure of the solar cell is given in Fig. 11. The structure consisted of glass coated with rough front ZnO:Al layer, a typical single-junction thin-film silicon *p-i-n* solar cell, a 700 nm thick ZnO:Al film used as back electrode. Three different back reflectors were applied at the back side of the solar cell, namely ZnO:Al / air (reference), ZnO:Al / Ag, and ZnO:Al / 1-D PC (see Figure 11).

The measured *EQE* of solar cells with different back reflectors is presented in Fig. 12. The *EQE* did not show the state-of-the-art performance because of some processing issues. Additionally, a high absorption in ZnO:Al front contact could be responsible for a low response in the short-wavelength region. The *EQE* increased in the long-wavelength region where the positive effect of the back reflectors was expected. The trend of increasing *EQE* is visualized by the arrows in the plot. In case of the textured metallic back reflector, surface plasmon absorption was responsible for a lower *EQE* in comparison with the 1-D PC back reflector, where the plasmon absorption was not expected.

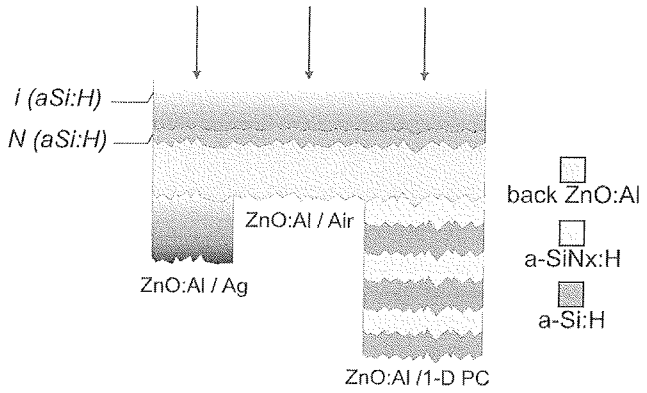

Fig. 11: Zoom-in at back side of the solar cell provided with three different back reflectors (the three red arrows indicate the place where the beam of EQE *setup is directed).*

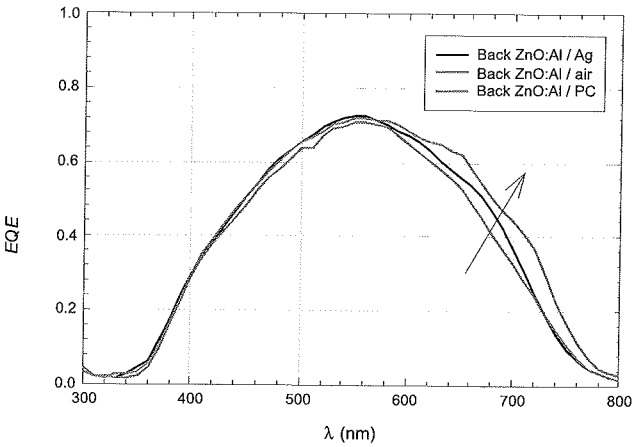

Fig. 12: EQE of solar cells on rough front ZnO:Al stacked with different back reflectors.

4 Conclusion

Approaches to improve the stability of *a*-Si:H solar cell against light-induced degradation and to enhance the absorption in absorber layers of thin-film silicon solar cells were presented.

Dilution of the silane source gas with hydrogen during the PECVD deposition of silicon films results in interesting modifications of the structural properties of the films in reference to undiluted ones. Although the phase transition is the most evident effect of the hydrogen dilution, more subtle changes do also occur in the amorphous silicon. The detailed XRD analysis of the pc-Si:H films revealed a narrowing of the FSP of the XRD patterns with increasing hydrogen dilution. The most important result from the XRD analysis of the pc-Si:H films is the presence of ordered domains of tetragonal silicon hydride in the films. A degradation experiment demonstrated the improved stability of the cells with absorber layers prepared at higher hydrogen dilution. However, the degradation of solar cells with absorber layers prepared at R > 20 is not further reduced with a

further increase of R. This result indicates that there is a strong link between the degradation behavior of the solar cells and the medium range order of the individual films (estimated from the FSP width of the XRD pattern), which also saturates for films prepared at R > 20.

There are several novel approaches to light trapping techniques such as the use of 1-D periodic gratings, modulated surface-texture substrates and design and implementation of distributed Bragg reflectors based on dielectric films. The gratings were successfully employed in single junction *a*-Si:H solar cells. High performance was obtained on solar cells using diffraction grating with P = 600 nm and h = 300 nm, where J_{SC} of this solar cell increased by 14.2% relative to the J_{SC} of the solar cell with flat interfaces. The concept of modulated surface texture and the spatial-frequency surface representation of the surface were presented. Solar cells deposited on modulated surface-textured ZnO:Al/glass substrate exhibited higher *EQE* in comparison to a solar cell deposited on surface-textured ZnO or glass due to improved anti-reflective and scattering properties of rough interfaces. 1-D PC can be used to obtain high reflectance at the back contact in a broad and tunable wavelength region. 1-D PCs based on *a*-Si:H and *a*-SiN_x:H layers were designed by computer simulations, fabricated and implemented in *a*-Si:H solar cells. The use of 1-D PC back reflector resulted in a higher *EQE* in the long-wavelength region in comparison to other types of back reflectors. The absence of absorption losses in the dielectric layers of 1-D PC makes the combination of ZnO:Al / PC a good candidate for back reflectors.

Acknowledgments

This work was carried out with a subsidy of the Dutch Ministry of Economic Affairs under EOS-LT program (project number EOSLT04029), supported by Delft University of Technology as a part of the SENECU project and partially funded through the project of Ministry of Education, Sports and Youth of the Czech Republic No. 1M06031. OM&T company is acknowledged for providing the 1-D grating.

References

/1/ W. Spear and P. LeComber,Solid State Comm. 17 (9), 1193 (1975).

/2/ D.E. Carlson and C.R. Wronski, Appl. Phys. Lett. 28 (11), 671 (1976).

/3/ J. Meier et al., in Proc. of the 1st World Conference on Photovoltaic Energy Conversion, Hawai (1994), p. 409-412.

/4/ J. Yang, A. Banerjee, K. Lord, and S. Guha, in Proc. of the 2nd World Conference and Exhibition on Photovoltaic Solar Energy Conversion, Vienna (1998), p. 387-390.

/5/ Photon International, March 2009.

/6/ L. Yang and L. F. Chen, Mater. Res. Soc. Proc. 336 (1994) 669.

/7/ J. Yang, X. Xu and S. Guha, Mater. Res. Soc. Proc. 336 (1994) 687.

/8/ C.R. Wronski, J.M. Pearce, R.J. Koval et al., Mater. Res. Soc. Proc. 715 (2002) A13.4.

/9/ G. van Elzakker, V. Nádaždy et al., Thin Solid Films 511-512 (2006) 252-257.

/10/ G. van Elzakker, P. Sutta, M. Zeman, Mater. Res. Soc. Symp. 1153 (2009) 1153-A18-02.

/11/ D.L. Williamson, Mater. Res. Soc. Symp. Proc. 559 (1999) 251.

/12/ S. Minomura, K. Tsuji et al., Journal of Non-Cryst. Solids 35&36 (1980) 513-518.

/13/ C. C. Tsai, G. B. Anderson, R. Thompson et al., Journal of Non-Cryst. Solids 114 (1989) 151.

/14/ O. Isabella et al., in Proc. of the 23rd EUPVSEC, Valencia (2008), 3AV.1.48.

/15/ F.-J. Haug et al., in Proc. of teh 21st EUPVSEC, Dresden, (2006).

/16/ O. Isabella et al., in Proc. of the 23rd ICANS, Utrecht, (2009).

/17/ J. Springer, A. Poruba, L. Mullerova, et al., , J. Appl. Phys. 95, 1427 (2004).

/18/ J. Krc, A. Campa, S. Luxembourg, M. Zeman and M. Topic, Mater. Res. Soc. Symp. Proc. 1101E, (2008), 1101-KK08-01.

/19/ O. Isabella, B. Lipovsek, J. Krč, M. Zeman, Mater. Res. Soc. Symp. Proc. 1153 (2009), 1153-A03-05.

M. Zeman, G. van Elzakker, O. Isabella
Delft University of Technology, PVMD /DIMES,
Feldmannweg 17, 26282 CT Delft, Netherlands

P. Sutta
University of West Bohemia, NTRC,
Univerzitní 8, 306 14 Plzeň, Czech Republic

J. Krc
University of Ljubljana, Faculty of Electrical
Engineering, SI-1000 Ljubljana, Slovenia
janez.krc@fe.uni-lj.si

Prispelo (Arrived): 15.08.2009 *Sprejeto (Accepted): 09.10.2009*

AN INTRODUCTION TO THE TECHNOLOGY OF THIN FILM SILICON PHOTOVOLTAICS

A. Feltrin, R. Bartlomé, C. Battaglia, M. Boccard, G. Bugnon, P. Bühlmann, O. Cubero, M. Despeisse, D. Dominé, F.-J. Haug, F. Meillaud, X. Niquille, G. Parascandolo, T. Söderström, B. Strahm, V. Terrazzoni, N. Wyrsch, C. Ballif

Ecole Polytechnique Fédérale de Lausanne (EPFL), Institute of Microengineering (IMT), Photovoltaics and thin film electronics laboratory, Neuchâtel, Switzerland.

Key words: thin film silicon, microcrystalline silicon, tandem solar cells

Abstract: Several aspects of the science and technology of thin film silicon for photovoltaic applications will be presented. The potential advantages of this technology over crystalline wafer technology will be discussed. A basic understanding of the material properties of thin film silicon layers enables to assess their potential and limitations when used in photovoltaic devices. A brief review of the production technology for thin films will be given with particular emphasis on amorphous and microcrystalline silicon. As for other photovoltaic technologies, the push for higher efficiency of thin film silicon devices is strong. An appealing feature of these materials is that they can be easily integrated in multi-junction tandem devices. For instance, stacking amorphous and microcrystalline silicon thin films in one tandem cell, the micromorph cell, increases the efficiency well above the characteristic values of single junction cells. The Institute of Microengineering (IMT) has been a pioneer in the research and development of thin film silicon photovoltaics over the last 20 years and several latest developments on are reviewed.

Uvod v tehnologijo tankoplastne silicijeve fotovoltaike

Kjučne besede: tankoplastni silicij, mikrokistalni silicij, tandemske sončne celice

Izvleček: Predstavljeni so številni vidiki znanosti in tehnologije uporabe tankoplastne silicijeve fotovoltaike. Razločene bodo potencialne prednosti omenjene tehnologije glede na kristalno silicijevo tehnologijo. Osnovno razumevanje lastnosti materiala plasti tankoplastnega silicija omogoča podati oceno prednosti in ovir pri uporabi v fotovoltaiki. Podan je kratek pregled tankoplastnih tehnologij s povdarkom na amorfnem in mikrokristalnem siliciju. Kot pri drugih tehnologijah, je tudi tukaj prisotna težnja k povečanju izkoristka sončnih celic. Izstopajoča lastnost teh materialov je njihova enostavna možnost integracije v večspojne strukture. Združevanje amorfnih in mikrokristalnih plasti v tandemsko mikromorfno sončno celic, na primer, povečuje izkoristek precej nad vrednosti enospojnih sončnih celic. predstavljeni so številni razvojni dosežki inštituta IMT (Institute of Microengineering), ki je pionir na področju raziskav in razvoja tankoplastne silicijeve fotovoltaike v zadnjih 20 letih.

1 Introduction

Thin film silicon photovoltaics is one of the emerging technologies to produce electricity from sunlight. Semiconductors like amorphous silicon (a-Si:H) and microcrystalline silicon (μc-Si:H) form the backbone of this technology. The use of a-Si:H as a photovoltaic material can be traced back to publications in the 1970s /1/, whereas microcrystalline silicon solar cells were first made in the mid 1990s at IMT /2/. Since then, this technology has attracted increasing interest in the academic and industrial environment. Despite lower efficiencies than wafer based crystalline photovoltaics, a particularly attractive feature of this technology is the versatility of the deposition techniques. Materials with different optical band gaps are synthesized by changing the silicon phase and by forming compounds with other elements like carbon or germanium /3/. Materials with different optical band gaps can be easily combined to form multiple stacks that exploit a larger part of the solar spectrum increasing the efficiency of the photovoltaic device /4/.

2 Deposition techniques

Crystalline and wafer based photovoltaic technology represents today the biggest market share. This technology uses a top-down approach to prepare solar cells: wafers are obtained by sawing silicon ingots drawn from melted silicon in crucibles. These wafers are processed in multiple steps to obtain solar cells successively assembled in modules. The technology used in thin film silicon is at the opposite. Solar cells are obtained in the so called bottom-up approach: atoms of silicon are stacked one on top of the other on a suitable substrate to form all the layers of a solar cell. Other technologies use this approach as well /5/, however there is a distinctive advantage in doing so in thin film silicon technology. The production technology used to deposit single solar cells is scalable to large surfaces and therefore modules can be prepared on large areas (> 1 m^2) without the need to assemble individual cells. In the following we will briefly describe the two main techniques used at IMT to prepare full solar cells, both scalable to large surfaces and presently employed for industrial production. Additional attractive features of this technology are extremely low material consumptions compared to wafer based technologies and low temperature processing steps (typically below 300°C) in contrast to wafer based technology where processes close to 1000°C are used. This last aspect opens up the possibility to use cheap substrates in thin film silicon technology.

2.1 Low pressure chemical vapor deposition

One of the characteristic components in the design of thin film solar cells are transparent conductive oxide (TCO) layers that have principally three functions: 1-to contact electrically the solar cell; 2- to be transparent to the sunlight; 3- to scatter the incoming sunlight. In the next section of this paper it will be explained how these requirements are intimately related to the material properties of the amorphous and microcrystalline silicon layers. Different techniques are available to deposit these layers. At IMT a modified low pressure chemical vapor deposition (LP-CVD) technique has been developed that allows growing TCO layers with excellent optical and electrical properties that satisfy the three requirements above /6/. Molecular precursors in gaseous form like water vapor, diethylzinc and the dopant diborane are injected at low pressure (< 1mbar) in a chamber and thermodynamically dissociate in the vicinity of a hot plate where substrates are heated up to temperatures between 100°C and 200°C. Depending on the process parameters, different growth modes can be obtained /6/. After optimization of the deposition process layers as shown in Fig. 1 are obtained. They display a characteristic surface roughness due to the presence of pyramidally shaped single ZnO crystals. The rough surface that spontaneously develops during the growth acts as a diffuser for the incoming light /7/. ZnO has excellent transparency in the wavelength range between 400nm and 1000 nm, that is to say in the same range where silicon absorbs light.

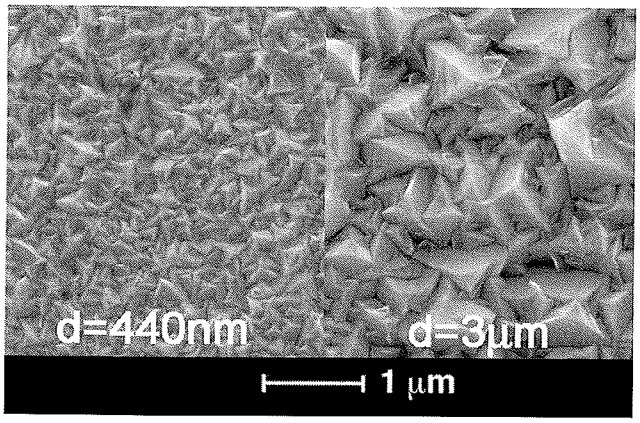

Fig. 1: SEM picture of typical ZnO samples with different thicknesses deposited by LP-CVD technique.

An interesting feature of ZnO deposited by LP-CVD is that by varying process and layer properties different electrical and optical properties can be obtained /8/ and the impact on solar cell performance studied.

2.2 Plasma enhanced chemical vapor deposition

For the deposition of silicon containing layers CVD alone cannot be used, because the dissociation rate of typical precursor gases like silane and hydrogen molecules is extremely low at typical process temperatures around 200°C. Therefore, dissociation has to be provided by another energy source than the hot plate. Electrons oscillating in an electromagnetic field driven at frequencies in the range between 13.56 MHz (RF) and typically 100 MHz can provide the necessary energy to dissociate the gas molecules by electron impact dissociation. In stable discharge conditions a plasma containing electrons and positive ions is obtained and the deposition technique is called plasma enhanced chemical vapor deposition (PE-CVD) /9/. Growth rates between a few Ångströms and a few nanometers per second can be obtained by varying the process parameters and reactor configurations. IMT has been a pioneer in studying the physical and chemical properties of plasmas driven at frequencies higher than 13.56 MHz /10-12/, the so called VHF domain /13-15/. It was shown that in VHF conditions higher deposition rates and smaller ion bombardment energies could be obtained, leading to more favorable conditions for the deposition of silicon layers.

3 Silicon material properties

A quite remarkable feature by of PE-CVD processes is that by varying deposition conditions, typically silane concentration in hydrogen or RF-VHF input power, a transition between the amorphous and microcrystalline phase of silicon can be observed /16/. Therefore, two different phases of this material can be easily deposited using the same technology. In the following of this section we will briefly review a few basic properties of a-Si:H and µc-Si:H.

3.1 Optical properties

The optical absorption spectrum of of a-Si:H and µc-Si:H are displayed in Fig. 2. The two materials are characterized by quite distinct optical band gaps: amorphous silicon has a band gap around 1.7 eV, whereas microcrystalline silicon has a band gap around 1.1 eV. As a result microcrystalline silicon absorbs light in a spectral range where amorphous silicon is already transparent to sunlight. To effectively absorb the sunlight the layer thickness should roughly equal the penetration depth. For amorphous silicon this would mean layer thicknesses of up to 10 µm and for microcrystalline silicon up to 1 mm. With deposition rates of a few Ångströms or even nanometers per second, these thicknesses are prohibitively large. From this simple analysis of the absorption spectrum the need to increase the light path in silicon while keeping an acceptable film thickness emerges as a priority in thin film silicon technology. The light path can effectively be increased in thin layers by scattering processes at rough interfaces that devi-

ate the light path from normal incidence into oblique directions.

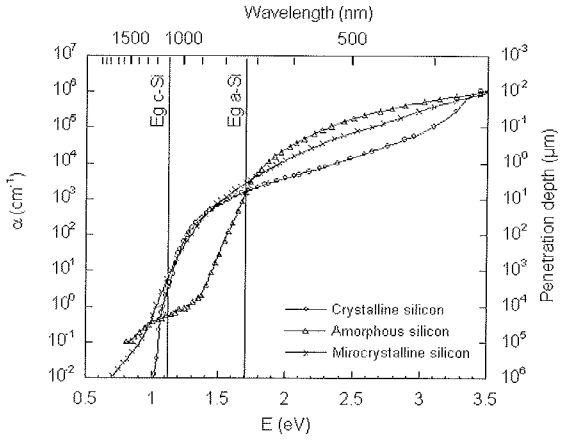

Fig. 2: Absorption spectrum of amorphous and microcrystalline silicon.

The usefulness of rough LP-CVD ZnO and the importance to study light trapping in thin films becomes thus apparent.

3.2 Electronic properties

Amorphous and microcrystalline silicon are primarily characterized by disorder in the atomic lattice /17-18/. As a result, defects play an important role in the electronic and transport properties of these materials. They drastically reduce the carrier diffusion lengths compared to their crystalline (i.e. highly ordered) counterpart by several orders of magnitude. Thin layers and transparent electrodes covering the whole cell surface are therefore needed to efficiently extract the carriers in these materials. In addition, amorphous silicon knowingly suffers from light-induced or Staebler-Wronsky degradation /19/. This process, which is reversible, increases the defect density in amorphous silicon when illuminated and critically depends on the thickness of the layer. Finally, doping n or p type thin film silicon layers further reduces the diffusion length to a few nanometers only.

4 Solar cells

The design of thin film silicon solar cells is basically determined by the electronic properties of amorphous and microcrystalline layers. Since doping drastically reduces diffusion length, doped layers are not photoactive. Therefore their role is to create an electric field in the photoactive intrinsic layer sandwiched between the two doped layers.

4.1 Substrate and superstrate configurations

Depending whether the substrate being used for silicon deposition is transparent or not, two different sequences of layer stacking are used in thin film silicon technology. Fig. 3 shows the two possible configurations. In the first one, called superstrate configuration, the substrate is glass. In the second one, called substrate configuration, the substrate is opaque like a plastic or metal and if the sheet is thin enough, flexible solar cell modules can be obtained.

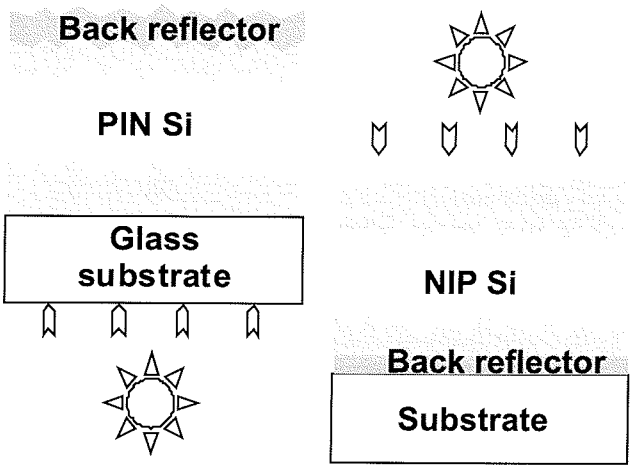

Fig. 3: Sketches of thin film silicon cells in superstrate (left) and substrate (right) configurations.

4.2 Single junction cells

Single junction amorphous and microcrystalline solar cells have been extensively investigated at IMT and high efficiencies of 9.5% after light soaking have been obtained for amorphous single junction cells grown on LP-CVD ZnO /20/.

The growth of μc-Si:H on LP-CVD ZnO has been extensively studied as well. It has been shown that in order to obtain cell efficiencies close to 10%, it was necessary to modify the ZnO surface morphology in order to obtain high open circuit voltages and fill factors. Thus, high efficiencies of 9.9% have been reported at IMT /21/. Plasma process studies have been conducted as well in order to understand the growth of μc-Si:H. Fig. 4 shows the efficiency of microcrystalline single junction solar cells deposited in a large area R&D PE-CVD system at IMT under different process conditions /22/. As can be seen, efficiencies are very sensitive to pressure. It was shown that the improvement in film quality and solar cell efficiency can be related to lower ion energies hitting the growth surface. However, pressure and ion energies are not the only important parameters determining the solar cell efficiencies. Cells deposited at 1.2 mbar, but under high silane depletion conditions show a remarkable improvement as well. Plasma chemistry is likely to be involved in this case, although the exact mechanism remains unclear.

In Fig. 4 some of the cells display deposition rates close to 1 nm/s. These cells have been obtained in plasma conditions where silane depletion is very high and they form the basis process for the development of high rate deposition processes for microcrystalline cells /23/.

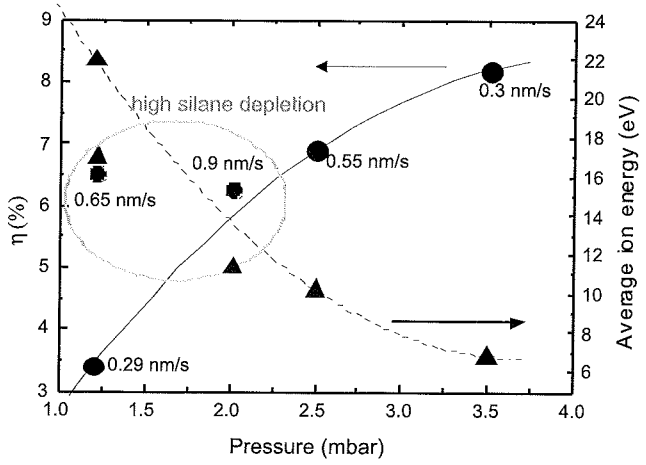

Fig. 4: Efficiency vs pressure of microcrystalline silicon single junction solar cells obtained at IMT.

4.3 Micromorph tandem cells

As mentioned in the introduction, stacking different materials is easily realized in thin film silicon technology because combining materials with different optical band gaps allows exploiting a larger part of the solar spectrum. In particular combining amorphous and microcrystalline silicon thin films in a serially connected tandem cell has first been proposed at IMT in the mid 1990s /4/. Since then, an increasing number of research institutes and companies have adopted this concept.

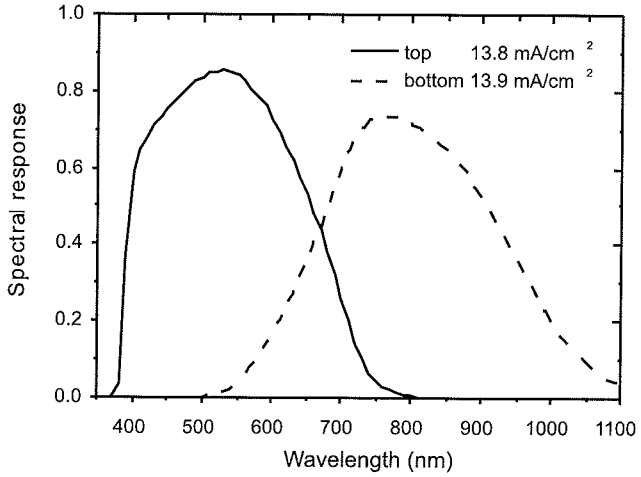

Fig. 5: Spectral response of a 13.3% initial efficiency micromorph tandem cell obtained at IMT.

In Fig. 5 the spectral response of 13.3% efficient micromorph tandem cell is presented. Such high efficiencies and current densities can be obtained only by carefully designing the light trapping in the device. In particular, a high current in the top, or amorphous, cell while keeping the thickness below 300 nm is highly desirable in order to reduce Stabler-Wronski degradation of the amorphous material. This can only be achieved by inserting between the two active layers an intermediate layer that selectively reflects and transmits light in the appropriate wavelength range. Different material options are available for the intermediate layer. At IMT silicon oxide based intermediate reflectors have been investigated for this purpose and current gains around 20% have been observed in the top cell /24/. Additionally, it has been observed that the texture of the front TCO influences the current gain as well /25/.

In substrate configuration the surface roughness of LP-CVD ZnO can be used easily as an intermediate reflector /26/. The device scheme with an AIR is presented in Fig. 6. The μc-Si:H is deposited on hot silver substrate which has morphology with large feature size (about 1 μm) for efficient light scattering for wavelengths between 750 nm and 1100 nm. The shape of the morphology has a moderate roughness in order to provide ideal condition for the growth of μc-Si:H material. The AIR is composed of 1.5 μm of LP-CVD ZnO deposited on the bottom cell. As shown in Fig. 6, it restores a feature size of about 300 nm and morphology needed for the a-Si:H top cell. Therefore, the blue-green light (500 nm - 750 nm) is back scattered at the AIR interface. The light is then trapped between the AIR and the top front contact in the a-Si:H top cell.

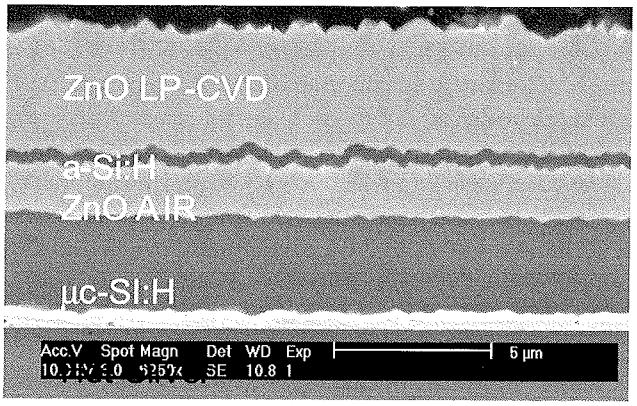

Fig. 6: SEM micrograph of a nip/nip micromorph tandem cell cross-section with a ZnO asymmetric intermediate reflector (AIR) obtained at IMT.

Fig. 7 shows the EQE of our device with thin 1.5 μm μc-Si:H cells. The initial and stabilized electrical parameters of cells without IR and with AIR are also compared. It shows that with the AIR, the top cell can be made as thin as 140 nm and still generates 11.4 mA/cm^2. In tandem cells, the degradation is reduced to 8 % with the AIR compared to 18 % without IR but thicker 300 nm top cell.

4.4 High rate deposition of bottom cell

The absorption coefficient of microcrystalline silicon extends well into the near infrared region compared to amorphous silicon. However, thick layers in the order of several microns are nevertheless necessary in order to achieve high current densities.

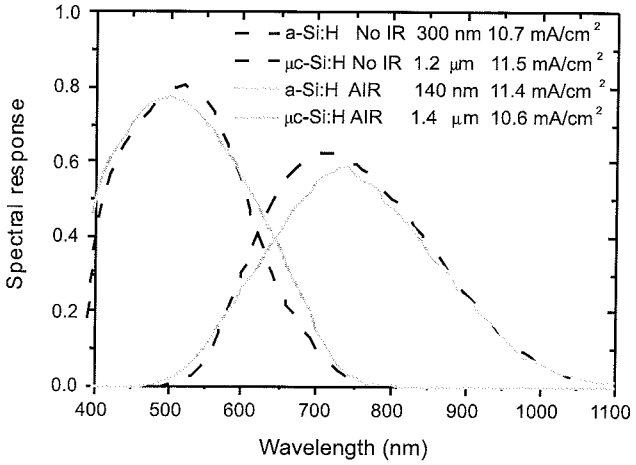

Fig. 7: Initial spectral response of nip/nip micromorph tandem solar cells without IR (300 nm a-Si:H, 1.2 μm μc-Si:H) and with AIR (140 nm a-Si:H, 1.4 μm μc-Si:H) deposited on hot silver coated glass.

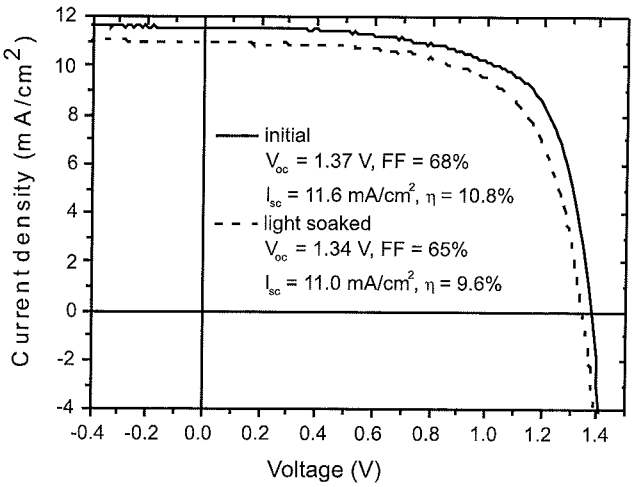

Fig. 8: Current-voltage curve of a micromorph tandem cell in its initial and stabilized state. The bottom cell has been deposited at 1 nm/s.

Therefore, fast deposition of microcrystalline silicon is desirable. In Fig. 8 the current-voltage curves of initial and stable (after 1000 hours light soaking) efficiencies of a micromorph solar cell with the bottom (or microcrystalline) cell deposited at 1 nm/s is shown. In this case the thickness of the top cell is only 230 nm, which limits the light induced degradation to about 12% to a stabilized value of 9.6%. Further improvements in the process conditions of the bottom cell will be necessary in order to lift this efficiency value above the 10% mark.

3 Conclusions

A short review of the main features and challenges in the technology of thin film silicon photovoltaics has been presented. This technology certainly offers great potential in terms of scalability to large surfaces and versatility of the deposition techniques. In addition, materials with different optical band gaps are easily combined in multi-junction structures that can significantly lift the efficiencies above the level of single junction solar cells. In order to achieve high efficiencies it is necessary to properly design all the layers of the stack. The design has to optimize optical and light scattering properties of TCOs and electrical properties of the materials by tailoring PE-CVD conditions, reducing defect densities in intrinsic materials and minimizing absorption in doped layers.

References

/1./ Carlson, D.E. and C.R. Wronski, *Amorphous Silicon Solar-Cell.* Applied Physics Letters, 1976. **28**(11): p. 671-673.

/2./ Meier, J., et al., *Complete Microcrystalline P-I-N Solar-Cell - Crystalline or Amorphous Cell Behavior.* Applied Physics Letters, 1994. **65**(7): p. 860-862.

/3./ Bernhard, N., G.H. Bauer, and W.H. Bloss, *BANDGAP ENGINEERING OF AMORPHOUS-SEMICONDUCTORS FOR SOLAR-CELL APPLICATIONS.* Progress in Photovoltaics, 1995. **3**(3): p. 149-176.

/4./ Fischer, D., et al., *The "micromorph" solar cell: Extending a-si:H technology towards thin film crystalline silicon.* Conference Record of the Twenty Fifth Ieee Photovoltaic Specialists Conference - 1996, 1996: p. 1053-1056

/5./ Yamaguchi, M., *III-V compound multi-junction solar cells: present and future.* Solar Energy Materials and Solar Cells, 2003. **75**(1-2): p. 261-269.

/6./ Fay, S., et al., *Low pressure chemical vapour deposition of ZnO layers for thin-film solar cells: temperature-induced morphological changes.* Solar Energy Materials and Solar Cells, 2005. **86**(3): p. 385-397.

/7./ Fay, S., et al. *Rough ZnO layers by LP-CVD process and their effect in improving performances of amorphous and microcrystalline silicon solar cells.* in *14th International Photovoltaic Science and Engineering Conference*. 2004. Bangkok, THAILAND.

/8./ Steinhauser, J., et al. *Electrical transport in boron-doped polycrystalline zinc oxide thin films.* in *E-MRS 2007 Spring Meeting Symposium on Advances in Transparent Electronics: From Materials to Devices II*. 2007. Strasbourg, FRANCE.

/9./ Levitskii, S.M., *An Investigation of the Breakdown Potential of a High-Frequency Plasma in the Frequency and Pressure Transition Regions.* Soviet Physics-Technical Physics, 1957. **2**(5): p. 887-893.

/10./ Fluckiger, R., et al., *Structural and Electrical Properties of Undoped Microcrystalline Silicon Grown by 70 Mhz and 13.56 Mhz Pecvd.* Microcrystalline and Nanocrystalline Semiconductors, 1995. **358**: p. 751-756

/11./ Fluckiger, R., et al., *Electrical-Properties and Degradation Kinetics of Compensated Hydrogenated Microcrystalline Silicon Deposited by Very High-Frequency-Glow Discharge.* Journal of Applied Physics, 1995. **77**(2): p. 712-716.

/12./ Finger, F., et al., *Influences of a High-Excitation Frequency (70 Mhz) in the Glow-Discharge Technique on the Process Plasma and the Properties of Hydrogenated Amorphous-Silicon.* Journal of Applied Physics, 1992. **71**(11): p. 5665-5674.

/13./ Curtins, H., N. Wyrsch, and A.V. Shah, *High-Rate Deposition of Amorphous Hydrogenated Silicon - Effect of Plasma Excitation-Frequency.* Electronics Letters, 1987. **23**(5): p. 228-230.

/14./ Howling, A.A., et al., *Frequency-Effects in Silane Plasmas for Plasma Enhanced Chemical Vapor-Deposition.* Journal of Vacuum Science & Technology a-Vacuum Surfaces and Films, 1992. **10**(4): p. 1080-1085.

/15./ Kroll, U., et al., *More Insight into the Vhf-Glow-Discharge by Plasma Impedance Measurements.* Amorphous Silicon Technology-1994, 1994. **336**: p. 115-120

/16./ Kroll, U., et al., *From amorphous to microcrystalline silicon films prepared by hydrogen dilution using the VHF (70 MHz) GD technique.* Journal of Non-Crystalline Solids, 1998. **227**: p. 68-72.

/17./ Finger, F., et al., *Electronic states in hydrogenated microcrystalline silicon.* Philosophical Magazine B-Physics of Condensed Matter Statistical Mechanics Electronic Optical and Magnetic Properties, 1998. **77**(3): p. 805-830.

/18./ Beck, N., A. Shah, and N. Wyrsch, *Determination of the quality of a-Si:H films: "True" transport parameters.* 1994 Ieee First World Conference on Photovoltaic Energy Conversion/Conference Record of the Twenty Fourth Ieee Photovoltaic Specialists Conference-1994, Vols I and Ii, 1994: p. 476-479

/19./ Staebler, D.L. and C.R. Wronski, *Reversible Conductivity Changes in Amorphous Silicon.* Journal of the Electrochemical Society, 1977. **124**(8): p. C303-C303.

/20./ Meier, J., et al., *Potential of amorphous and microcrystalline silicon solar cells.* Thin Solid Films, 2004. **451-52**: p. 518-524.

/21./ Bailat, J., et al., *High-efficiency p-i-n microcrystalline and micromorph thin film silicon solar cells deposited on LPCVD ZnO coated glass substrates.* Conference Record of the 2006 IEEE 4th World Conference on Photovoltaic Energy Conversion, Vols 1 and 2, 2006: p. 1533-1536

/22./ Bugnon, G., et al., *Influence of pressure and silane depletion on microcrystalline silicon material quality and solar cell performance.* Journal of Applied Physics, 2009. **105**(6).

/23./ Strahm, B., et al., *Microcrystalline silicon deposited at high rate on large areas from pure silane with efficient gas utilization.* Solar Energy Materials and Solar Cells, 2007. **91**(6): p. 495-502.

/24./ Buehlmann, P., et al., *In situ silicon oxide based intermediate reflector for thin-film silicon micromorph solar cells.* Applied Physics Letters, 2007. **91**(14): p. -.

/25./ Domine, D., et al., *Optical management in high-efficiency thin-film silicon micromorph solar cells with a silicon oxide based intermediate reflector.* Physica Status Solidi-Rapid Research Letters, 2008. **2**(4): p. 163-165.

/26./ Soderstrom, T., et al., *Asymmetric intermediate reflector for tandem micromorph thin film silicon solar cells.* Applied Physics Letters, 2009. **94**(6): p. -.

A. Feltrin, R. Bartlomé, C. Battaglia, M. Boccard, G. Bugnon, P. Bühlmann, O. Cubero, M. Despeisse, D. Dominé, F.-J. Haug, F. Meillaud, X. Niquille, G. Parascandolo, T. Söderström, B. Strahm, V. Terrazzoni, N. Wyrsch, C. Ballif
Ecole Polytechnique Fédérale de Lausanne (EPFL), Institute of Microengineering (IMT), Photovoltaics and thin film electronics laboratory, Breguet 2, 2000 Neuchâtel, Switzerland.

Prispelo (Arrived): 15.08.2009 *Sprejeto (Accepted): 09.10.2009*

45. Mednarodna konferenca o mikroelektroniki, elektronskih sestavnih delih in materialih - MIDEM 2009
45nd International Conference on Microelectronics, Devices and Materials - MIDEM 2009

9. - 11- september 2009 Jamski Dvorec, Postojna

Petinštirideseta mednarodna konferenca o mikroelektroniki, elektronskih sestavnih delih in materialih - MIDEM 2009 (45th International Conference on Microelectronics, Devices and Materials) nadaljuje uspešno tradicijo mednarodnih konferenc MIDEM, ki jih vsako leto prireja Strokovno društvo za mikroelektroniko, elektronske sestavne dele in materiale - MIDEM.

Na konferenci, ki sta ji predsedovala prof. dr. Marko Topič in izr. prof. dr. Janez Krč (UL FE), je bilo letos predstavljeno 59 rednih in 11 vabljenih predavanj v šestih sekcijah z naslednjimi vsebinami:

- Materiali, tehnologije in elektronskih sestavnih delov
- Elektronika
- Optoelektronika
- Tanki in debeli filmi
- Integrirana vezja
- Senzorji in aktuatorji

Kot vsako leto je osrednji dogodek konference predstavljala enodnevna delavnica, tokrat na temo fotovoltaike z naslovom »Advanced photovoltaic technologies and devices«

Na konferenci so bili predstavljeni najnovejši dosežki raziskovalcev iz domačih in tujih raziskovalnih skupin in podjetij. Pomembno vlogo so odigrala vabljena predavanja, ki so povzemala zadnje dosežke iz evropskega in svetovnega vrha izbranih tematik.

Na področju materialov, tehnologij in elektronskih elementov je bilo predstavljeno vabljeno predavanje:

J.Krupka: Measurements of Materials at Microwave Frequencies

Na področju elektronike in optoelektronike je bilo izvedeno naslednje vabljeno predavanje:

M.A.Morris, J.D.Holmes: Scaling Beyond Lithographic Limits - Polymer Self-Assembly Mediated Sub-20 nm FET devices

Na področju tankih in debelih filmov je bilo vabljeno predavanje z naslovom:

A.Dziedzic; Modern Thick-Film and LTCC Passives and Passive Integrated Components

V delavnici je bilo predstavljeno osem vabljenih predavanj:

W.C.Sinke: Trends in Wafer-Based Silicon Photovoltaic Cell and Module Technology

S.P.Philipps, W.Guter, M.Steiner, E.Oliva, G.Siefer, E.Welser, B.M.George, M.Hermle, F.Dimroth, A.W.Bett: III-V Multi-junction Solar Cells - Simulation and Experimental Realization

A.Luque and A.Martí: Progress in understanding the intermediate band solar cell

J.Rakovec: Exploiting Solar Energy with Photovoltaics

H.Fechner: High penetration of Photovoltaic Systems in Electricity Networks

J.R.Sites: Impact of Grain Boundaries on Thin-Film Photovoltaics

M.Zeman, G. van Elzakker, P.Sutta, O.Isabella: Thin-film silicon solar cells: stability and light trapping

A. Feltrin, R. Bartlomé, C. Battaglia, M. Boccard, G. Bugnon, P. Bühlmann, O. Cubero, M. Despeisse, D. Dominé, F.-J. Haug, F. Meillaud, X. Niquille, G. Parascandolo, T. Söderström, B. Strahm, V. Terrazzoni, N. Wyrsch, C. Ballif: An Introduction to the Technology of Thin Film Silicon Photovoltaics

Kot je razvidno iz naslovov vabljenih predavanj (in rednih prispevkov, gl. celotni program), je delavnica pokrivala širok spekter aktivnosti na področju fotovoltaike, vključujoč najnovejše strukture in tehnologije sončnih celic in fotonapetostnih (PV) modulov, od tehnologij celic na osnovi tankih rezin, rekordnih več-spojnih sončnih celic na osnovi III-V materialov, novih konceptov celic (vmesni pas v osnovni energijski reži), tehnologije tankoplastnih celic (CIGS, a-Si, uc-Si, tandemske), vse do naprednih konceptov in sestavnih gradnikov na sistemskem nivoju, priključevanju PV sistemov na omrežje ter nenazadnje vplivi geografskih in vremenskih pogojev (sončno obsevanje) na energijski izplen PV sistemov in elektrarn.

Delavnica je privabila več kot 60 poslušalcev.

Pred konferenco je bil izdelan zbornik z 69 referati (26 tuji avtorji), skupaj v obsegu 396 strani (najobsežnejši zbornik doslej). Skupno število udeležencev konference je bilo 85, od tega 60 domačih in 25 tujih udeležencev, kar kaže na visok trend naraščanja obiska konferenc MIDEM.

Glede na navedene podatke in kvaliteto vabljenih in rednih prispevkov smo organizatorji, upamo pa tudi da udeleženci konference, z letošnjo konferenco zelo zadovoljni. To nam je v motivacijo in izziv pri pripravi aktualnih znanstvenih in razvojnih tem ter organizacije konference MIDEM 2010.

CONFERENCE MIDEM 2009 - SHORT PROGRAM

Jamski dvorec - Postojna, September 9. - September 11. 2009

DAY/ HOUR	sep.09 Wednesday	sep.10 Thursday	sep.11 Friday
9:00	OPENING CEREMONY	WORKSHOP - OPENING	INVITED PAPER
9:15	INVITED PAPER	INVITED PAPERS	Andrzej Dziedzic
9:30	Jerzy Krupka		Chairman: M. Hrovat
9:45	Chairman :B. Malič	Wim Sinke	Coffee Break
10:00	Coffee Break	S.P. Philipps	SESSION ON
10:15	SESSION ON	Antonio Luque	THIN&THICK FILMS
10:30	MATERIALS,		
10:45	AND DEVICES	Chairman: J. Krč	Chairman: A.Dziedzic
11:00		Coffee Break	
11:15	Chairman : B. Malič	INVITED PAPERS	
11:30		Jože Rakovec	
11:45		Hubert Fechner	
12:00			
12:15		Chairman: J. Krč	
12:30	LUNCH	LUNCH	LUNCH
12:45			
13:00			
13:15			
13:30	SESSION ON	WORKSHOP	
13:45	MATERIALS,	INVITED PAPERS	SESSION ON
14:00	AND DEVICES	James R. Sites	INTEGRATED CIRCUITS
14:15	Chairman: B. Malič	Miro Zeman	
14:30	Coffee Break	Andrea Feltrin	
14:45	SESSION ON	Chairman: M. Topič	Chairman: J. Trontelj
15:00	ELECTRONICS		
15:15	Chairman: D. Vrtačnik	Coffee Break	
15:30		WORKSHOP	
15:45			Coffee Break
16:00			SESSION ON
16:15		REGULAR PAPERS	SENSORS AND ACTUATORS
16:30	SESSION ON	Chairman: J. Krč	
16:45	OPTOELECTRONICS		
17:00	Chairman: M. Topič		Chairman: S. Amon
17:15			
17:30			
17:45			CLOSING CEREMONY
18:00			
18:15			
18:30			
18:45			
19:00			
19:15	REUNION IN FRONT OF THE ENTRANCE		
19:30	VISIT TO POSTOJNA CAVE	DINNER	
19:45			
20:00			
20:15			
20:30			
20:45			
21:00			

UTRINKI S KONFERENCE

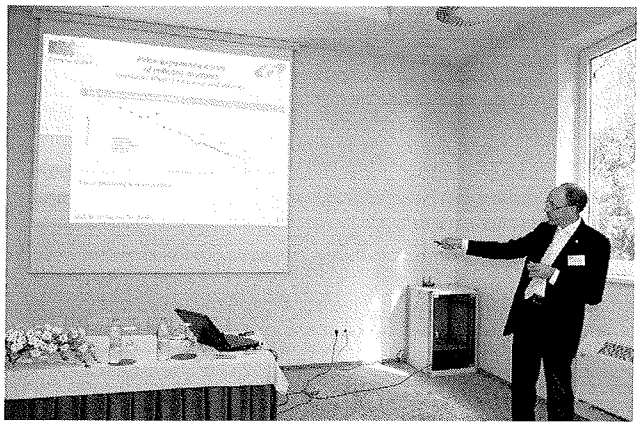

Vabljeno predavanje prof. Wima Sinke o kristalno silicijevih sončnih celicah in modulih (Energy Research Center of the Netherlands, koordinator največjega evropskega projekta na področju kristalnih silicijevih sončnih celic in modulov Crystalclear OP6)

Vabljeno predavanje prof. Jamesa Sitesa o tankoplastnih CIGS celicah (Colorado State University ZDA, vodja PV laboratorija in prodekan na omenjeni univerzi)

Skupinska slika pred Jamskim dvorcem, v ozadju vhod v Postojnsko jamo.

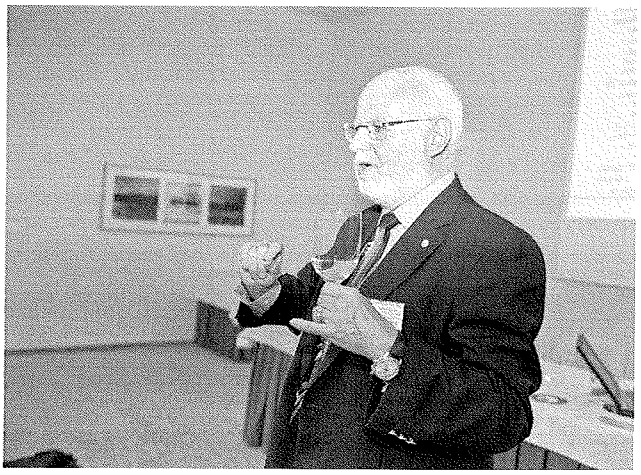

Vabljeno predavanje prof. Antonia Luque o niovih konceptih sončnih celic z vmesnim pasom (Polytechnic University Madrid, izumitelj dvostranske celice, član kraljeve akademije Španije, dobitnik prestižnih nagrad kot je evropska nagrada Alexandra-Edmonda Becquerela s področja fotovoltaike)

Del udeležencev delavnice o fotovoltaiki

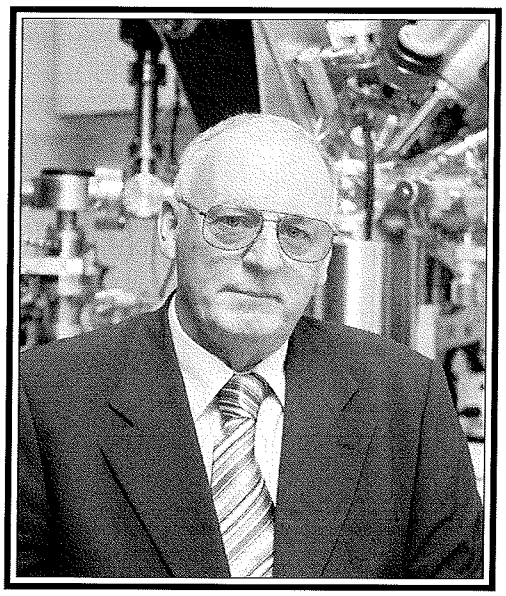

V SLOVO PROF. DR. ANTONU ZALARJU

Pred časom smo se poslovili od našega pokojnega sodelavca Toneta Zalarja, vendar je v naših mislih še vedno živa njegova podoba. Naj ob tej priložnosti na kratko opišem strokovno pot pokojnega prof. Antona Zalarja.

Profesor Anton Zalar je bil rojen sredi 2. svetovne vojne, leta 1943 v Ljubljani. Tu se je šolal na srednji tehnični šoli, smer metalurgija, nadaljeval visokošolski študij metalurgije na Fakulteti za naravoslovje in tehnologijo Univerze v Ljubljani, kjer je leta 1969 diplomiral, leta 1981 zaključil magisterij in leta 1987 doktoriral. Nadaljeval je z akademsko kariero na Fakulteti za naravoslovje in tehnologijo, Univerze v Ljubljani, kjer je leta 2004 pridobil naziv redni profesor za področje fizikalne metalurgije. Profesor Anton Zalar je bil do leta 1995 zaposlen na Inštitutu za elektroniko in vakuumsko tehniko - IEVT, zatem pa je vodil Inštitut za tehnologijo površin in optoelektroniko. Po priključitvi tega instituta v okvir Instituta »Jožef Stefan« leta 2003 pa je bil uspešni vodja Odseka za tehnologijo površin in optoelektroniko. Prof. Zalar je vseskozi vodil tudi Laboratorij za preiskavo površin in tankih plasti in raziskovalno skupino, ki je opravljala temeljne in aplikativne raziskave, med drugim tudi s področja materialov za elektroniko.

Pokojni Anton Zalar je zadnja leta sicer opravljal vodstvene funkcije, vendar pa je bil v svojem srcu predvsem raziskovalec in je to ostal tudi do konca. Do konca je pozorno spremljal svoje raziskovalno področje, to je preiskave površin in tankih plasti z elektronskimi spektroskopskimi tehnikami, oziroma bolj natančno s spektroskopijo Augerjevih elektronov. Do konca je Anton Zalar aktivno sodeloval pri eksperimentalnem delu. Žal so nekatere njegove preiskave ostale nedokončane in nekatere njegove ideje neuresničene. Na svojem raziskovalnem področju se je uveljavil doma in v mednarodnih strokovnih krogih. Med posebej izstopajočimi dosežki naj omenim, da je prof. Anton Zalar v osemdesetih letih prvi na svetu uvedel zelo odmevno metodo za natančno preiskavo tankoplastnih struktur, ki so še posebej pomembne na področju mikroelektronike. Ta raziskovalna metoda nosi ime po profesorju Zalarju (ang. »Zalar rotation«) in je še danes sestavni del vseh naprednih analitskih instrumentov za preiskavo površin in tankih plasti. Metoda »Zalar rotation« za natančno preiskavo notranjih faznih mej v večplastnih strukturah je še danes nepogrešljiva pri razvoju sodobnih mikroelektronskih elementov in jo redno uporabljajo v vseh razvojnih laboratorijih pomembnih svetovnih firm s področja mikroelektronike. Prof. Zalar je avtor tudi večih tehničnih izboljšav in enega patenta. Kot mednarodno priznani strokovnjak je imel profesor Anton Zalar intenzivne stike s tujino. Uspešno je sodeloval z Max-Planck institutom »Institut für Metallforschung« iz Stuttgarta, kakor tudi s »Kernforschungszentrum Karlsruhe«. Sodeloval je z Institutom za tehnično fiziko pri Madžarski akademiji za znanost v Budimpešti, z Inštitutom za fiziko iz Prage, z Oddelkom za tehnično fiziko Univerze Kaiserslautern, ter mnogimi drugimi. Posebej velja omeniti tudi njegovo sodelavo z ameriško firmo Physical Electronics. Rezultati njegovega znanstveno-raziskovalnega dela so zajeti v 360 bibliografskih enotah, med njimi je 208 znanstvenih in strokovnih člankov. Na tujih inštitutih in univerzah je imel okrog štirideset vabljenih predavanj. Njegova dela so bila citirana več kot 1400 krat, kar nam priča o izredni odmevnosti dela profesorja Antona Zalarja. Za svoje delo je profesor Anton Zalar dvakrat prejel nagrado Sklada Borisa Kidriča, in sicer 1980 in 1987. Oktobra 2006 je bila njegova raziskovalna skupina uvrščena v skupino najboljših raziskovalnih programov v letu 2005 v Sloveniji. Profesor Anton Zalar je bil tudi uspešen pedagog in visokošolski učitelj. Od leta 1995 je bil visokošolski profesor na Naravoslovnotehniški fakulteti Univerze v Ljubljani, predaval je tudi na Fakulteti za elektrotehniko in računalništvo na Univerzi v Mariboru ter na Mednarodni podiplomski šoli

Jožefa Stefana. Bil je tudi delovni mentor več mladim raziskovalcem, ki so vsi svoj študij uspešno zaključili.

Pokojni prof. Zalar je bil član društva MIDEM, član uredniškega odbora revije Informacije MIDEM in član Društva za vakuumsko tehniko Slovenije, katerega 50-letnico praznujemo letos. O zelo visokem mednarodnem ugledu profesorja Antona Zalarja nam pričajo podatki, da je bil v letih od 1986 do 1988 predsednik Zveze društev za vakuumsko tehniko Jugoslavije - JUVAK, od leta 1986 do 1992 pa je bil član Izvršilnega odbora Mednarodne zveze za vakuumsko znanost, tehniko in aplikacije (IUVSTA). Prof. Zalar je bil tudi član ameriškega vakuumskega društva AVS. Od leta 1990 do 1994 je bil izvoljen za poslanca Mestne skupščine Ljubljana za raziskovalno področje.

Prof. Zalar je sodeloval v številnih mednarodnih programskih komitejih različnih znanstvenih konferenc. Bil je član mednarodnega svetovalnega odbora Evropske konference o uporabni analizi površin in faznih mej (ECASIA). V Sloveniji je prof. Zalar od leta 1997 sodeloval v mednarodnem programskem komiteju konference MIDEM, ki je namenjena strokovnjakom s področja mikroelektronike. Pri Mednarodni organizaciji za standardizacijo je bil prof. Zalar od leta 1992 član Komiteja ISO/TC 201, Surface Chemical Analysis, kjer je tudi zastopal Urad za standardizacijo in meroslovje, Slovenije. V letu 1992 je opravljal povezavo med navedenim komitejem ISO in Mednarodno zvezo za vakuumsko znanost, tehniko in aplikacije (IUVSTA) in sicer preko Povezovalnega komiteja IUVSTA, katerega predsednik je bil. Prof. Zalar je opravljal tudi recenzijska dela za dve najpomembnejši mednarodni reviji za področje tankih plasti in površin: Thin Solid Films in Surface and Interface Analysis.

Pokojni prof. Anton Zalar je bil tudi veliki ljubitelj Slovenije in slovenskega jezika, še posebno si je prizadeval za kvalitetno izrazoslovje na svojem raziskovalnem področju.

Sodelavci pokojnega Antona Zalarja se ga bomo spominjali predvsem po njegovi natančnosti, doslednosti oziroma pedantnosti, to je lastnostih, za katere danes velikokrat ni več ne prostora in ne časa. Ravno tako je pokojnega Toneta odlikovala pokončna drža, trma in vztrajnost. Imel je vedno tudi pogum, da je naredi korak dlje v neznano kot drugi. Bil je rahločuten in pravičen človek, ki je znal prisluhniti človekovim težavam in stiskam in mu, če se je le dalo, tudi pomagal. Pokojni Tone je bil med sodelavci, znanci in prijatelji poznan tudi po svoji sproščenosti, gostoljubnost in prijetnem vzdušju v družbi. Zelo rad se je po delovnih obveznostih srečal s sodelavci in prijatelji in običajno na teh srečanjih ostal do zadnjega.

Institut Jožef Stefan, Naravoslovnotehniška Fakulteta Univerze v Ljubljani, Društvo MIIDEM, Društvo za vakuumsko tehniko Slovenije in celotno slovensko naravoslovje so s smrtjo profesorja Antona Zalarja izgubili izrednega raziskovalca, uspešnega visokošolskega učitelja, aktivnega člana ter mednarodno visoko priznanega strokovnjaka, ki je v spominu slovenskega naravoslovja pustil trajno in vidno sled.

Doc. dr. Janez Kovač,

Odsek za tehnologijo površin in optoelektroniko – F4
Institut Jožef Stefan

UDK621.3:(53+54+621+66), ISSN0352-9045 Informacije MIDEM 39(2009)1, Ljubljana

VSEBINA **CONTENT**

UDK621.3:(53+54+621+66), ISSN0352-9045 Informacije MIDEM 39(2009)2, Ljubljana

VSEBINA CONTENT

UDK621.3:(53+54+621+66), ISSN0352-9045 Informacije MIDEM 39(2009)3, Ljubljana

UDK621.3:(53+54+621+66), ISSN0352-9045 Informacije MIDEM 39(2009)4, Ljubljana

VSEBINA CONTENT

Informacije MIDEM
Strokovna revija za mikroelektroniko, elektronske sestavine dele in materiale

NAVODILA AVTORJEM

Informacije MIDEM je znanstveno-strokovno-društvena publikacija Strokovnega društva za mikroelektroniko, elektronske sestavne dele in materiale - MIDEM. Revija objavlja prispevke s področja mikroelektronike, elektronskih sestavnih delov in materialov. Ob oddaji člankov morajo avtorji predlagati uredništvu razvrstitev dela v skladu s tipologijo za vodenje bibliografij v okviru sistema COBISS.
Znanstveni in strokovni prispevki bodo recenzirani.

Znanstveno-strokovni prispevki morajo biti pripravljeni na naslednji način:

1. Naslov dela, imena in priimki avtorjev brez titul, imena institucij in firm
2. Ključne besede in povzetek (največ 250 besed).
3. Naslov dela v angleščini.
4. Ključne besede v angleščini (Key words) in podaljšani povzetek (Extended Abstract) v angleščini, če je članek napisan v slovenščini
5. Uvod, glavni del, zaključek, zahvale, dodatki in literatura v skladu z IMRAD shemo (Introduction, Methods, Results And Discsussion).
6. Polna imena in priimki avtorjev s titulami, naslovi institucij in firm, v katerih so zaposleni ter tel./Fax/Email podatki.
7. Prispevki naj bodo oblikovani enostransko na A4 straneh v enem stolpcu z dvojnim razmikom, velikost črk namanj 12pt. Priporočena dolžina članka je 12-15 strani brez slik.

Ostali prispevki, kot so poljudni cčlanki, aplikacijski članki, novice iz stroke, vesti iz delovnih organizacij, inštitutov in fakultet, obvestila o akcijah društva MIDEM in njegovih članov ter drugi prispevki so dobrodošli.

Ostala splošna navodila

1. V članku je potrebno uporabljati SI sistem enot oz. v oklepaju navesti alternativne enote.
2. Risbe je potrebno izdelati ali iztiskati na belem papirju. Širina risb naj bo do 7.5 oz.15 cm. Vsaka risba, tabela ali fotografija naj ima številko in podnapis, ki označuje njeno vsebino. Risb, tabel in fotografij ni potrebno lepiti med tekst, ampak jih je potrebno ločeno priložiti članku. V tekstu je treba označiti mesto, kjer jih je potrebno vstaviti.
3. Delo je lahko napisano in bo objavljeno v slovenščini ali v angleščini.
4. Uredniški odbor ne bo sprejel strokovnih prispevkov, ki ne bodo poslani v dveh izvodih skupaj z elektronsko verzijo prispevka na disketi ali zgoščenki v formatih ASCII ali Word for Windows. Grafične datoteke naj bodo priložene ločeno in so lahko v formatu TIFF, EPS, JPEG, VMF ali GIF.
5. Avtorji so v celoti odgovorni za vsebino objavljenega sestavka.

Rokopisov ne vračamo. Rokopise pošljite na spodnji naslov.

Uredništvo Informacije MIDEM
MIDEM pri MIKROIKS
Stegne 11, 1521 Ljubljana, Slovenia
Email: Iztok.Sorli@guest.arnes.si
tel. (01) 5133 768, fax. (01) 5133 771

Informacije MIDEM
Journal of Microelectronics, Electronic Components and Materials

INSTRUCTIONS FOR AUTHORS

Informacije MIDEM is a scientific-professional-social publication of Professional Society for Microelectronics, Electronic Components and Materials – MIDEM. In the Journal, scientific and professional contributions are published covering the field of microelectronics, electronic components and materials.
Authors should suggest to the Editorial board the classification of their contribution such as : original scientific paper, review scientific paper, professional paper...
Scientific and professional papers are subject to review.

Each scientific contribution should include the following:

1. Title of the paper, authors' names, name of the institution/company.
2. Key Words (5-10 words) and Abstract (200-250 words), stating how the work advances state of the art in the field.
3. Introduction, main text, conclusion, acknowledgements, appendix and references following the IMRAD scheme (Introduction, Methods, Results And Discsussion).
4. Full authors' names, titles and complete company/institution address, including Tel./Fax/Email.
5. Manuscripts should be typed double-spaced on one side of A4 page format in font size 12pt. Recommended length of manuscript (figures not included) is 12-15 pages
6. Slovene authors writing in English language must submit title, key words and abstract also in Slovene language.
7. Authors writing in Slovene language must submit title, key words and extended abstract (500-700 words) also in English language.

Other types of contributions such as popular papers, application papers, scientific news, news from companies, institutes and universities, reports on actions of MIDEM Society and its members as well as other relevant contributions, of appropriate length , are also welcome.

General informations

1. Authors should use SI units and provide alternative units in parentheses wherever necessary.
2. Illustrations should be in black on white paper. Their width should be up to 7.5 or 15 cm. Each illustration, table or photograph should be numbered and with legend added. Illustrations, tables and photographs must not be included in the text but added separately. However, their position in the text should be clearly marked.
3. Contributions may be written and will be published in Slovene or English language.
4. Authors must send two hard copies of the complete contributon, together with all files on diskette or CD, in ASCII or Word for Windows format. Graphic files must be added separately and may be in TIFF, EPS, JPEG, VMF or GIF format.
5. Authors are fully responsible for the content of the paper.

Contributions are to be sent to the address below.

Uredništvo Informacije MIDEM
MIDEM pri MIKROIKS
Stegne 11, 1521 Ljubljana, Slovenia
Email: Iztok.Sorli@guest.arnes.si
tel.+386 1 5133 768, fax.+386 1 5133 771